GEORGIA INSTITUTE OF TECHNOLOGY — OFFICE OF CONTRACT ADMINISTRATION

PROJECT ADMINISTRATION DATA SHEET

[X] ORIGINAL
[ ] REVISION NO. ____

Project No. A-2920 DATE: 5/6/81

Project Directors: Dr. J. W. Amoss & Dr. E. L. Meeks ~~School~~/Lab EML/PSD

Sponsor: Naval Research Laboratory; Washington, D. C. 20375

Type Agreement: Short Form Research Contract No. N00014-81-K-2004

Award Period: From 4/1/81 To ~~3/31/82~~ 6/30/83 (Performance) flexible (Reports)

Sponsor Amount: $99,965 ($50,000 authorized thru 9/30/81) Contracted through:

Cost Sharing: None GTRI/~~GIT~~

Title: Application of Molecular Beam Epitaxy to Millimeter Wave GaAs IMPATTs

ADMINISTRATIVE DATA OCA CONTACT Duane Hutchison x 4820

1) Sponsor Technical Contact: Dr. John Davey; Code 6811; Naval Research Laboratory; 4555 Overlook Ave., S. W.; Washington, D. C. 20375

2) Sponsor Admin./Contractual Contact: Mr. Thomas A. Bryant; ONR Resident Representative; Georgia Institute of Technology; 206 O'Keefe Building; Atlanta, GA. 30332

Reports: See Deliverable Schedule Security Classification: Unclassified

Defense Priority Rating: None

RESTRICTIONS

See Attached DOD Supplemental Information Sheet for Additional Requirements.

Travel: Foreign travel must have prior approval - Contact OCA in each case. Domestic travel requires sponsor approval where total will exceed greater of $500 or 125% of approved proposal budget category.

Equipment: Title vests with GIT if specified in the proposal and not otherwise indicated in Short Form Research Contract.

COMMENTS:

COPIES TO:

Administrative Coordinator
Research Property Management
Accounting Office
Procurement/EES Supply Services
Research Security Services
~~Reports Coordinator~~ (OCA)
Legal Services (OCA)
Library, Technical Reports
EES Research Public Relations (2
Project File (OCA)
Other: ____

GEORGIA INSTITUTE OF TECHNOLOGY OFFICE OF CONTRACT ADMINISTRATION

SPONSORED PROJECT TERMINATION/CLOSEOUT SHEET

Date 12/23/83

Project No. A-2920 ~~School~~/Lab EML

Includes Subproject No.(s)

Project Director(s) J.W. Amoss & E.L. Meeks GTRI / ~~GTRI~~

Sponsor Naval Research Laboratory

Title Application of Molecular Beam Epitaxy to Millimeter Wave GaAs IMPATTs

Effective Completion Date: 6/30/83 (Performance) flexible * (Reports)

Grant/Contract Closeout Actions Remaining:

- [ ] None
- [x] Final Invoice or Final Fiscal Report
- [x] Closing Documents
- [x] Final Report of Inventions
- [x] Govt. Property Inventory & Related Certificate
- [ ] Classified Material Certificate
- [ ] Other

* 30 days after receipt of draft report. Final Report charges allowed after 6/30/83.

Continues Project No. Continued by Project No.

COPIES TO:

Project Director
Research Administrative Network
Research Property Management
Accounting
Procurement/EES Supply Services
Research ~~Security~~ Services
Reports Coordinator (OCA)
~~Legal Services~~

Library
GTRI
Research Communications (2)
Project File
Other

Form OCA 60:1028

Application of Molecular Beam Epitaxy to Millimeter Wave GaAs IMPATTs

Quarterly Report No. 1

J. W. Amoss, E. L. Meeks, and N. W. Cox

Engineering Experiment Station
Georgia Institute of Technology
Atlanta, Georgia 30332

10 July 1981
Report for Period 1 April 1981 - 30 June 1981
Contract No. N00014-81-K-2004

Prepared for

Naval Research Laboratory
Washington, D.C. 20375

PREFACE

This report describes work performed at the Georgia Institute of Technology Engineering Experiment Station under Contract No. N00014-81-K-2004 during the period 1 April 1981 to 30 June 1981. Funding for the program was provided by the Naval Electronics Systems Command with technical administration by Dr. John Davey of the Naval Research Laboratory.

1.0 INTRODUCTION

This report summarizes recent research directed toward the application of molecular beam epitaxy material to millimeter wave GaAs IMPATTs. The program is a one year effort to utilize MBE epitaxial growth techniques to produce improved and reproducable, highly efficient millimeter wave GaAs IMPATT devices. Specific tasks of the program are:

1) define initial target profiles for 40 GHz IMPATTs,
2) grow GaAs material to desired target profile
3) determine actual profile,
4) process material,
5) evaluate RF performance,
6) simulate via computer model, and
7) excercise computer model to obtain new target profile and repeat steps 2-7.

1.1 Summary of Principal Results

During this report period, most of the efforts were concerned with tasks 1, 3, and 6. The tasks related to material growth and processing, device fabrication and testing, etc. are awaiting completion of the new MBE system which is being constructed at Georgia Tech. The rather low-level expenditures during this period is reflected in the manpower and financial status report in a subsequent section. The following results were obtained during this period:

° An improved MBE system was designed and is being assembled (under internal funding) for exclusive use during this program. The growth chamber of this system is significantly smaller than its predecessor,

which should improve the pump-down and bake-out capability and, hopefully, lower the residual background doping level. The system contains six source furnaces and shutters, thereby allowing the growth of double-drift Read-Read type devices. The source shutters have been redesigned and should be more positive acting than those contained in the previous system.

° A number of GaAs millimeter wave IMPATT profiles were chosen for initial investigations. They are based partially on computer simulations and partially on actual designs as reported by other laboratories. These will serve as initial target profiles for the MBE devices.

° Computer software for generating and interpreting CV data of double-drift devices was developed.

° Voltage contrast experiments were made on an available X-band double drift device. Such experiments may prove helpful in evaluating the doping profile of millimeter wave devices.

1.2 Plans for Next Quarter

° Complete assembly and test of new MBE system.

° Grow and optimize single-drift low-high and hybrid-Read material.

° fabricate and test IMPATTs

II DEVICE DESIGN

IMPATT design necessitates a thorough understanding of the factors effecting IMPATT operation. An accurate mathematical description of IMPATT operation, however, requires a highly complicated model and a precise knowledge of the structural and the material parameters. The more general computer simulations involve methods in which the equations governing IMPATT operation are solved numerically without introducing any simplifying assumptions. This usually involves finite difference equations in which the solution starts with initial conditions and proceeds through the transient to a final steady - state solution. Fourier analysis of the steady-state wave forms then leads to output power, efficiency, and admittance data. Simulations of this type are far too costly for use in general device design because of the many structural and material parameters involved. Furthermore, disputes still remain about the values of drift velocities and ionization rates of GaAs at high-field levels, which add further to the uncertainty of the model. Because of the many inherent uncertainties and the expens of the more general solutions, most device developers resort to a s emperical design approach based on approximate models. The desir approach and the models used during this program are described

In general, an IMPATT device is a semiconductor diode w in the reverse breakdown region. Under reverse bias, the is such that majority carriers are forced away or depleted fr junction area, forming a depletion region. When the electric field the vicinity of the junction reaches a certain level, avalanche multiplication occurs creating, hole-electron pairs which drift through the

remainder of the depletion region. To help visualize IMPATT operation and the factors effecting efficiency, the active region of the diode can be seperated into two distinct parts: a part in which mobile carriers (holes and electrons) are generated through impact ionization and the remaining part in which the carriers drift at saturated velocity. Read has shown that this device can generate power (or act as a negative resistor) at microwave frequencies.

The negative resistance can be attributed to two mechanisms. In the avalanche region, the generation of carriers is proportional to the density of carriers and to the electric field. This results in the current density generated within the avalanche region lagging the RF field, or terminal voltage, by 90°. A further 90° phase lag between the terminal current and terminal voltage is introduced via the drift of carriers through the drift region(s).

The dc to RF energy conversion occurs within the drift region via the interaction of drifting carriers with the electric field. Although necessary for the generation of carriers, the avalanche region does not contribute to the energy conversion processes. This "idealized" model leads to a simple approximation for the efficiency of an IMPATT device in terms of the dc voltage across the avalanche region V_a and the voltage across the drift region V_d, i.e.

$$\eta = \frac{1}{\pi} \frac{V_d}{V_d + V_a} \tag{1}$$

Despite it's simplicity, this expression is being used extensively here and at other laboratories as a guide in device development. The voltages across the avalanche and drift regions are obtained from a static solution

of the ionization integral equation and Poisson's equation.

Another approach which was used to help select initial target profiles utilized a large-signal quasi-static IMPATT computer program based on the analytic formulation of Kuvas and Lee (1). An existing computer program was modified to include double-drift devices with abritrary profiles. In brief the large-signal solution begins with a dc solution at the desired operating current. The electric field intensity and the ratio of hole-to-electron particle current density calculated for the dc case are assumed to remain unchanged in the large-signal case (2).

The efficiency of a number of potential single-drift and double-drift devices were calculated using these two approaches. Typical devices are shown in Figures 1 and 2 with selected device structures and calculated efficiencies tabulated below. The distances associated with each device are measured from the junction. The quasi-static efficiencies were calculated at 40 GHZ assuming the an RF voltage of .6 V_{DC}.

Flat profile:

doping density - 9.6×10^{16} cm^{-3}
efficiency - 12.9% (static)
12.1% (quasi-static)

High-low:

doping density - 30.0×10^{16} cm^{-3}
6.7×10^{16} cm^{-3}
interface - .13 microns
efficiency - 17.5% (static)
19.2% (quasi-static)

Low-high-low:

doping density - 6.7×10^{16} cm^{-3}
69.0×10^{16} cm^{-3}
6.7×10^{16} cm^{-3}
spike position - .09 microns
spike width - .02 microns
efficiency - 16.9% (static)
- 17.9% (quasi-static)

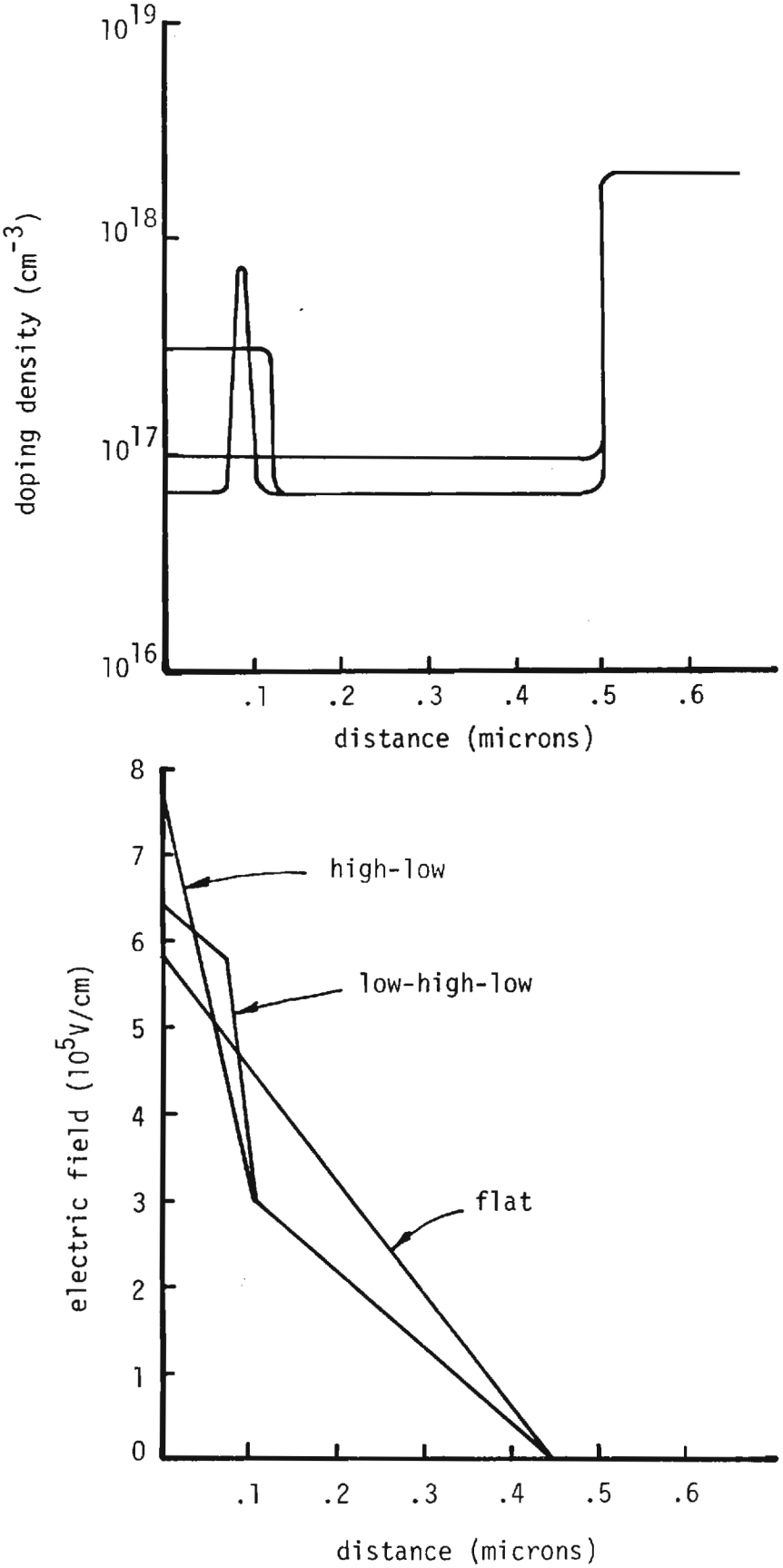

Figure 1. Single-drift millimeter wave IMPATT doping profiles and electric field intensity

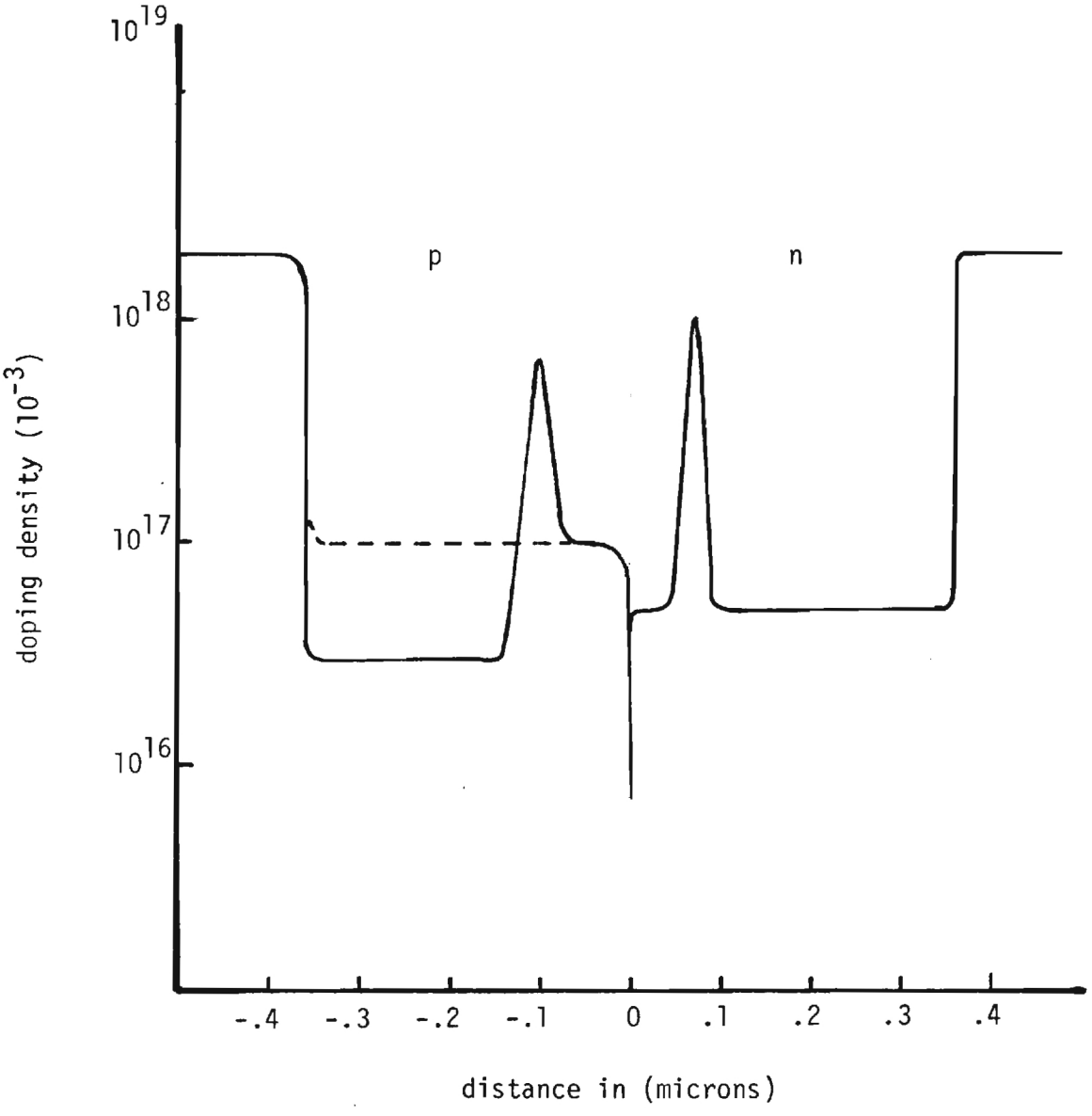

Figure 2. Double-drift millimeter wave IMPATT doping profiles.

Read-Read: (p-side)

doping density - 20.0×10^{16} cm^{-3}
- 60.0×10^{16} cm^{-3}
- 2.8×10^{16} cm^{-3}

spike position - .07 microns
apike width - .02 microns

(n -side)

doping density - 6.0×10^{16} cm^{-3}
- 125.0×10^{16} cm^{-3}
- $.6 \times 10^{16}$ cm^{-3}

spike position - .07 microns
spike width - .02 microns
efficiency - 23.9% (static
- 21.9% (quasi-static)

Low-high-low single-drift Schottky devices will be attempted first. These devices are relatively easy to profile and should be a good indicator as to the ability to grow a particular structure. A hybrid-Read profile will be grown next. This structure requires the growth of both n and p type material and requires a more elaborate profiling technique, as discussed in the next section. Following this, a Read-Read structure similar to the one described above will be grown and variations thereof made to optimize the structure using a semi-emperical approach.

III PROFILE EVALUATION

An accurate knowledge of doping profiles is crucial to any device development program. Although profile measurements for single-drift devices are considered straightforward, the conventional techniques do not provide a complete profile description within the zero bias depletion region. This problem becomes more accute for millimeter wave low-high-low (spike) devices where the zero bias depletion region may include the spike (highly doped region). In addition, the devices often enter low-level breakdown before the active or operating region is completely depleted. Step etching is often used to provide a profile description throughout the remaining region.

Establishing the doping profile of the double-drift device is considerably more complicated. In general, conventional techniques yields an effective concentration N_E and total depletion width W in terms of a change in capacitance, dC, with a change in applied voltage, dV, as given by

$$N_E(W) = -\frac{C^3}{q\epsilon A^2} \cdot \frac{1}{dC/dV} \quad \text{and} \tag{2}$$

$$W = \epsilon A/C, \quad \text{where}$$

$$\frac{1}{N_E(W)} = \frac{1}{N_A(y_p)} + \frac{1}{N_D(X_n)}, \tag{3}$$

$$W = y_p + X_n, \quad \text{and}$$

N_A and N_D are the net acceptor and donor concentrations at the edges of the depletion region (y_p, X_n) resulting from the applied voltage V.

These equations are a consequence of the more general equations given by

$$V + V_b = \frac{q}{\varepsilon} \left\{ \int_o^{y_p} \left[\int_o^{y} N_A(y)dy \right] dy + \int_o^{x_n} \left[\int_o^{X} N_D(X)dx \right] dx \right\} \quad (4)$$

and

$$\int_o^{y_p} N_A(y)dy = \int_o^{x_n} N_D(X)dx. \quad (5)$$

which of course, result from integrating Poissons equations twice and invoking conservation of charge. For a given doping profile $N_A(y)$ and $N_D(X)$, an applied voltage V will result in a depletion width $W = y_p + X_n$ and a corresponding capacitor C.

As stated previously, the conventional technique of determining doping profile directly from CV measurements yields an effective doping profile which does not represent the true profile throughout the composite material. A computer program based on the above equations was developed for interpreting CV data and for reconstructing doping profiles. The computer program can also simulate CV data of double-drift devices of abritrary doping profile.

Figures 3 and 5 show the effective profile, as obtained from simulated CV data, of typical hybrid-Read and Read-Read devices where actual profiles are shown in Figures 4 and 6.

Note the unusually wide rectangular "spike" shown in the "effective" doping profile of the hybrid-Read device. For the uniformly doped p-region, the total depletion width changes as $W = (1 + N_D(X)/N_A)X$ which causes the width of the actual spike of thickness δ and doping N_D to show up as a spike of thickness $(1 + N_D/N_A)\delta$ and doping $N_D N_A/(N_D + N_A)$ in the effective profile. For practical cases where both p and n regions

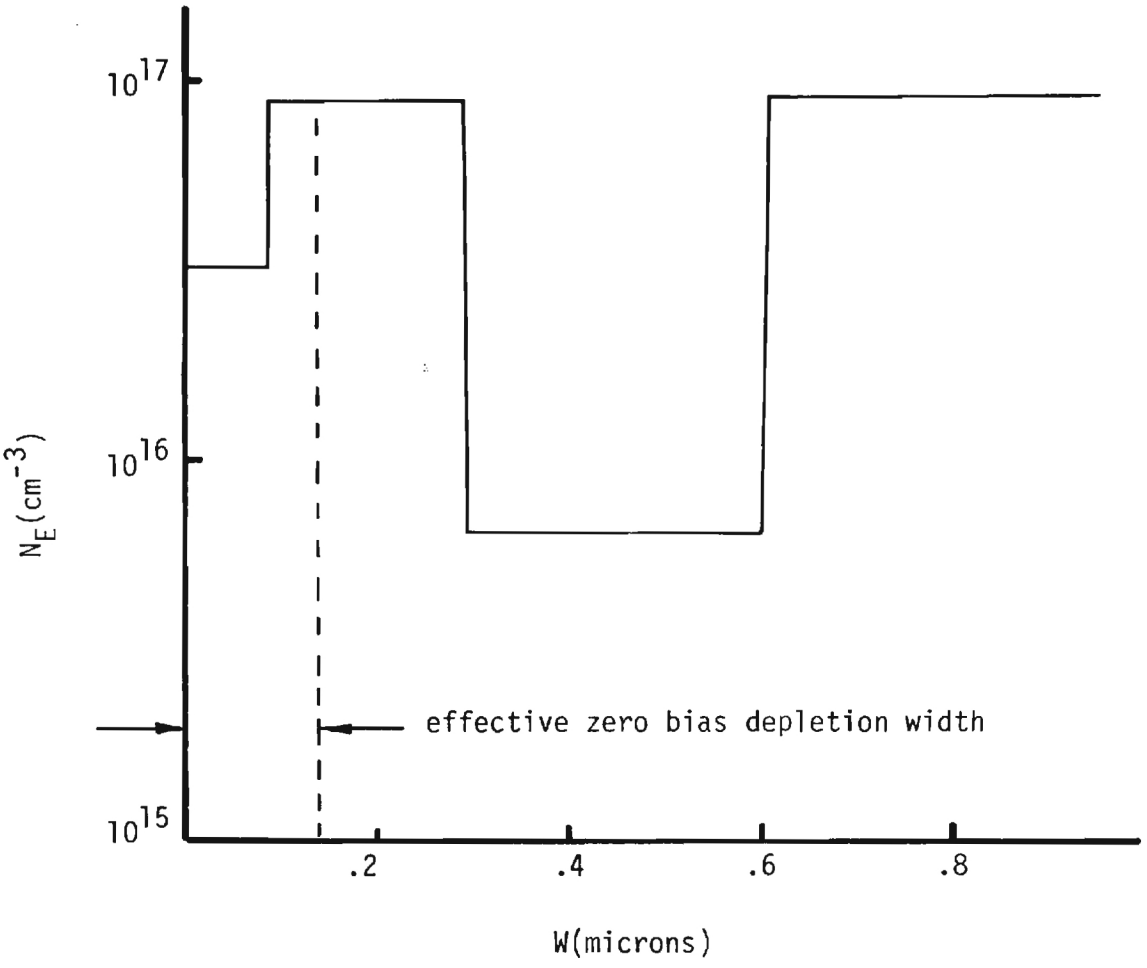

Figure 3. Effective Profile of Hybrid-Read Double-Drift Device

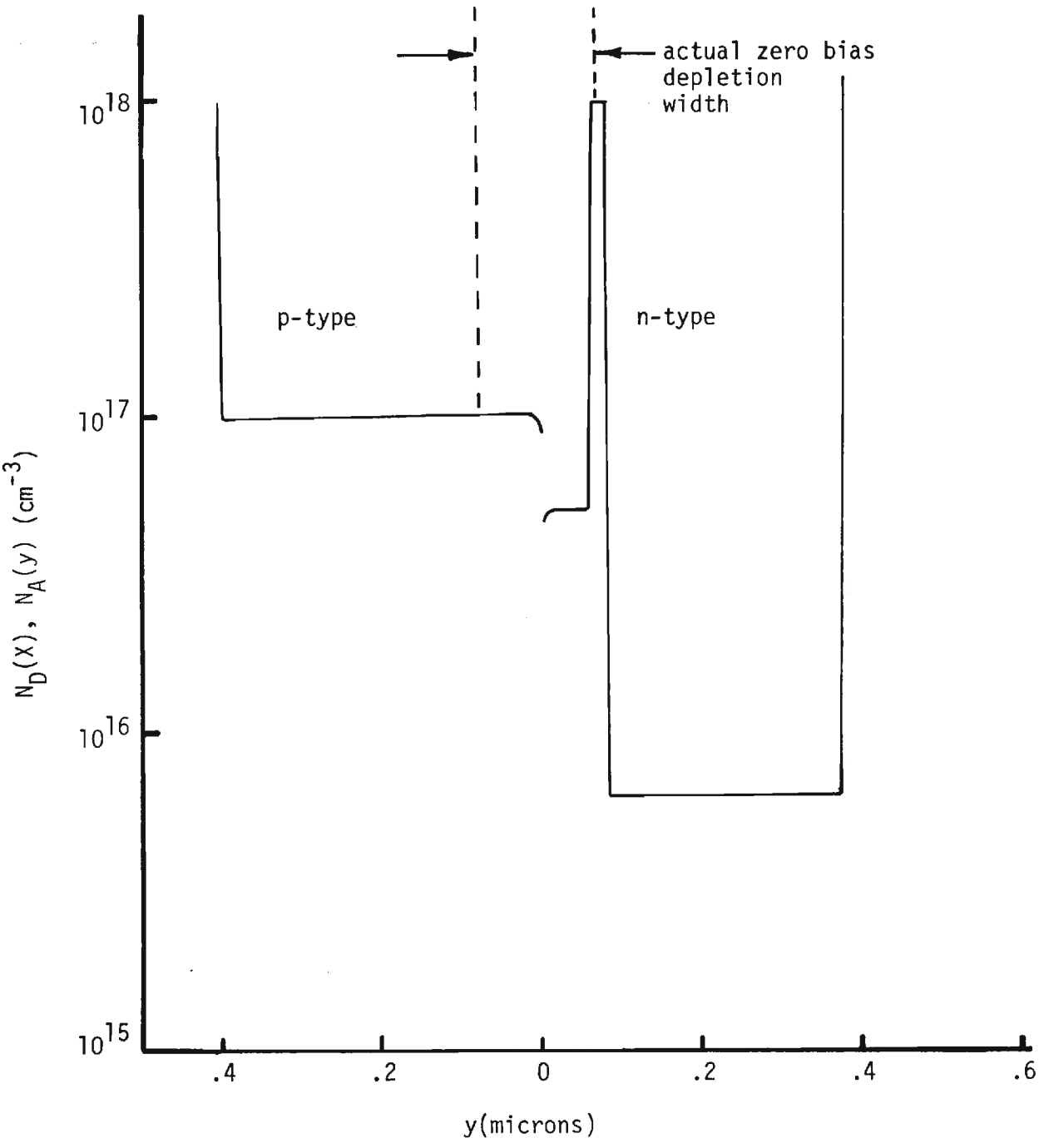

Figure 4. Actual Profile of Hybrid-Read Double-Drift Device

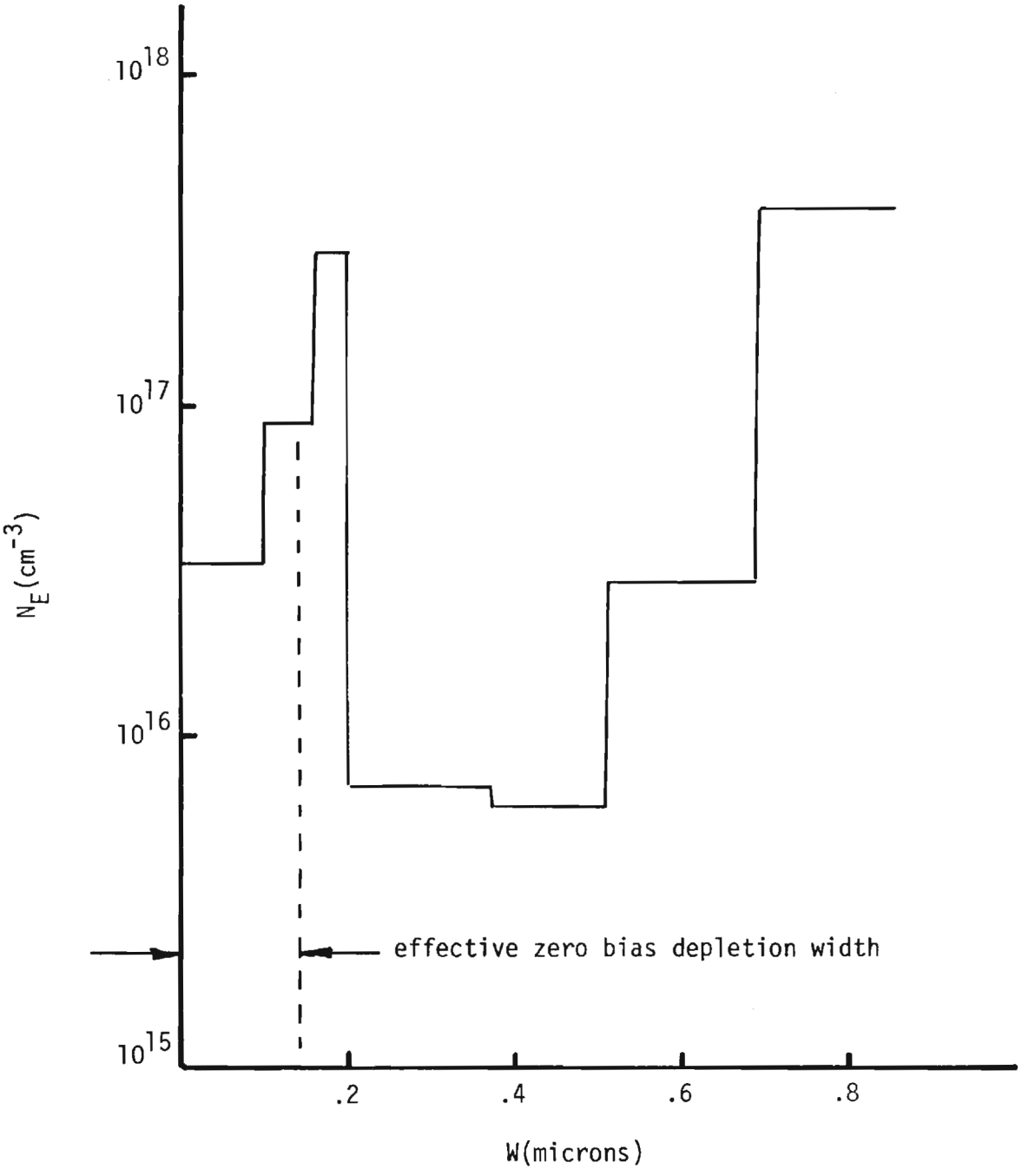

Figure 5. Effective Profile of Read-Read Double-Drift Device

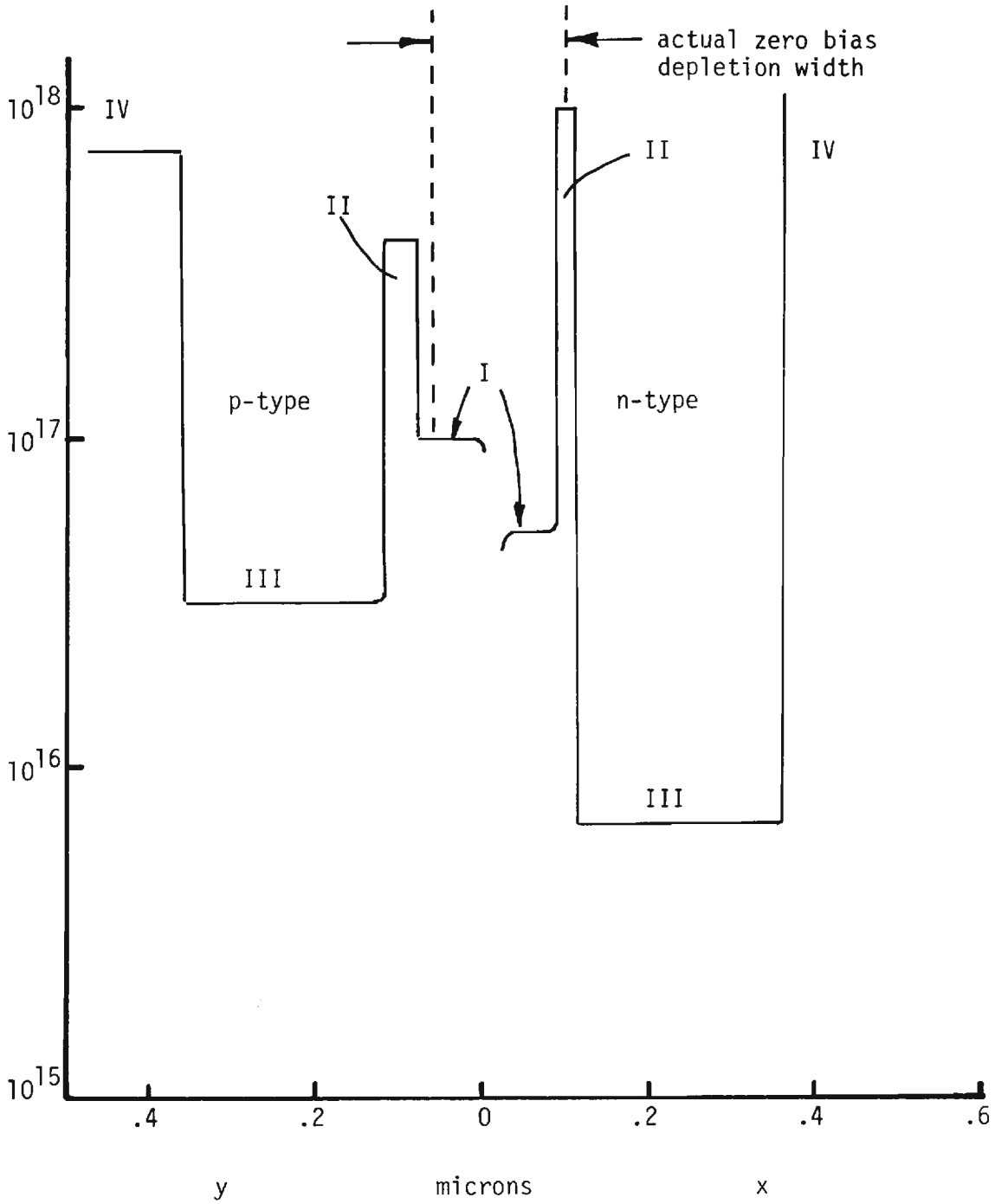

Figure 6. Actual Profile of Read-Read Double-Drift Device

may have complicated profiles (as in the Read-Read device), the effective doping can be quite complicated. Also note the arrows shown in the Figures. These represent the approximate extent of the zero bias depletion region. Little information on profile can be obtained from CV data for this region. A slight extension of the profile towards the junction can be obtained by applying slight positive bias. No information on $N_A(y)$ individually can be deduced from the effective doping distribution without first knowing the distribution of one side. One approach helpful in confirming whether or not a particular target profile had been grown would be to compare calculated values of $N_E(W)$ based on the target profile with values of $N_E(W)$ obtained from CV data measured on the grown material. If agreement is good one can be more confident in the profile grown. One should be aware, however, that the effective profile of a double-drift device is not unique and that an infinite combination of $N_A(y)$ and $N_p(y)$ can theoretically give the same $N_E(W)$. The task then is to determine uniquely $N_A(y)$ and $N_D(X)$ from measured C-V data.

There are two methods commonly used in reconstructing the doping profiles of double-drift devices. The first method involves etching a series of steps into both the p and n region, forming Schottky junctions at the various etch levels, and then evaluating the doping profile about those levels in the conventional manner. Unfortunately, this requires Schottky junctions on both p and n type material. In addition, the thickness of the active regions of millimeter wave IMPATTs are such that limited information can be obtained on the p-side because of the close proximity of the p-type Schottky with the p-n junction[3].

The other method involves etching just through the pn interface, forming a Schottky junction at that position, and evaluating the remaining

layer in the conventional manner. The profile of the other layer can then; in theory, be uniquely determined by using integrated charge expessions[3]. Equation (5) can be rewritten as

$$E_Q \begin{pmatrix} X \\ y \\ W \end{pmatrix} = \frac{q}{\varepsilon} \int_o^X N_D(X)dx = \frac{q}{\varepsilon} \int_o^X N_A(y)dy = \frac{q}{\varepsilon} \int_o^y N_{eff}(W)dx \qquad (6)$$

The field at any point in terms of integrated charge is $E\binom{X}{y} = E_{max} - E_Q\binom{X}{y}$. The integrated charge expression can be rewritten and generalized to

$$E_Q(z) = \frac{q}{\varepsilon} \int_o^z N(z)dz + \frac{1}{\varepsilon A} \int_o^V CdV \qquad (7)$$

which shows that the field in the swept out region can be expressed as a function of distance z and can be obtained (except in the zero bias depletion region, z^o) from C-V measurements. By treating E_Q as an independent variable and distance z (either x, y or z) as the dependent variable, then $y(E_Q) = W(E_Q) - X(E_Q)$ as depicted graphically in Figure 7. The Roman numericals denote the regions (with subscripts L for left and R for right) that the electric field sweeps through as E_Q increases. The doping profile $N_D(y)$ can theoretically be determined from $E_Q(y)$ using equation (6). In actual practice, however, the data about the origin (within the zero bias depletion width) can not be determined. Furthermore, the Schottky junction used to determine the profile of one side cannot always be placed just within that side. Both introduce an uncertainty in the proper orientation of the $W(E_Q)$ curve with respect to the $X(E_Q)$ curve. This can cause significant errors in the $y(E_Q)$ curve and hence in the reconstructed doping profile for the remaining side.

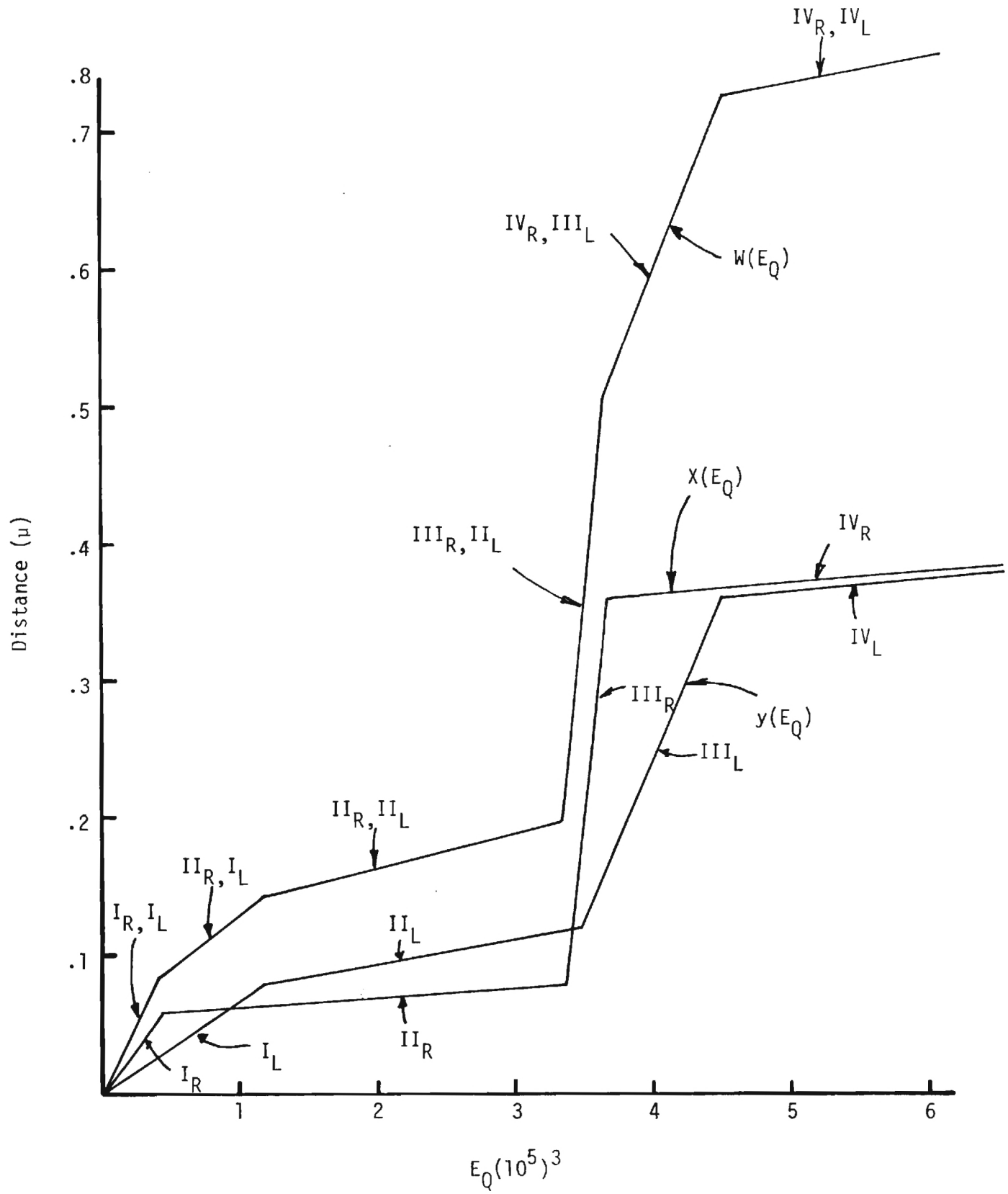

Figure 7. Integrated Charge Technique for reconstructing profile of one side knowing composite profile and profile of other side.

The scanning Electron Microscope (SEM) may prove useful orientating the two curves. This instrument has been used extensively in other IMPATT programs conducted at Georgia Tech to assess device geometry and to perform failure analysis. One of these programs (AFAL-TR-78-63) utilized the SEM for depltion width evaluation using the voltage contrast (V.C.) mode. This task was unique in that most prior V.C. work had been performed on planar device geometries while the tests on IMPATTs require contrast resolution in the mesa-height direction.

One of these tests was recently repeated to determine if this technique could be used to gain more information on the doping profile of double-drift devices. The results of this test is shown in Figure 8 as a composite of the series of photographics of a flat profile double-drift X-band device under different bias conditions. These photographs were taken using both the usual V.C. mode and specimen current mode. The middle band shows the depletion region as it widens with an increase in reverse bias. This image is formed from the specimen current which is caused by charge current multiplication resulting from the impingement of the electron beam within the depletion region.

Note the position of the junction shown as the relatively narrow line for .71 volts positive bias where the depletion region has narrowed considerably. It is also worthwhile to note the fuzziness and striations in the vicinity of the junction at low bias levels. The fuzziness is throught to be due to charge accumulation at the surface (charging from the beam). Increasing the voltage in either direction removes this charge. The straitions are thought to be due to nonuniform charging

Figure 8. Voltage contrast of flat double-drift IMPATT.

caused by nonuniform doping (the transition between the pn doping).

If the striations are cuased by a nonuniformity in doping, this type analysis could be very useful in providing additional profile data, especially for the millimeter devices. These test will be pursued further on the MBE grown devices.

IV MANPOWER AND FINANCIAL STATUS

Man Hours

Categories		Cumulative Total
Principal Research Engineer/Scientist	0.0	0.0
Senior Research Engineer/Scientist	112.0	112.0
Research Engineer/Scientist	0.0	0.0
Assistant Research Engineer/ Scientist/Technologist	0.0	0.0
Graduate Research Assistant	0.0	0.0
Student Co-op	0.0	0.0
Total	112.0	112.0

Financial

Budgeted	99,965.00
Expended	5,207.41
Balance	94,757.59

REFERENCES

1. R. Kuvas and C. A. Lee, "Quasi-static approximation for semiconductor avalanches," J. Appl. Physics, Vol. 41, no. 4, pp. 1743-1755, March 1970.

2. D. R. Decker, "IMPATT Diode Quasi-Static Large-Signal Model," IEEE Transactions on Electron Devices, Vol. ED-21, no. 8, pp. 469-479, August 1974.

3. D. Massé, M. Alderstien, A. D. Barlas, K. K. Johnson, L. Holway, and R. Mozzi, "EHF GaAs Double-Drfit IMPATT Diodes," Final Report, Contract AFAL-TR-79-1204, December 1979.

Application of Molecular Beam Epitaxy to Millimeter Wave GaAs IMPATTs

Quarterly Report No. 2

J. W. Amoss, E. L. Meeks, and N. W. Cox

Engineering Experiment Station
Georgia Institute of Technology
Atlanta, Georgia 30332

10 October 1981
Report for Period 1 July 1981 - 30 September 1981
Contract No. N00014-81-K-2004

Prepared for

Naval Research Laboratory
Washington, D.C. 20375

INTRODUCTION

This report summarizes recent research directed toward the application of molecular beam epitaxy material to millimeter wave GaAs IMPATTs. The program is a one year effort to utilize MBE epitaxial growth techniques to produce improved and reproducible, highly efficient millimeter wave GaAs IMPATT devices. Specific tasks of the program are:

1) define initial target profiles for 40 GHz IMPATTs,
2) grow GaAs material to desired target profile
3) determine actual profile,
4) process material,
5) evaluate RF performance,
6) simulate via computer model, and
7) exercise computer model to obtain new target profile and repeat steps 2-7.

Summary of Principal Results

During this report period, most of the efforts were concerned with completion of the new MBE system. The low-level expenditures during this period is again reflected in the manpower and financial status report in a subsequent section.

Plans for Next Quarter

- Grow and optimize single-drift low-high and hybrid-Read material.
- fabricate and test IMPATTs

IV MANPOWER AND FINANCIAL STATUS

Man Hours

Categories		Cumulative Total
Principal Research Engineer/Scientist	0.0	0.0
Senior Research Engineer/Scientist	96.0	208.0
Research Engineer/Scientist	0.0	0.0
Assistant Research Engineer/ Scientist/Technologist	0.0	0.0
Graduate Research Assistant	0.0	0.0
Student Co-op	0.0	0.0
Total	96.0	208.0

Financial

Budgeted	99,965.00
Expended	9,195.90
Balance	90,769.10

Application of Molecular Beam Epitaxy to Millimeter Wave GaAs IMPATTs

Quarterly Report No. 3

J. W. Amoss, E. L. Meeks, and N. W. Cox

Engineering Experiment Station
Georgia Institute of Technology
Atlanta, Georgia 30332

10 January 1982
Report for Period 1 October 1981 - 31 December 1981
Contract No. N00014-81-K-2004

Prepared for

Naval Research Laboratory
Washington, D.C. 20375

INTRODUCTION

This report summarizes recent research directed toward the application of molecular beam epitaxy material to millimeter wave GaAs IMPATTs. The program is a one year effort to utilize MBE epitaxial growth techniques to produce improved and reproducible, highly efficient millimeter wave GaAs IMPATT devices. Specific tasks of the program are:

1) define initial target profiles for 40 GHz IMPATTs,
2) grow GaAs material to desired target profile
3) determine actual profile,
4) process material,
5) evaluate RF performance,
6) simulate via computer model, and
7) exercise computer model to obtain new target profile and repeat steps 2-7.

Summary of Principal Results

The MBE system was completed and several calibration runs were made during this report period. Since the expenses for the MBE system construction efforts are being borne by Georgia Tech, the actual program expenditures during this period is again low as reflected in the man power and financial status reported in a subsequent section. As of January 1, about 20% of the total amount allocated by NRL for this project had been expended although 75% of the time period had elapsed. Consequently, a nine month no-cost time extension has been requested. Dr. John Davey, NRL's technical contact, was made aware of the need and reasons for this request during the most recent program review.

A minor but delaying problem with the shutter design was encountered during the initial runs. Under high vacuum conditions, the shutter alignment mechanism tended to gall and seize in the open position. This problem has been corrected and calibration runs are proceeding with great success.

Since the geometry of the new system is somewhat different and the source ovens are significantly different from our other systems, new growth parameters must be established. The growth rate of GaAs is determined by the Ga flux which is controlled by measuring the pressure change with the Ga source shutter open and closed. An ion gauge mounted directly behind the substrate position is used to measure the source fluxes before and after growth. The Ga flux control parameter and the growth rate are shown in Figure 1.

The system is also loaded with a Si source (n-type dopant) which will be calibrated immediately.

Plans for Next Quarter

- Grow and optimize single-drift low-high and hybrid-Read material.
- Fabricate and test IMPATTs.

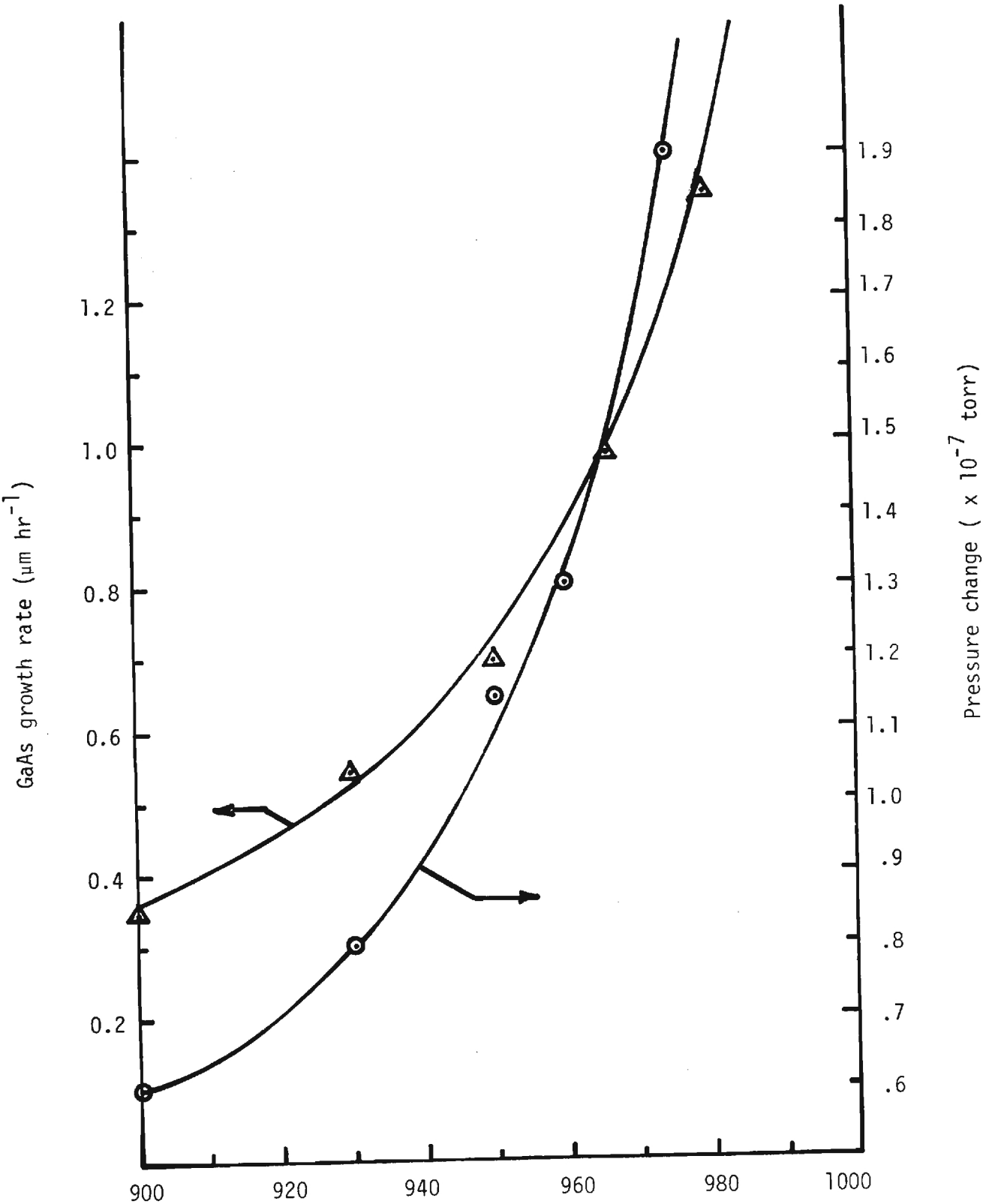
GaAs growth rate (μm hr^{-1})
Pressure change (x 10^{-7} torr)
0.2
0.4
0.6
0.8
1.0
1.2
.6
.7
.8
.9
1.0
1.1
1.2
1.3
1.4
1.5
1.6
1.7
1.8
1.9
900
920
940
960
980
1000
Ga control set point °C
System III (PBN)

IV MANPOWER AND FINANCIAL STATUS

Man Hours

Categories		Cumulative Total
Principal Research Engineer/Scientist	0.0	0.0
Senior Research Engineer/Scientist	140.0	348.0
Research Engineer/Scientist	20.0	20.0
Assistant Research Engineer/ Scientist/Technologist	0.0	0.0
Graduate Research Assistant	0.0	0.0
Student Co-op	0.0	0.0
Total	160.0	368.0

Financial

Budgeted	99,965.00
Expended	21,249.76
Balance	78,715.24

A-2920

Application of Molecular Beam Epitaxy to Millimeter Wave GaAs IMPATTs

Quarterly Report No. 4

J. W. Amoss, E. L. Meeks, and N. W. Cox

Engineering Experiment Station
Georgia Institute of Technology
Atlanta, Georgia 30332

10 April 1982
Report for Period 1 January 1981 - 31 March 1981
Contract No. N00014-81-K-2004

Prepared for

Naval Research Laboratory
Washington, D.C. 20375

INTRODUCTION

This report summarizes recent research directed toward the application of molecular beam epitaxy material to millimeter wave GaAs IMPATTs. The program is a one year effort to utilize MBE epitaxial growth techniques to produce improved and reproducible, highly efficient millimeter wave GaAs IMPATT devices. Specific tasks of the program are:

1) define initial target profiles for 40 GHz IMPATTs,
2) grow GaAs material to desired target profile,
3) determine actual profile,
4) process material,
5) evaluate RF performance,
6) simulate via computer model, and
7) excercise computer model to obtain new target profile and repeat steps 2-7.

Summary of Principal Results

During this report period, signficiant progress has been made in the major goals of the program. All sources required to grow double drift IMPATTs have been installed and calibrated. The system is being used to grow material for this and other programs with outstanding results. The topography of the surfaces grown are exceptionally smooth and featureless. The system routinely pumps down to the 10^{-10} tor range. In all respects, the new system has, thus far, proven superior to the other MBE systems constructed and operated at Georgia Tech.

Three millimeter wave IMPATT profiles have been grown and partially evaluated. The first, a single drift profile, was grown primarily to confirm the growth calibration curves. The other two, hybrid-Read profiles, were grown to be tested and processed as active operating IMPATTs. The latter materials have been taken through the processing steps, mounted in an EHF micropill package, and tested in a Ka-band waveguide structure with moderate success.

Details of major technical accomplishments are discussed in the next section.

Technical Discussions

The Si source (n-type dopant) and the Be source (p-type dopant) calibration curves used to grow the IMPATT profiles are shown in Figure 1. The impurity concentrations of the test samples were obtained from Hall mobility and capacitance versus voltage data. The temperatures during growth were measured with thermocouples located within the source ovens.

All IMPATT runs to date have used highly conducting, silicon doped substrates purchased from Laser Diode Laboratories. They were polished by the supplier and cleaned prior to loading by a procedure that has been used successfully for many years in this laboratory for the growth of CVD and MBE epitaxial layers.

The cleaning procedure used is listed in Table I.

Table I. GaAs Substrate Cleaning Procedure

1. Vapor degrease in boiling trichlorethylene vapor.
2. While still in tri vapor, rinse with methanol and keep covered with methanol until blown off with dry nitrogen.
3. Etch 1 minute in $H_2SO_4H_2O_2:H_2O$, 5:1:1 and rinse in hot DI water.
4. Rinse in methanol and keep wet until Br etch.
5. Etch 1 minute in Br:methanol 1:50.
6. Rinse in methanol. Blow dry with N_2.
8. Rinse in hot DI water.
9. Blow dry with N_2.

Figure 2 depicts the hybrid-Read profile choosen for initial growth of double-drift device material. This profile is based on material previously grown by others using CVD epi-reactors. When processed into IMPATTs, single chip packaged devices with similar structures have nominally delivered 1.5 watts at 35 GHz with an efficiency of 15%. Breakdown voltages at 1 mA were typically 17-18 volts.

The growth schedule for the profile shown in Figure 2, using the calibration curves of Figure 1 and a growth rate of 1 micron per hour, is shown in Table II.

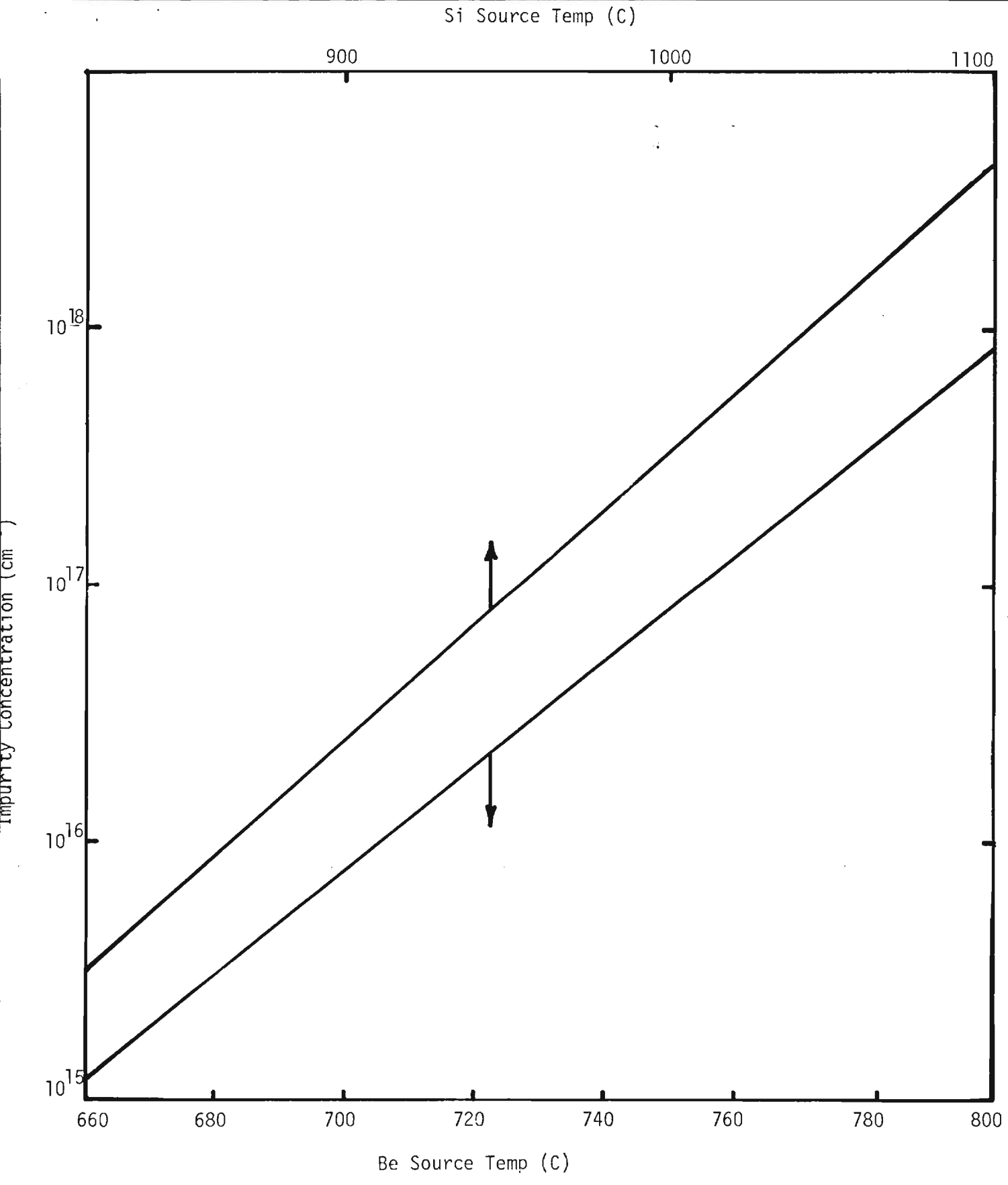

Figure 1. Calibration Curves for Be and Si Sources.

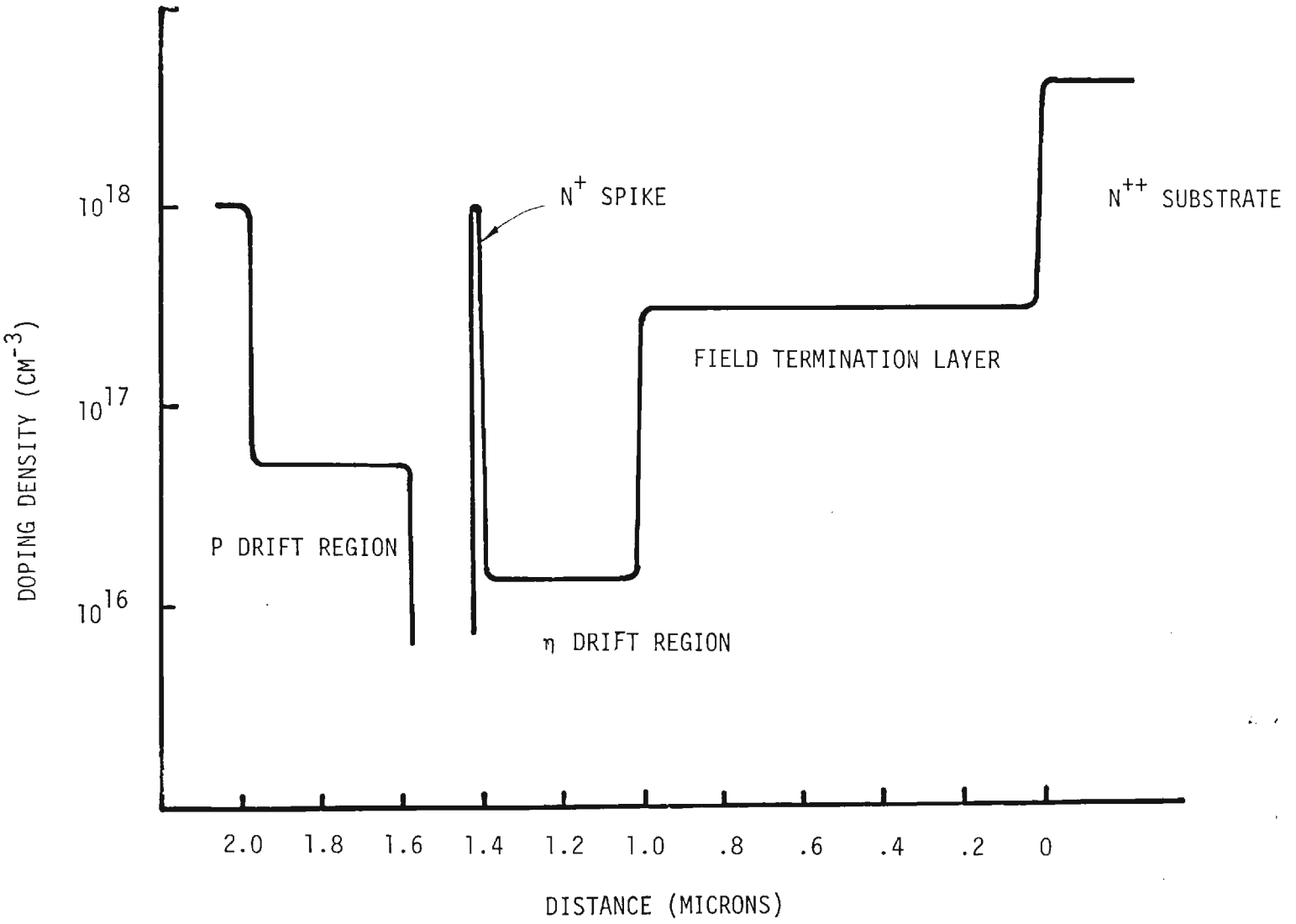

Figure 2. Doping density profile of double drift hybrid structure.

TABLE II. GROWTH SCHEDULE

SAMPLE NO. E 0329 -III DATE/OPERATOR EM/JL

RUN OBJECTIVE: DOUBLE DRIFT IMPATT

SYSTEM MODIFICATIONS:

SUBSTRATE: TYPE ____ LOT A1457P DOPING Si ORIENTATION 2° off [100]

PUMP DOWN DETAILS:

BACKGROUND PRESSURE: $1. \times 10^{-8}$ Torr

$\Delta P]_{GA}$ $4. \times 10^{-7}$

$\Delta P]_{As}$ 1.6×10^{-6}

SHUTTER	OPEN	SHUT
Ga Oven		
___ Oven		
___ Oven		
___ Oven		
___ Oven		

GROWTH CONDITIONS/RUN PROFILE						
Time 8:36	60 min	24 min	1 min 12 sec	9 Mm 30 sec	20 min	6 min
Ga Oven Cont/Temp(°C)	990	OPEN				
#1 Voltage (V)	18.5					
#1 Current (A)	7.3					
Si Oven Cont/Temp(°C)	1000	880	1060	off		
#2 Voltage (V)	18					
#2 Current (A)	7.0					
Se Oven Cont/Temp(°C)	200	CLOSED			740	880
#4 Voltage (V)						
#4 Current (A)						
As Oven Cont/Temp(°C)	296	OPEN				
#3 Voltage (V)	3					
#3 Current (A)	2.4					
___ Oven Cont/Temp(°C)						
Voltage (V)						
Current (A)						
Substrate Cont/Temp(°C)	580					
Voltage (V)	16.3					
Current (A)	2.8					
Ionization Gauge (Torr)	3×10^{-7}					

After growth, the total thickness of the grown layers was measured using a step-profiler (profiling across a region partially masked by the substrate holder) and found to be 2.05 μm for one sample and 2.15 μm for the other. Since these were in excellent agreement with the 2.0 micron target thickness, the materials were processed for further tests. This processing consisted of forming ohmic contacts on both the substrate and epitaxial sides of the wafer. Six mil mesas were then formed on the epitaxial side allowing breakdown voltages to be measured. All devices showed sharp breakdown characteristics with voltages at 1 mA to be between 16.5 and 17.5 volts. The fact that these values compare well with calculations and measured breakdown voltages of devices with similar profiles was very encouraging.

Because of the close agreement in both thicknesses and breakdown voltages, this material was processed into IMPATTs using a procedure developed on a previous IMPATT program. This is a rather time consuming procedure involving several delicate steps.

Fabrication of diodes from epitaxial material consists of wafer thinning, metallization of both sides, and diode delineation by etching. Figure 3 shown the GaAs thickness and metalization scheme used at Georgia Tech. Gold plated heat sinks were chosen to optimize heat sinking and to facilitate possible thermocompression chip bonding.

Ohmic contacts to both sides of the material are required as shown. Contact to the p^+ layer is accomplished by an RF sputter deposited trimetal system of Pt-Ti-Au. The contact to the n^+ material is Au-Ge-Ni, Au evaporated to the thicknesses indicated and then alloyed at 440^0C for 20 seconds.

A flow chart of the complete fabrication procedure is shown in Figure 4. Many of these steps are standard; however several steps are unique to high frequency IMPATT processing and will be described below.

GaAs thinning to less than 10 μm is performed to minimize undercutting of the back contact. Thickness measurements requiring an accuracy on the order of 1 μm are difficult to make with conventional means. To facilitate this measurement, a dot pattern consisting of 7 mil diameter dots on 1/32 inch centers is delineated on the p side of the wafer. Holes are then etched 10 μm deep using methanol: hydrogen peroxide: phosphoric acid in the ratio 1:1:1. During the wafer thinning

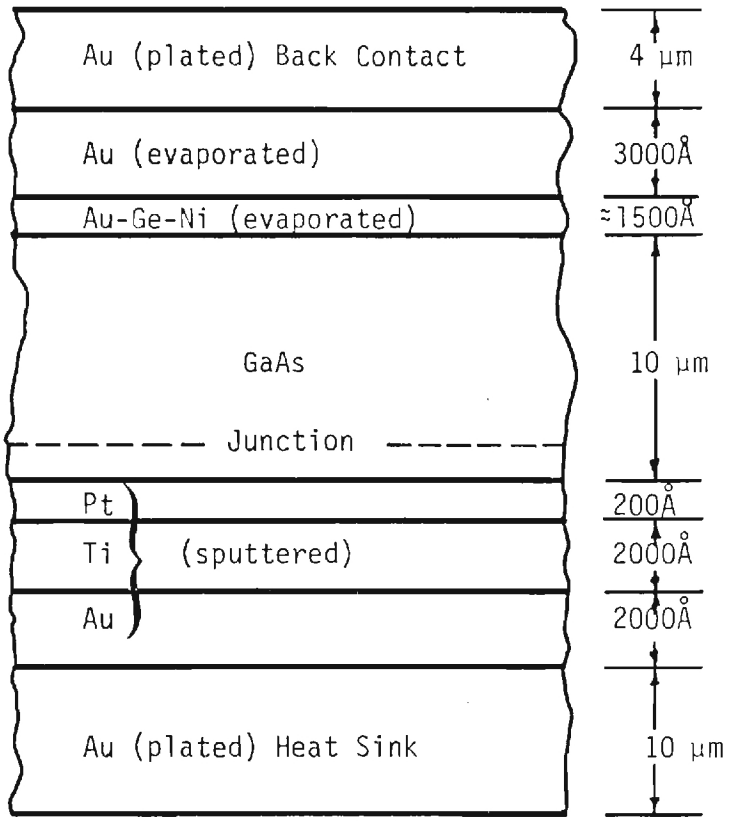

Figure 3. Material Structure for IMPATT Diodes

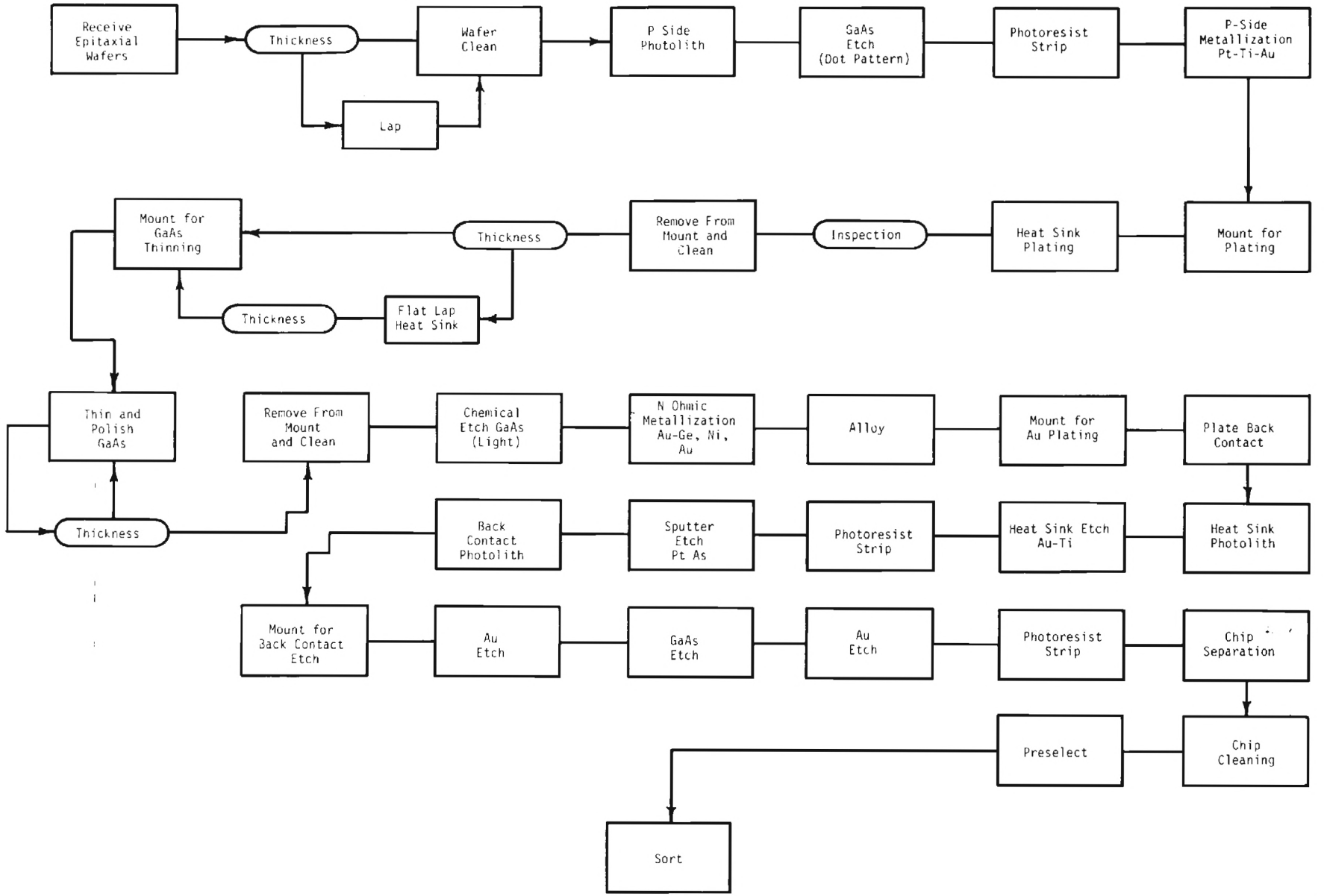

Figure 4. Process Flow Chart for Double Drift IMPATT Diodes

and polishing process, the appearance of the dots indicates completion of the process.

Target materials of 99.999% purity, mounted in a Perkin-Elmer, (model 2400) sputtering system were used to form the ohmic contact to the p^+ material. All targets were presputtered for 2 min at 500 watts prior to substrate metalization. Platinum was deposited for 1.5 min at 150 watts, titanium for 25 min at 500 watts, followed by gold for 4 min at 500 watts.

Gold plating to form the diode heat sink is the next processing step. Devices normally processed at Georgia Tech are typically greater than 1 mil in thickness. As a result, any stresses imposed on the GaAs by the plating have little effect on the mechanical stability of the wafer. With thicknesses less than 0.5 mil, thermal expansion-mismatches often cause severe warping of the wafer.

Periodic reverse current (PR) plating is a recognized procedure for reducing stress in plated layers. This procedure, which is used extensively in copper and silver plating, also has the reported advantages of substantial leveling of the base surface and improved uniformity on irregularly shaped samples (1). PR plating is a process wherein the plated layer is deplated during a periodic time interval which is short compared to the time interval in the forward direction. Although this procedure is common for silver and copper plating, literature concerning gold deposition by this method is limited. Reid and Goldie (2) indicate that PR plating of gold has been performed using a simple cyanide electrolyte with 25-40 g/l of gold and 10 g/l of free potassium cyanide at a temperature of 60-75^{o}C. Current density was specified at 1-15 mA/cm^2 with an anodic -to cathodic time ratio of 15:2. No actual plating and deplating times were given.

PR current plating requires a means of periodically exchanging the connections to the plating bath anode and cathode. Georgia Tech has developed a circuit which periodically reverses the anode and cathode potential and maintains desired forward and reverse plating currents.

Forward and reverse times were adjusted to 35 seconds and 5 seconds, respectively, while the forward and reverse current densities were maintained at 3 mA/cm^2 and 2.25 mA/cm^2. Plating rate was measured to be approximately 3.5 microns per hour.

After plating, the material was lapped and polished. Slices, 13 mils thick were mounted on a lapping fixture and thined to 4 mils using a Majur horizontal-action lapping machine. Further thinning to 10 microns was accomplished by a chemical mechanical operation utilizing a Beuhler polishing wheel saturated with a 1:4 Clorex-water etching solution. The appearance of the dot pattern indicates a final wafer thickness of 10 microns.

Figure 5 a scale drawing of the mesa structure and the heat sink arrangement used for this effort. The iron oxide mask set consists of two IMPATTs fabricated on a common 5 x 10 mil heat sink. Front to back alignment is accomplished by optically aligning the heat sink-defined material to the heat sink mask and then aligning that assembly to the back contact mask.

Figure 6 shows SEM photographs of an actual mesa after completion of the processing steps. The jagged material around the heat sink edge is thought to be platinum which was not sufficiently removed prior to device separation. In some instances, this material can curl up and place a short between the heat sink and top contact (notice left chip). Most of the chips, however, showed essentially the same breakdown characteristics after processing as they did before.

The IMPATTs are then seperated by clearing through the Au heat sink with a razor blade, stressed to 60 mA to eliminate those subject to premature burn out, and then mounted in an EHF micropill package. Contact is made to the top contact via a crossed wire connection. Each chip is then etched within the package until the overall capacitance is between .6 - .9 pF. The devices are then RF tested in a Ka band waveguide structure which basically consists of a post-mount in which the diode can be positioned across the guide or recessed within the waveguide floor, an adjustable back short, and an EH tuner positioned between the post-mounted diode and output port. Preliminary RF tests resulted in oscillations at 35 GHz.

The fact that these first diodes did oscillate within band,

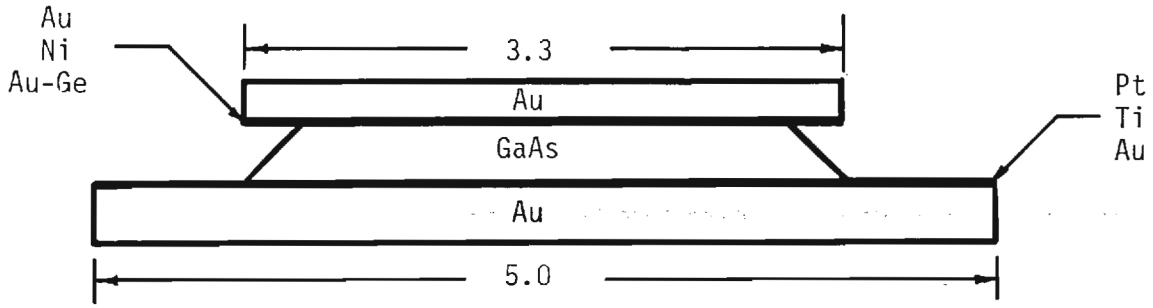

Dimensions in mils

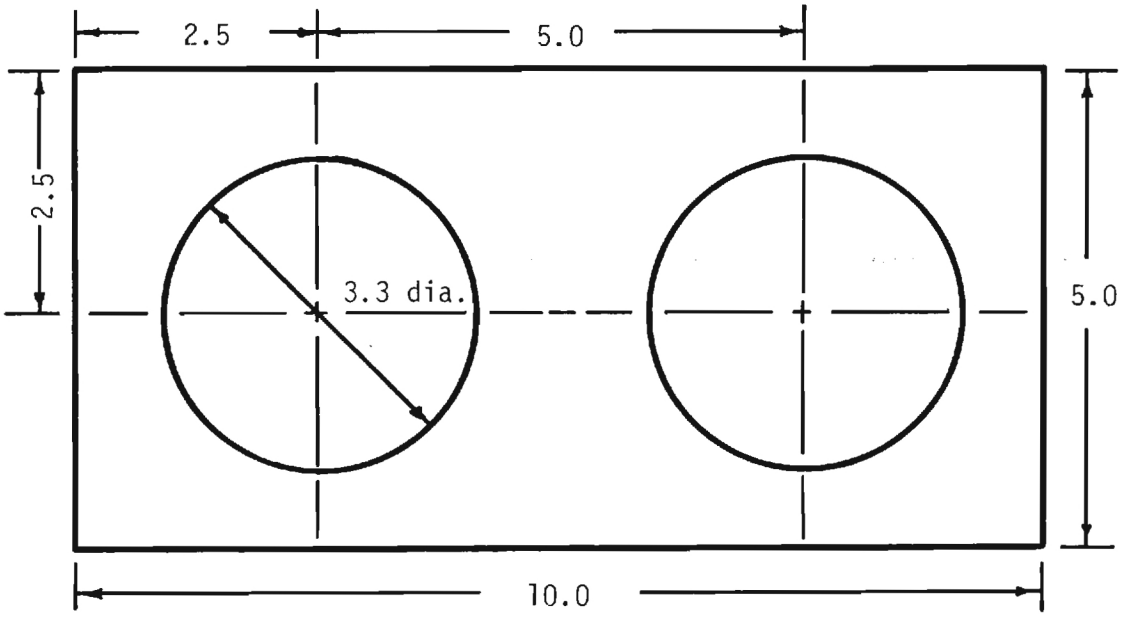

Figure 5. Mesa Structure and Heat Sink

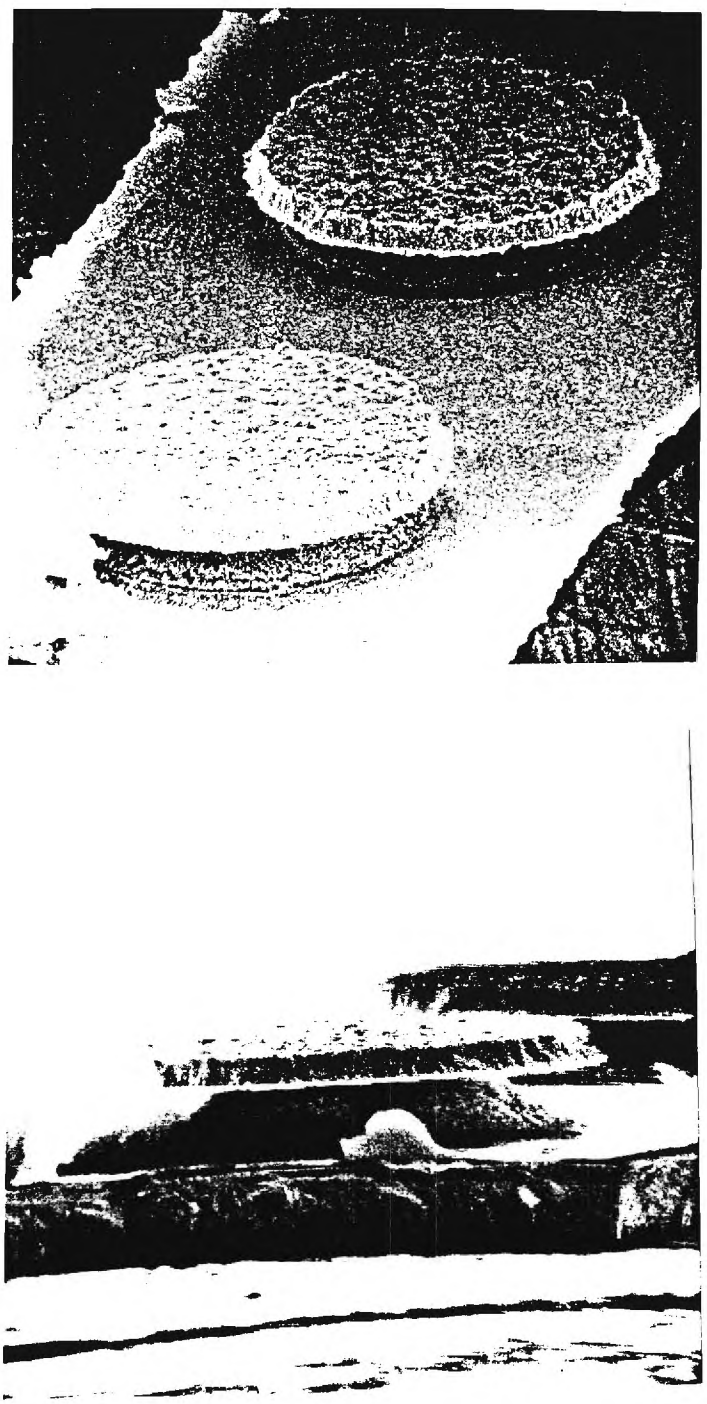

Figure 6. SEM photographs of IMPATT mesa.

although with low output power (40 mW), is very encouraging. Tests are continuing in an attempt to determine if the low power is due to non-optimized profile, poor heat sinking, or to increase in series resistance introduced in the processing procedure. Steps are also underway to fabricate the top contact in the form of crossed beam leads which can then be connected directly to the package.

Plans for Next Quarter

- o Continue growth and optimization of hybrid-Read material
- o Develop beam lead process
- o Continue processing and testing of IMPATT material.

REFERENCES

1. A. Kenneth Graham, Electroplating Engineering, Van Nostrand Reinhold, New York, 1971.

2. F. H. Reid and W. Goldie, Gold Plating Technology, Electrochemical Publications Limited, Scotland, 1974.

Man Hours

Categories		Cumulative Total
Principal Research Engineer/Scientist	13.0	13.0
Senior Research Engineer/Scientist	341.0	689.0
Research Engineer/Scientist	272.0	292.0
Assistant Research Engineer/ Scientist/Technologist	0.0	0.0
Graduate Research Assistant	0.0	0.0
Student Co-op	0.0	0.0
Total	626.0	994.0

Financial

Budgeted - $99.965.00
Expended - $46,808.72

Balance $53,156.28

Application of Molecular Beam Epitaxy to Millimeter Wave GaAs IMPATTs

Quarterly Report No. 5 & 6

J. W. Amoss, E. L. Meeks, and N. W. Cox

Engineering Experiment Station
Georgia Institute of Technology
Atlanta, Georgia 30332

10 July 1982
Report for Period 1 April 1982 - 30 September 1982
Contract No. N00014-81-K-2004

Prepared for

Naval Research Laboratory
Washington, D.C. 20375

INTRODUCTION

This report summarizes recent research directed toward the application of molecular beam epitaxy material to millimeter wave GaAs IMPATTs. The program is a one year effort to utilize MBE epitaxial growth techniques to produce improved and reproducible, highly efficient millimeter wave GaAs IMPATT devices. Specific tasks of the program are:

1) define initial target profiles for 40 GHz IMPATTs,
2) grow GaAs material to desired target profile,
3) determine actual profile,
4) evaluate RF performance,
6) simulate via computer model, and
7) exercise computer model to obtain new target profile and repeat steps 2-7.

Summary of Principal Results

A number of wafers were grown, processed, and RF tested as IMPATT devices during this reporting period. Most of the wafers were grown as hybrid-Read structures in which the p region was flat (uniformly doped) and the n region contained a spike approximately .15 microns from the p-n junctions. The most critical device parameter seems to be the position of the spike and the amount of charge contained therein. A series of structures was grown in which the spike position was fixed and the amount of charge varied. Based on the system calibration curves, the total charge contained within the spike was varied from 2.0×10^{12} cm^{-2} to $8.0 \times 10^{11} cm^{-2}$. This change resulted in an increase in output power from 41 mW to 135 mW. Other experiments indicate that the charge contained within the spike should be reduced further. These experiments also suggest that the system calibration may have changed. Attempts are being made to rectify these problems.

Another "unknown" in the material growth process is the abruptness of the transition between different doping levels and the "shape" of the spike when the source ovens are changed abruptly. Two samples of hybrid-Read material have been sent to two different material evaluation companies for analysis by SIMS.

Technical Discussions

The hybrid-Read structure initially grown and tested was the E0329-III wafer described in the previous quarterly report and whose target profile is reproduced in Figure 1. The spike of this structure contained approximately 2×10^{12} Coulombs cm^{-2} and was nominally .16 microns from the junction. These devices had very sharp breakdown characteristics with breakdown voltages between 17.5 - 18.5 volts at 1 mA. The maximum output power obtained was about 20 mW when biased to approximately 200 mA. As stated previously, the E0329-III MBE grown profile was based on material previously grown by others using CVD epi-reactors and which nominally delivered 1.5 watts at 35 GHz with an efficiency of 15%. The breakdown voltages of the E0329-III MBE material and the CVD devices on which it was based are in good agreement yet the output powers differed by orders of magnitude.

Measurements were made in an attempt to determine the reasons for the vast difference in output power between the devices. Figure 2 shows the composite profiles of two Georgia Tech (GT) MBE devices and two CVD devices on which the GT profile was based. Also shown is a theoretical composite profile based on a rectilinear profile of Figure 1. It should be kept in mind that the impurity concentration shown is an effective value which is related to the impurity concentration on boh sides of the junction by $1/N_{eff} = 1/N_A + 1/N_D$ and the depth is the total distance

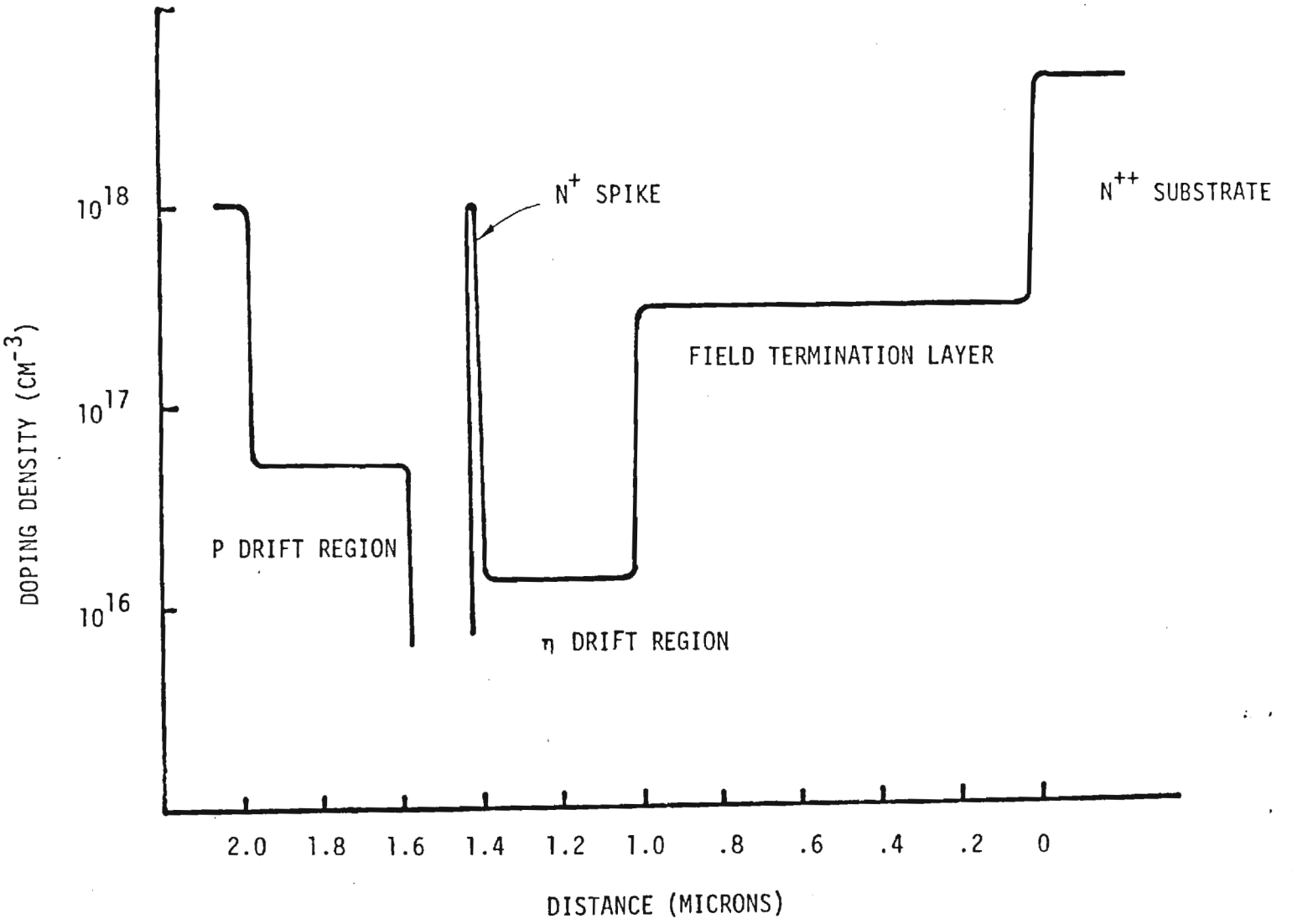

Figure 1. E0329-III Target Structure.

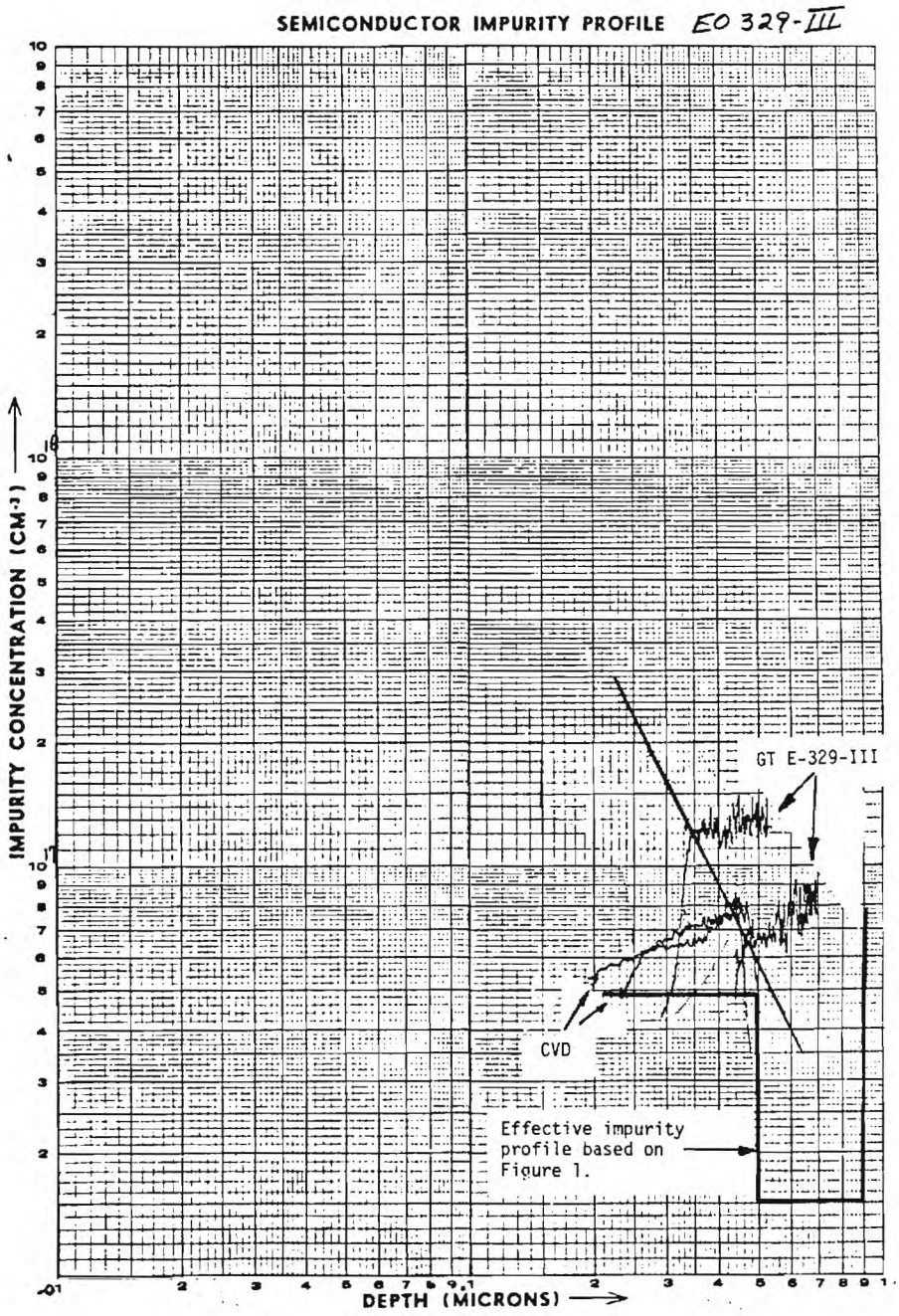

Figure 2. EO329-III Measured profile, CVD Measured profile, and calculated profile of target structure.

depleted on both sides of the junction. The accuracy of a profile measurement depends upon accurately knowing the device area. Since measured or calculated impurity concentration is inversly proportioalnal to the square of the area and the depth is directly proportional to the area, any error in device area will shift the measured profile along a line with slope of -2. Since the one of the Georgia Tech profiles shifted along a line with slope of -2 coincides with the other profile, the profile of the two devices (impurity concentration and depth) are probably very similar and the indicated difference is more likely a difference in their areas. All four devices had been etched in the package which prevented an accurate determination of device area. If the lower GT profile were shifted up to the higher one, all four devices would show essentially the same depth relationship but with significant differences between impurity concentrations. The zero bias depletion edge does not extend into the spike for the MBE grown material whereas it appears to extend into this region for the CVD material. For most of the profile (near horizontal portion), one depletion edge moves through the uniformly doped p region and the other edge moves through the highly doped spike region. For the CVD grown device the depletion edge moves out of the spike region and into the n-type drift region for an applied bias of about 14 volts. For the MBE grown device, the depletion edge remains in the spike region even up to the breakdown voltage of about 18 volts.

These differences in performance are thought to be due to excess charge contained between the junction and spike-drift interface region. Decreasing this charge (decreasing the impurity concentration) would result in a smaller change in electric field in this region and deplete more of the n-type drift region. That portion of the drift region not

depleted would introduce loss and consequently decrease output power and efficiency. This could possibly explain a difference in output power capability between the two devices.

There was also a significant difference in the dc bias capability of the two devices. The MBE grown chips burned out at about 200 mA bias whereas the CVD chips fabricated at Raytheon would withstand bias currents typically greater than 600 mA. Figure 3 compares the reverse I-V characteristics of these devices. The slope of the I-V curve is equal to $1/R_{TH} + 1/R_{SC}$ where R_{TH} is the thermal resistance and R_{SC} is the space charge resistance. Note that the slopes of the I-V curves for the MBE devices are equal to or greater than those for the CVD devices. Although not conclusive, this test indicates that the MBE devices are heat sunk as well as the CVD devices. More tests will have to be devised to determine why the MBE devices are susceptable to burnout at about 200 mA. This low burn out level has been observed with all MBE devices processed to date.

A single drift structure (E0401-III) was grown having the same doping profile as the n-side of wafer E0329-III. Measured profiles of chips from this material are shown in Figure 5. Again a rectilinear plot of the idealized target profile is shown for comparison. The actual profiles shown (not the same chip) were measured on an automatic profiler and on a C-V bridge. There is an obvious discrepancy in the measured drift width (.15 to .20 microns) and the desired drift width (.40 microns). At the time the measurements were made, it was thought that the discrepancy was due to premature or soft breakdown characteristics of the Schottky junctions since the sample measured on the automatic profiler did have a softer breakdown than the other

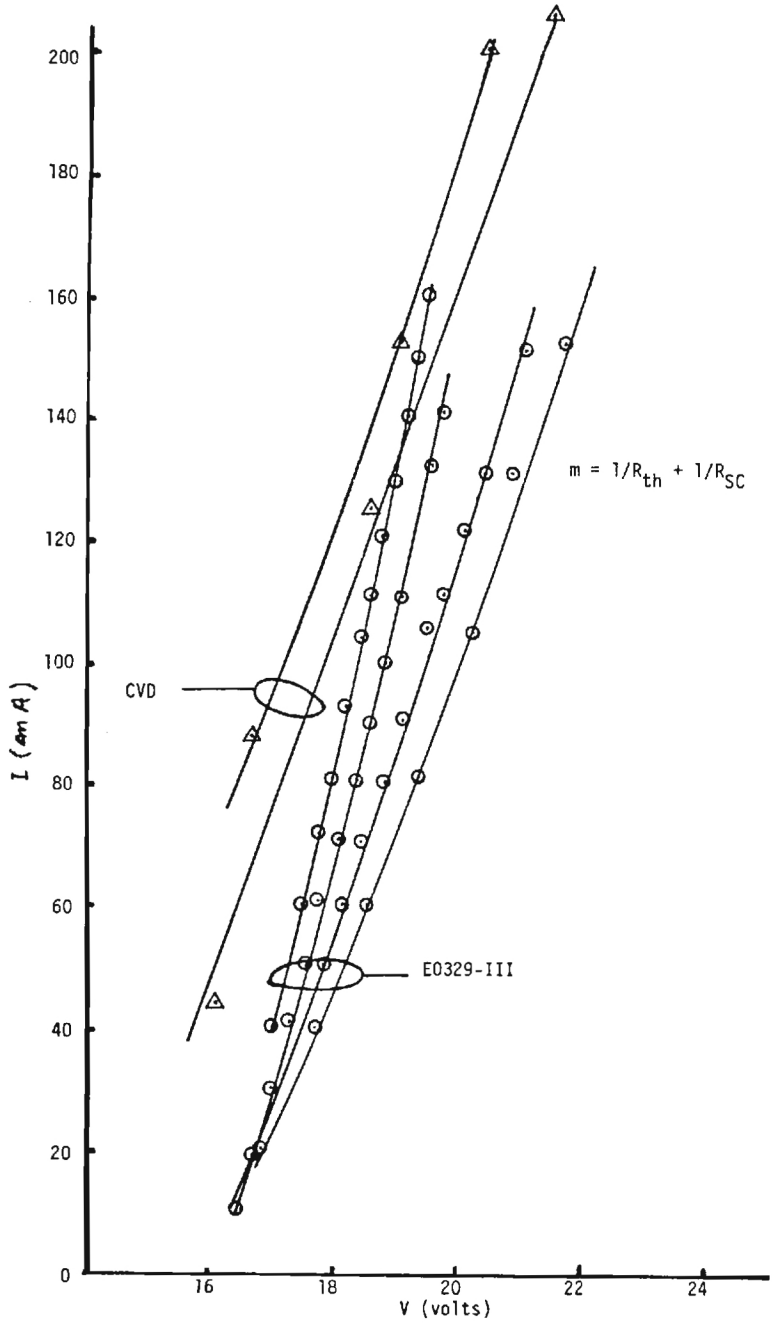

Figure 3. I-V Characteristics of E0329-III and CVD Devices.

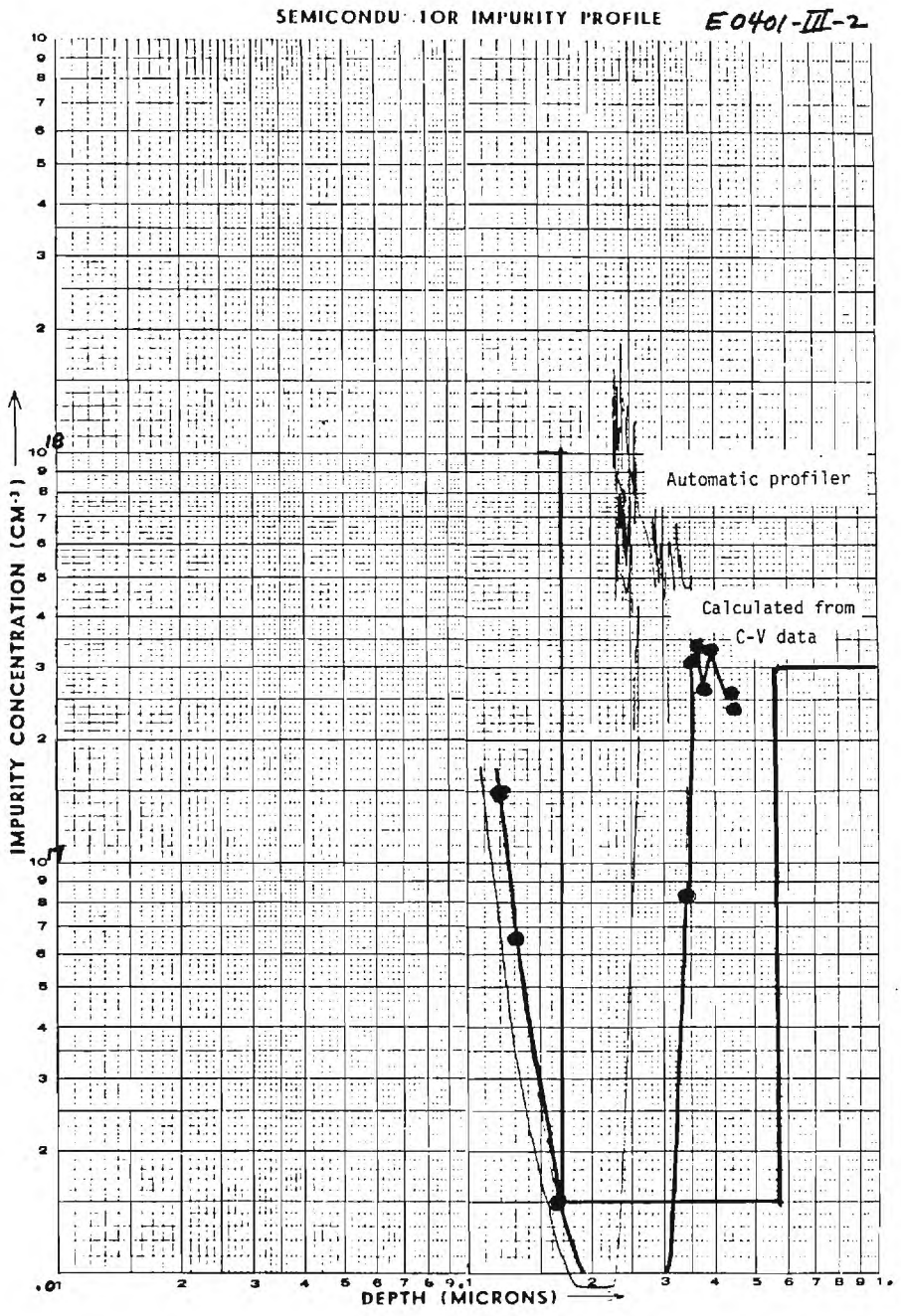

Figure 4. E0401-III-2 Measured profiles and calculated profile of target structure.

sample. The cluster of points about the doping of the field termination layer (3×10^{17}) displaced approximately .2 microns (12 min growth time) is not understood. It is not likely due to an uncertainty in device area nor is it likely due to a delay in source temperature. No devices were processed from this material. It was grown mainly as a check on the growth of the n-type region of E0329-III.

The next double drift IMPATT materials (E0511-III and E0512-III) grown were similar to the E0329-III except that the peak impurity concentration in the spike was decreased from 1×10^{18} to $.8 \times 10^{18}$, the impurity concentration in the p-drift region was increased to 8×10^{16}, and the doping between junction and spike was increased to 6×10^{16}. The measured impurity concentration versus depth for this material is shown in Figure 5. Also shown for comparison is a calculated profile based on an ideal rectilinear model. Note that the spike is still not depleted. The effective impurity concentration during the spike "sweep out" should be slightly lower than the doping in the p-region. This profile and the preceeding one suggests that the p-type doping may already be larger than that intended.

Material E0512-III was processed and tested as IMPATTs. One device yielded an output power to 41 mw at 34.6 GHz when biased to 235 mA. All of the other devices tested burned out at current levels less than 235 mA with output powers in the 25-30 mW range.

Since most of the profile measurements and RF tests performed at this point suggested that the n-type drift region may not be depleting prior to breakdown, the spike width was decreased to 100A (the growth time for the spike was halved) for the next growth run. In other respects this device was similar to E0512-III. Several devices from

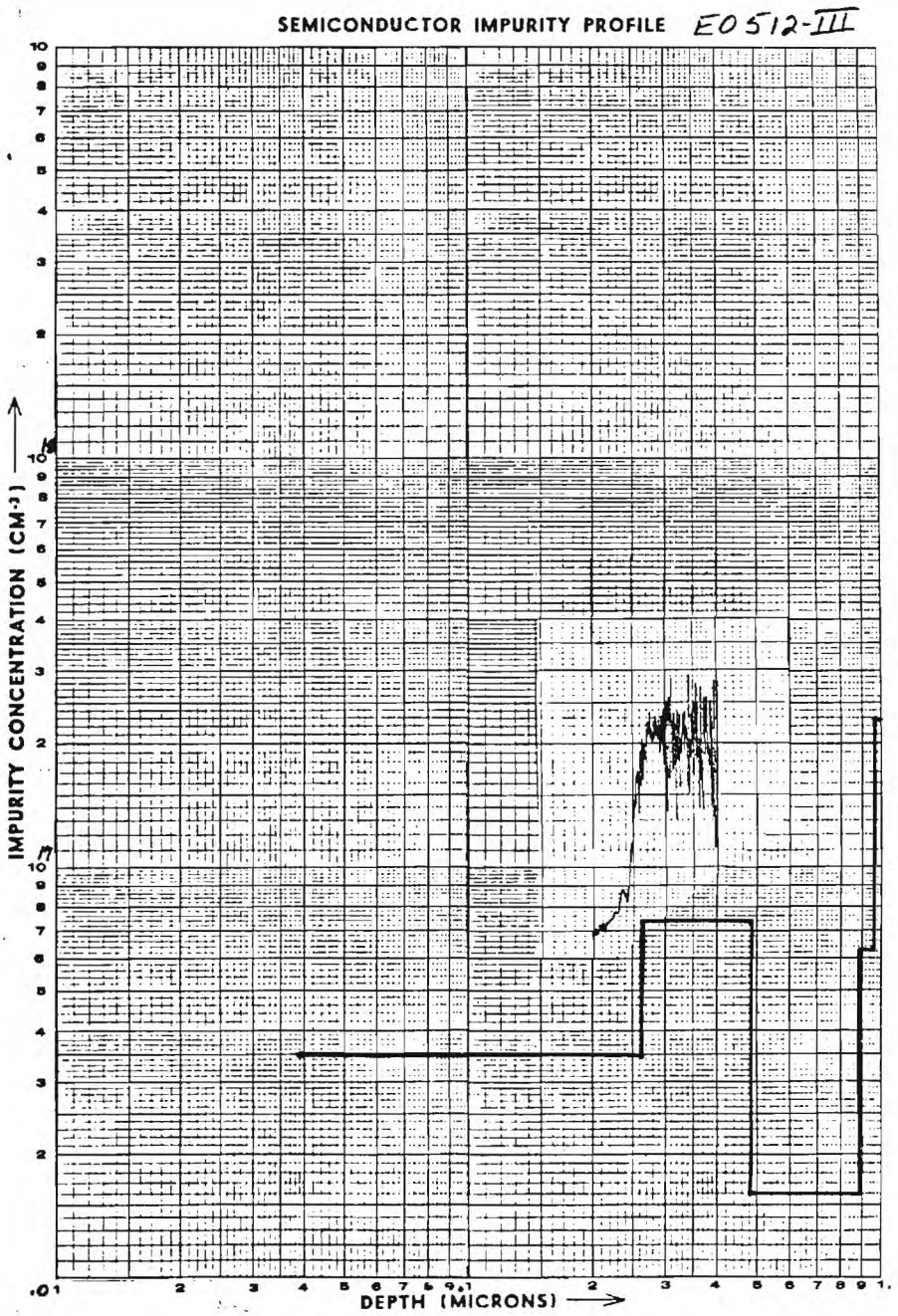

Figure 5. E0512-III measured profile and calculated profile of target structure.

this run oscillated at 36 GHz with output powers between 100 and 140 mw. Again, however, the diodes burned out at current levels less than 250 mA.

The last growth run during this quarter completely eliminated the spike. The structure was a double drift flat-flat profile in which the impurity concentrations and the depths of both type materials were choosen to be fully depleted at a peak electric field of 5.0×10^5 V/cm. Each region was doped to $7 \times 10^{16} cm^{-3}$ over a distance of $.5 \times 10^{-4} cm$. Although this structure was grown primarily to check the system calibration, the material was processed and tested as IMPATTs. Maximum output power obtained with these devices was 21 mW at dc bias currents up to 219 mA. The devices operated at about 31 GHz. All devices tested burned out at current levels less than 219 mA.

As stated, the flat profile double drift devices were grown primarily to check system calibration. Since both p and n-type impurity concentrations were to be 7×10^{16} cm^{-3}, the effective concentration should measure 3.5×10^{16} cm^{-3} and the total depletion depth should measure 1.0×10^{-4} cm prior to breakdown.

The results of this experiment are shown in Figure 6. The idealized profile (based on abrupt transitions) is designated as I, the effective impurity concentration measured on this devices is designated as A, and the "best fit" idealized profile is designated as III. An idealized rectlitinear impurity concentration which would give this best fit effective profile is shown on Figure 7 as II. It should be mentioned here that a measured effective profile of a double drift device is not uniquely related to only one set of p and n-type profiles. There is an infinite set of p- and n-type profiles that will give the

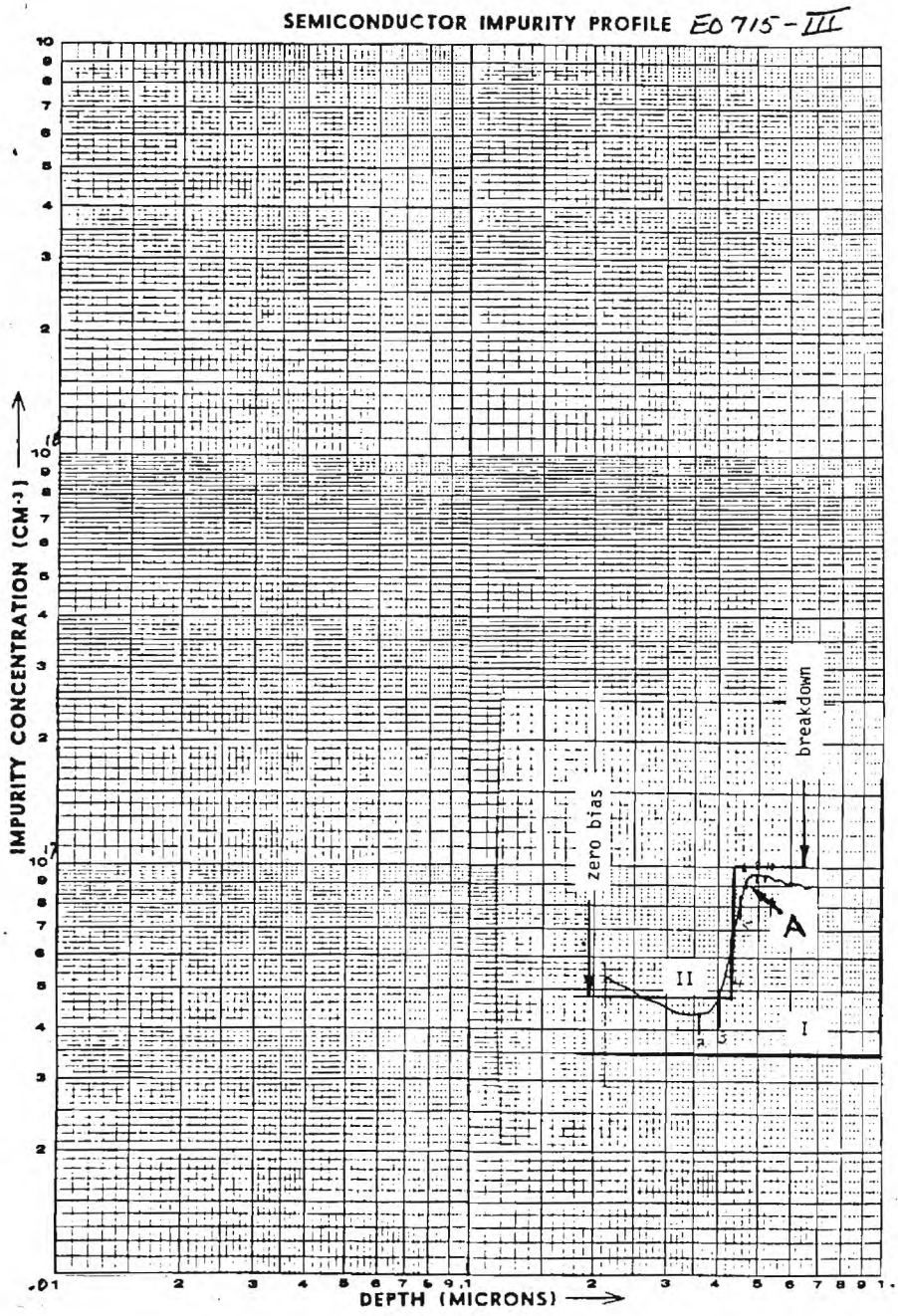

Figure 6. E0715-III measured profile, calculated profile of target structure (I), and calculated "best fit" profile.

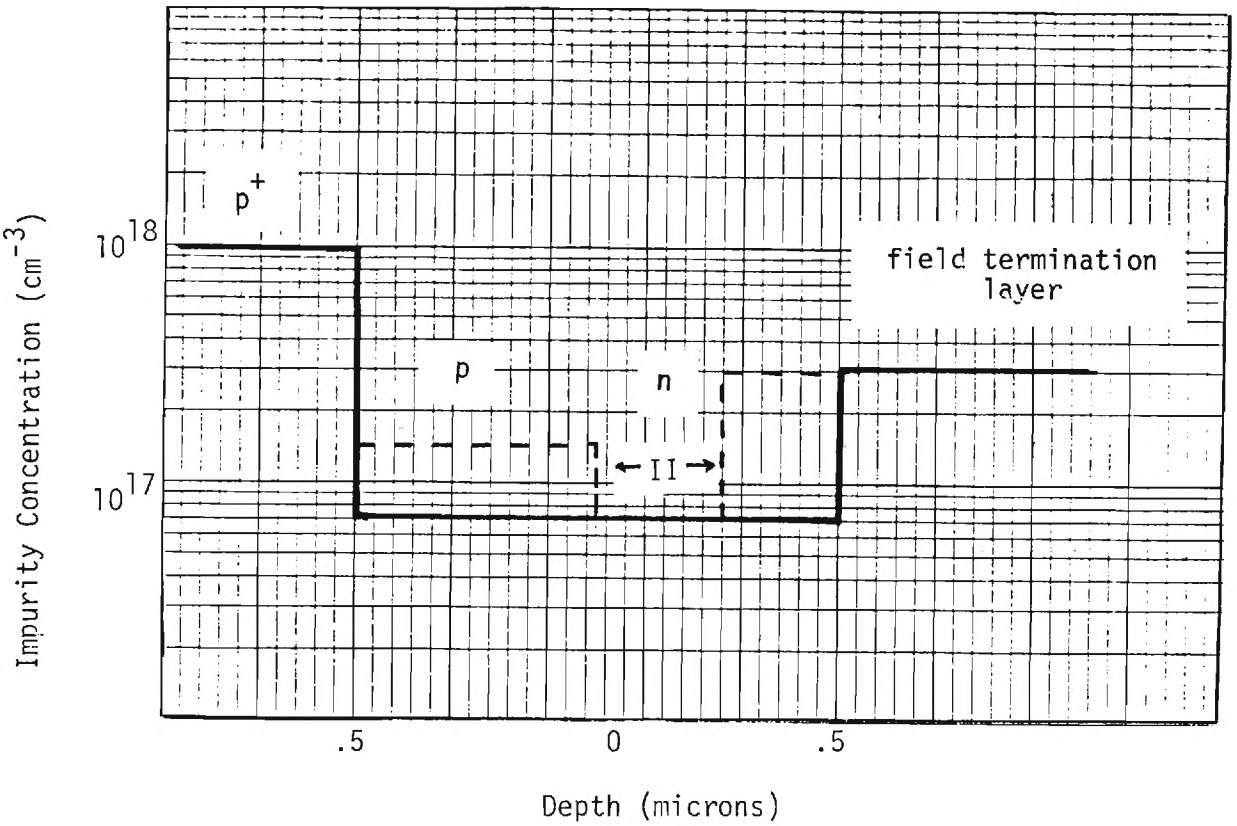

Figure 7. E-715-III Target structure and deviation for "best fit" (- - -).

same effective profile. Profile II of Figure 7 was choosen to be consistent with the deviations mentioned previously, i.e., the actual p-type doping is higher than that intended (Figure 2, 5 and 6) and the the field termination layer extends into the n-type drift region (Figure 4, 6 and 7).

Samples from material E0329-III were sent to Raytheon, who is known to be one of the leaders in the area of double-drift GaAs IMPATT devices, for the purpose of analyzing the impurity concentration. This company has devoted considerable effort and funds to set up an automated digital profilometer which is controlled by an Intel 8080 microprocessor-based digital computer. The measurements entails step-etching the structure, forming Schottky junctions at each step, and calculating impurity concentration from C-V measurements. The results of this analysis is shown in figure 8 along with the idealized rectilinear profile.

The first measurement was made with the Schottky placed on the p^+ contact layer (XI = 0). The zero bias depletion width was XO = 0.104 microns which allowed the impurity concentration of part of the p^+p transistion layer to be obtained (curve 1). After etching .200 microns, the zero bias depletion edge extended through the p-n junction making any conclusions from the data therby obtained subject to error (curve 2). The second etch (.400 microns from original surface) was close to the junction and identified as n-type material. From there the zero bias depletion edge extended to .291 microns where the results of C-V data reduction indicated a relatively high impurity concentration (curve 3) approximately .1 micron further into the n-drift region than where the spike was thought to be. The fifth etch went to .7 microns and showed a zero bias depletion depth of .207 microns. C-V data indicated

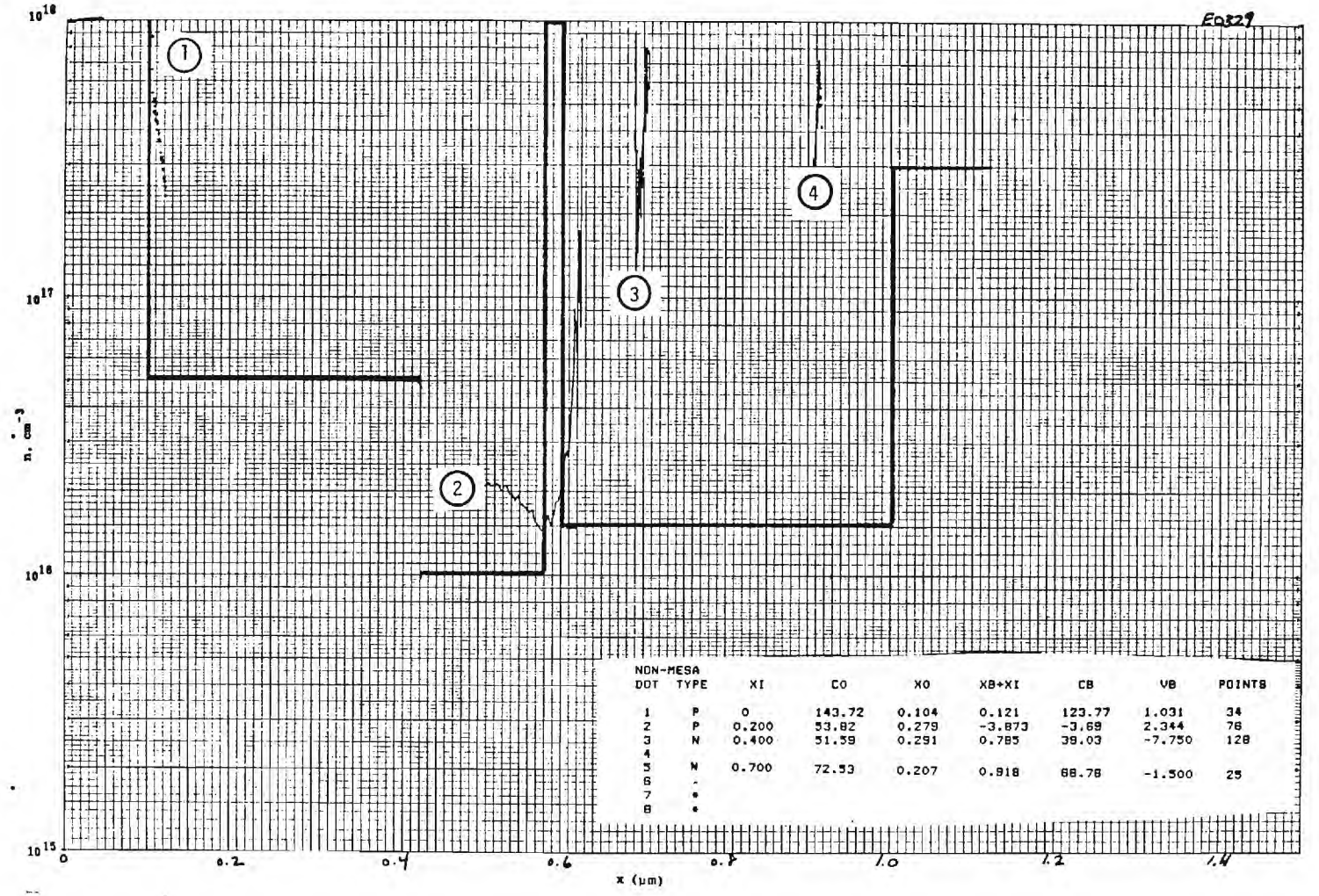

Figure 8. E0329-III measured profiles at selected etch depths.

an abrupt interface at this position of relatively high doping. This is thought to be the interface between the n-drift region and the field termination layer. The drift termination interface seems to be displaced into the drift region by about .1 micron consistent with Figures 4 and 6.

Figure 8 shows the composite or effective impurity concentration measured by Raytheon. The near horizontal trace is thought to result when one edge of the depletion remains in the highly doped spike while the other edge sweeps through the p-type drift layer. The deduced p-type impurity concentration from this plot is more consistent with the growth target of 5×10^{16} cm^{-3} but is not consistent with an actual higher impurity concentration implied from Figure 2, 4 and 6.

Conclusions

At the outset of the program, an accurate evaluation of the impurity concentration profile after growth was recognized as a critial task in millimeter wave IMPATT development. Setting up an automated computer controlled system to more efficiently and accurately obtain these profiles was beyond the scope of the present program.* Rather than resorting to such equipment we were planning to make use of the precise control and reproducibility of MBE GaAs growth and interpret the measured effective impurity concentration via calculated effective impurity concentrations. Although this method has been partially successful, it depends on the system being precisely calibrated. Considerable scatter was present in the data of the initial calibration runs. Efforts are underway to decrease the uncertainly in the system calibration curves.

---

*Georgia Tech is now in the process of including such capabilities in a new comprehensive semiconductor materials measurements laboratory.

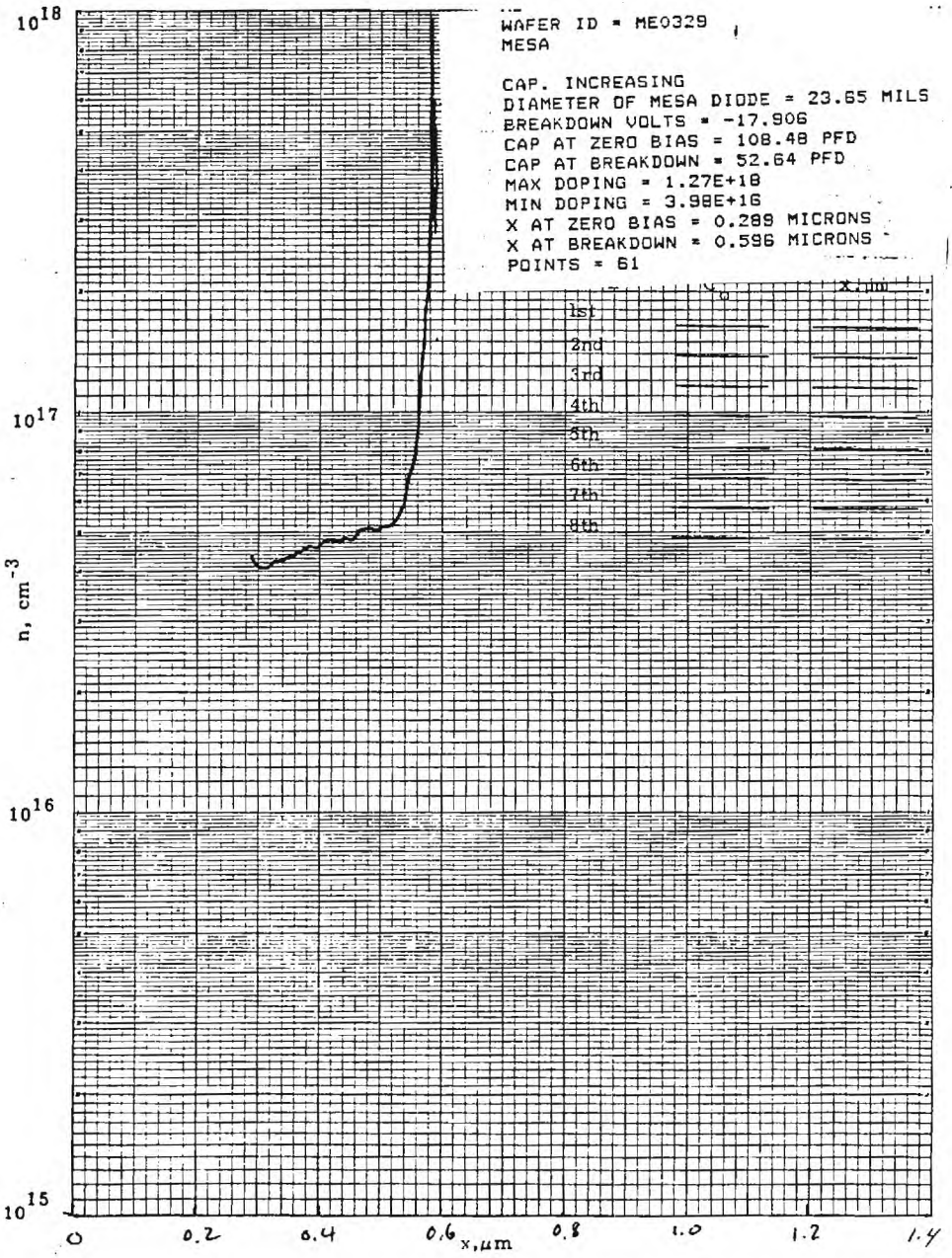

Figure 9. E0329-III measured effective profile of composite material.

All measurements made thus far indicate that excess charge is contained between the junction and the spike-drift interface. Whether too much charge is within the spike or too much within the tail of the spike can not be determined. The next hybrid-Read structure will place a 100A spike closer to the junction, thereby eliminating some of the charge contained within this region. Decreasing the charge between the junction and spike will, hopefully, cause the n-type drift region to become depleted.

Plans for Next Quarter

- Recheck calibration of system
- Continue growth and optimization of hybrid-Read material
- Continue processing and testing of IMPATT devices.

Man Hours

Categories		Cumulative Total
Principal Research Engineer/Scientist	25.6	38.6
Senior Research Engineer/Scientist	704.0	1393.0
Research Engineer/Scientist	176.3	468.3
Assistant Research Engineer/ Scientist/Technologist	0.0	0.0
Graduate Research Assistant	0.0	0.0
Student Co-op	0.0	0.0
Total	905.9	1899.9

Financial*

Budgeted - $99,965.00
Expended - $82,840.40
Balance $17,124.60

*Includes charges through August.

APPLICATION OF MOLECULAR BEAM EPITAXY TO MILLIMETER WAVE GaAs IMPATTs

Quarterly Report No.7 & 8

J. W. Amoss, E. L. Meeks, and N. W. Cox

Engineering Experiment Station
Georgia Institute of Technology
Atlanta, Georgia 30332

10 April 1983

Report for Period 1 August 1982 - 31 March 1983
Contract No. N00014-81-K-2004

Prepared for

Naval Research Laboratory
Washington, D.C. 20375

INTRODUCTION

This report summarizes recent research directed toward the application of molecular beam epitaxy material to millimeter wave GaAs IMPATTs. The program is a one year effort to utilize MBE epitaxial growth techniques to produce improved and reproducible, highly efficient millimeter wave GaAs IMPATT devices. Specific tasks of the program are:

1) define initial target profiles for 40 GHz IMPATTs,
2) grow GaAs material to desired target profile,
3) determine actual profile
4) evalute RF performance,
6) simulate via computer model, and
7) exercise computer model to obtain new target profile and repeat steps 2-7.

Summary of Principal Results

The power level of the devices produced on this program to date has been disappointing. Changes in the doping profile, position of the impurity spike, and charge content of the spike have made little difference on device performance. Rather than continue processing devices in the shadow of the continued disappointing performance, it was decided to discontinue device work and concentrate on material evaluation.

Material from one of the early double drift IMPATT runs was sent to Charles Evans and Associates for evaluation of the SI and Be impurity concentration profiles. When this data was returned it was immediately obvious from the Be profile that the

Ga source was contaminated with Be. The level of contamination was such that the Ga source was contributing 1.2×10^{17} cm^{-3} Be doping at all times during growth. All materials grown on the program after May 12 were certainly similarly contaminated. Also, since it is not known how or when the contamination occured, probably all the layers grown for this program were contaiminated.

The Ga and SI sources were removed, cleaned and replaced, and the Be source was moved to a position less likely to cause contamination of the Ga source. After cleanup a calibration layer was grown and sent for a second SIMS analysis of the Be and SI concentration profiles. The second SIMS profiles showed no Be doping from the Ga souce but the doping level was 50 to 100 times higher at the same Be source temperature as the previous SIMS data and the previous C-V and Hall data. No explanation for the discrepancy can be given at this time.

The SIMS data for both samples show excellent control of the SI impurity level, excellent control of the layer thickness, and very sharp interfaces between layers. The control is such as to inspire confidence that good double drift IMPATT layers can be grown with the Ga Tech MBE system.

The unfortunate contamination of the Ga source has obviously delayed progress on this program greatly but may be turned into an advantage if full control of the Be doping level with the elemental souce remains elusive. According to the SIMS data the contaminated Ga source produced a constant $1.2 \times 10^{17} cm^{-3}$ Be doping. Thus the introduction of a second Ga source deliberately contaminated with Be may be the answer to the Be doping control.

Further work on the program will be to: resolve if posible the discrepancy in the SIMS data for Be doping profile to grow new double-drift IMPATT layers and to test devices made from this new material. If the power obtained from the new devices is still poor, single drift devices will be made to evaluate the device processing procedures.

Technical Discussions

Figure 1 shows the SIMS depth profile for Si and Be as obtained on sample E0512-III. The SIMS analyst claims an uncertainty of 7% in depth and a factor of two in concentration. For comparison, the target profile is drawn on the experimental data. For one familar with MBE growth procedures, it is immediately obvious from the data in figure 1 that the Ga source is contributing a Be doping of 1.2×10^{17} cm^{-3}.

The growth rate of GaAs MBE is determined by the Ga flux. Thus, for precise control of layer thickness and doping concentration the Ga flux is calibrated before the start of each run. An ion gauge placed 1-2 cm behind the sample growth position is used to measure the Ga and As flux before the sample is introduced. Precise control of the flux is obtained by adjusting the source temperature until the desired pressure change is observed when the source shutter is opened and closed. After calibration, the Ga temperature is reduced $50^{o}C$ and held until the As flux is calibrated and growth is initiated. A full As flux is always used when the substrates are heated to temperature, and growth is initiated by opening the Ga source shutter and increasing the temperature to the calibrated set point. This

procedure is necessary in order to avoid an initial high Ga flux that occurs when the shutter is opened and the source has been held closed at the calibrated temperature for more than 30-40 seconds. It also avoids excess Ga deposit on the back of the shutter which can drop off and contaminate the heater coils.

At position A marked in figure 1 the increase in Be doping corresponding to the increase in Ga temperature when growth is initiated can be seen. This is the obvious indication of Ga source contamination. The only other action taken at this time during growth is the opening of the Si source shutter and when the temperature of the Si source is changed at latter times during growth no corresponding change in Be doping is observed.

Positions A on the Be curve and B on the Si curve in figure 1 must necessarily be at the same depth in the layer at any one position on the sample since both indicate the start of the growth. The depth discrepancy may be due to the fact that the profiles where taken at different positions on the sample. In any case it is within the 7% uncertainty. There is good agreement between the experimental data and the target profile for Si. The field termination layer at C in figure 1 is low but within the concentration uncertainly quoted by the SIMS analyst. The doping level, thickness of the drift region and the position of the spike are excellent. If the target profile is correct, a single drift device with identical Si profile should perform very well. There is a gradual increase in Si doping from 0.7 μm depth to the surface that would be disturbing since the Si source is closed and off during this growth but no such effect is seen in the

second SIMS profile.

In order to correct the problems discussed above, the Si and Ga source materials were dumped and the empty ovens baked out at 1400°C in a separate vacuum system. Also, the Be oven was moved to a position less likely to cause contamination problems. After replacing the source ovens and refilling them with new materials, a calibration layer was grown specifically for SIMS analysis.

The Si depth profile for the calibration run is shown in figure 2 and again the Si data shows excellent control. The target concentrations and layer thicknesses are very close and the background concentration is 3-5 x 10^{15} cm^{-3} when doping at 10^{17} cm^{-3} or less. When doping at 10^{18} cm^{-3} the background level is an order of magnitude higher. In both cases the Si background may possibly be reduced by changing from water cooling to LN_2 cooling in the source shroud.

The SIMS profile for Be in the calibration layer is shown in figure 3. The Be level is 50 to 100 times higher than the target profile, reaching a maximum of 2 x 10^{19} cm^{-3} near the surface. It is encouraging to know doping of this magnitude can be achieved with Be since it should facilitate the fabrication of ohmic contacts to p-type materials. However, the data in figure 3 are also 50-100 times higher than the data in figure 1 and the data obtained by Hall and C/V measurements at identical source temperatures. No explanation can be given at this time for the discrepancy in the data for Be in the calibration layer.

Further work on the program will proceed with the growth of several Be doped layers which will be evaluated for doping

concentration by C/V measurements. If these runs exhibit the necessary control of the Be concentration, layers will be grown for double drift IMPATT devices. If control of the elemental Be source remains a problem it may be necesary to add a Ga source deliberately contaminated with Be. According to Hansen[1], Ga will dissolve 4 PPM Be which is enough to dope to a level of about $10^{17}cm^{-3}$. This agrees well with the observed level of Be doping from the contaminated Ga source. P-type layers could be grown with the Be contaminated source and n-type layers with the pure source. Some measure of impurity control would be afforded by using both Ga sourcse and changing the ratio of their individual contributions. Highly doped surface layers could still be achieved for ohmic contacts by using the elemental Be source since precise control is not important in this application.

Conclusion

It is easy to understand the poor device performance obtained thus far. The profile shown in figure 1 shows three p-n junctions because of the added Be from the Ga source. What was supposed to be the n-type drift region is p-type and the n^+ spike is in a p-type region causing two p-n junctions. If the other layers grown were similarly contaminated it is surprising that the devices functioned at all. It is also clear that interpretation of C/V data would not likely lead to the correct impurity profile.

The capability and applicability of SIMS to this work is impressive. Continuation of the work on this program should certainly include SIMS analysis as an early standard procedure.

[1] Hansen, Constitution of Binary Alloys.

The control of the Si doping profile that can be otained with MBE is also impressive. When the same control of the p-type dopant can be exhibited, material for double drift IMPATT devices should be easily achieved.

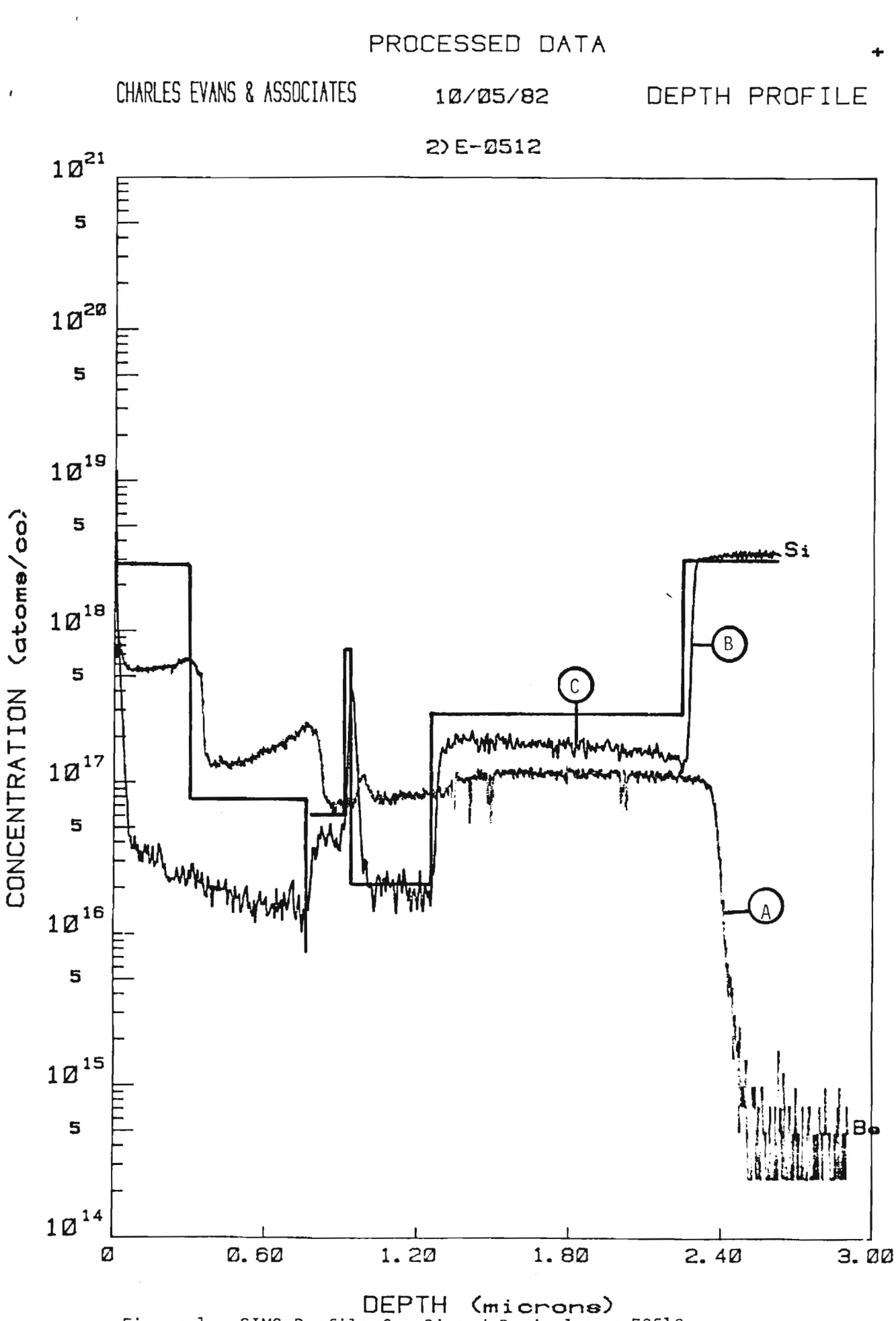

Figure 1. SIMS Profile for Si and Be in layer E0512.

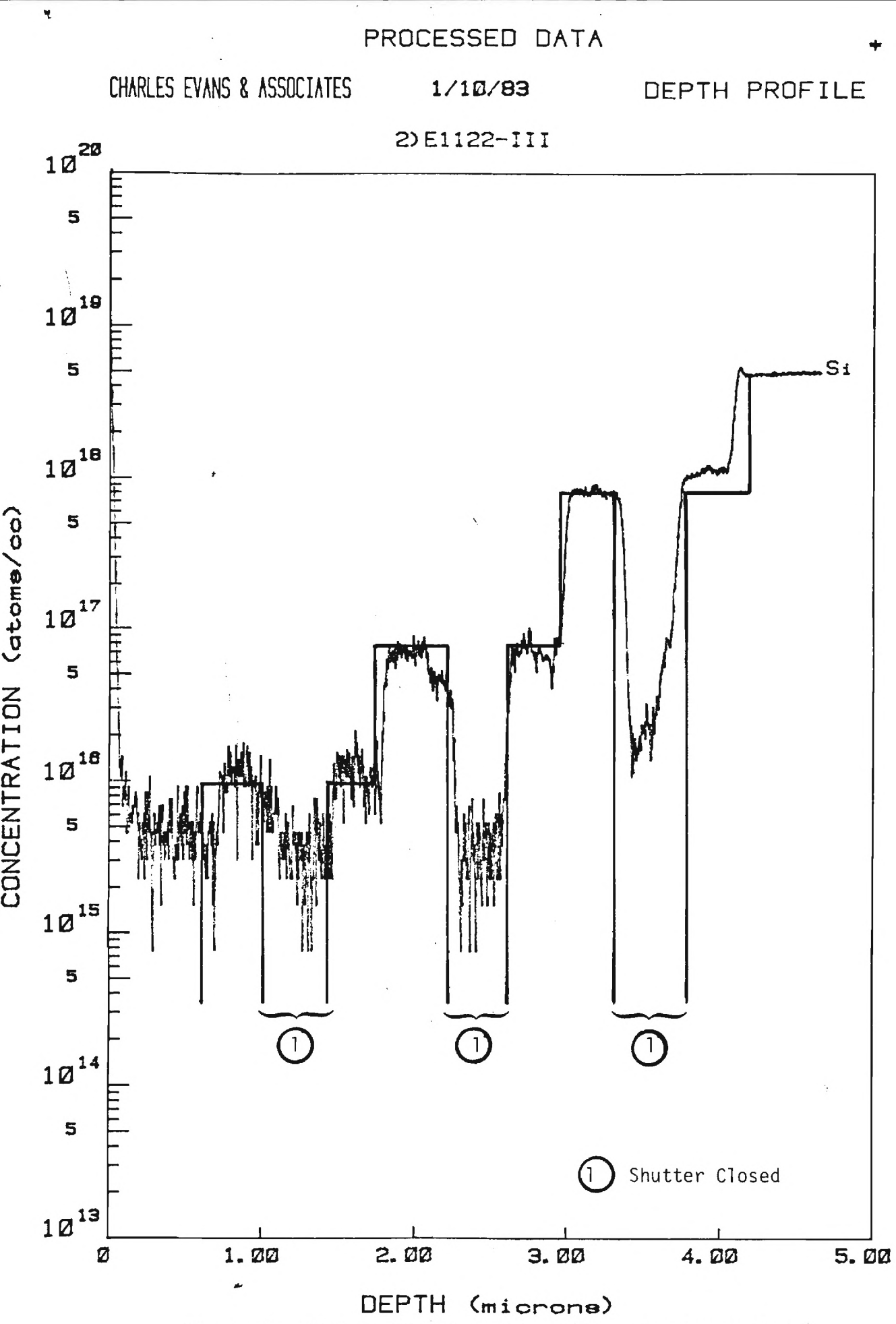

Figure 2. SIMS Profile for Si in calibration layer E1122.

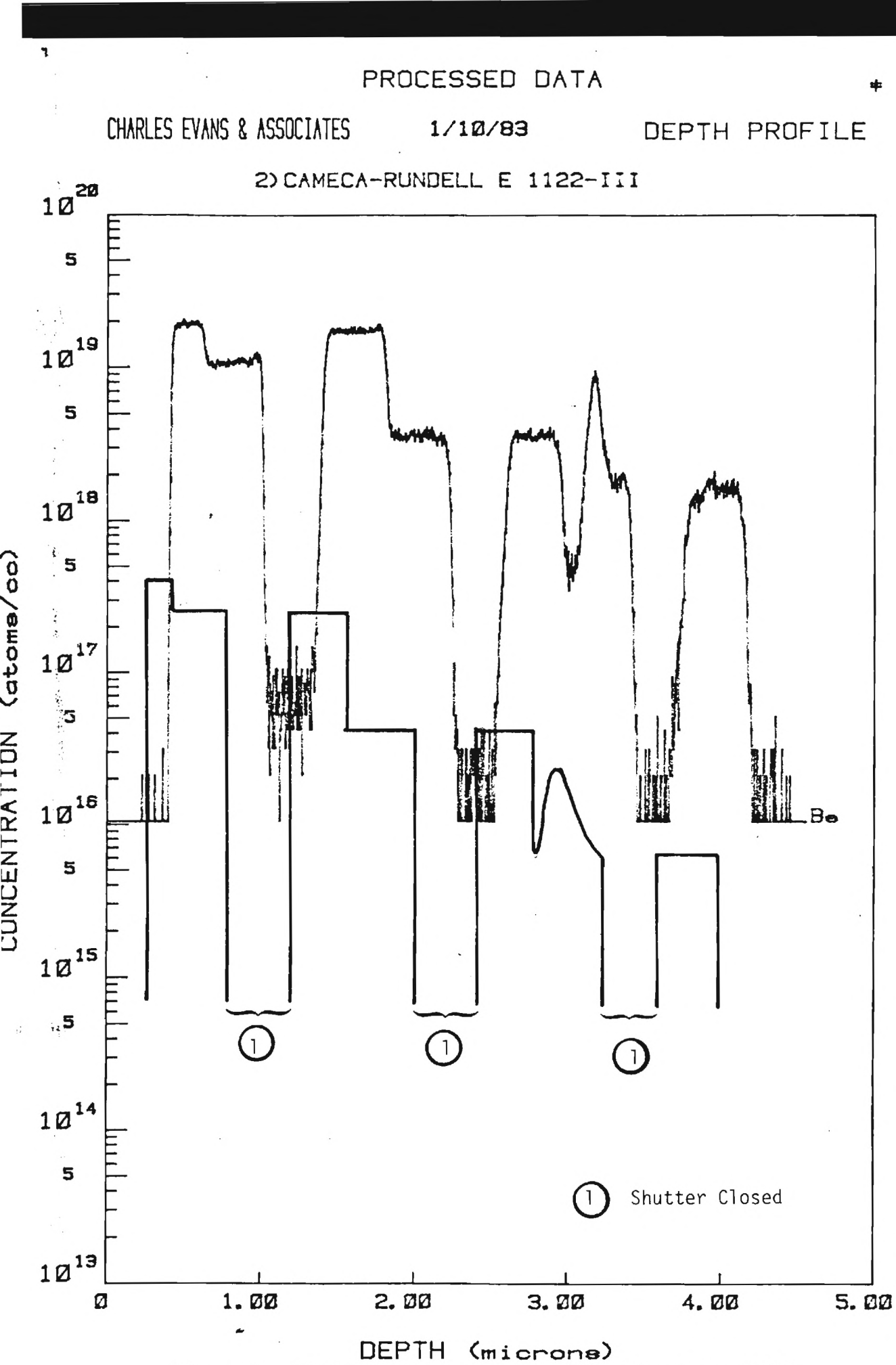

Figure 3. SIMS Profile for Be in calibration layer E1122.

Man Hours

Categories		Cumulative Total
Principal Research Engineer/Scientist	1.6	39.2
Senior Research Engineer/Scientist	211.2	1604.2
Research Engineer/Scientist	100.8	569.1
Assistant Research Engineer/ Scientist/Technologist	0.0	0.0
Graduate Research Assistant	0.0	0.0
Student Co-op	0.0	0.0
Total	313.6	2212.5

Financial*

Budgeted - $99,965.00
Expended - 97,551.09
Balance $2,413.91

*Includes charges through February.

APPLICATION OF MOLECULAR BEAM EPITAXY TO MILLIMETER WAVE GAAS IMPATTS

FINAL REPORT

J. W. Amoss, E. L. Meeks, and N. W. Cox

Engineering Experiment Station
Georgia Institute of Technology
Atlanta, Georgia 30332

Report for Period April 1, 1981 - June 30, 1983
Contract No. N00014-81-K-2004

Prepared for

Naval Research Laboratory
Washington, D. C. 20375

October 25, 1983

PREFACE

This report describes work primarily performed at the Georgia Institute of Technology Engineering Experiment Station under Contract No. N00014-81-K-2004 during the period April 1st 1981 through 30 June 1983. Funding for the program is provided by the Naval Electronics Systems Command. The Scientific Officers responsible for the technical administration of the program are Dr. John E. Davey and Dr. Harry Dietrich of the Naval Research Laboratory.

SUMMARY

This report describes the technical accomplishments of a basic research program directed towards a study of the application of molecular beam epitaxy to millimeter wave GaAs IMPATTs.

A computer program was developed for simulations of the RF characteristics of millimeter wave IMPATTs and was used to help establish a set of material parameters that optimize device performance.

Layers for single drift and double drift devices were grown and evaluated. The breakdown voltage of packaged and unpackaged chips were very consistent but the RF characteristics always varied widely for devices from the same material. This inconsistency indicated that the packaging methods used introduced wide variations in the devices even though the methods were applied as consistently as possible.

Devices produced from the best material had RF output powers as high as .540 watts which could be extrapolated to .825 watts if mounted on diamond heat sinks.

TABLE OF CONTENTS

LIST OF TABLES

LIST OF ILLUSTRATIONS

SECTION I

INTRODUCTION

BACKGROUND

Recent advances in the performance of both pulsed and CW microwave and millimeter wave IMPATT diodes have mainly resulted from improvements in material technologies. For example, the highly efficient GaAs IMPATTs developed by industrial firms over the last several years resulted from their ability to realize more sophisticated doping profiles. The further development of high quality, reproducible GaAs millimeter wave IMPATTs using conventional chemical vapor deposition (CVD) or liquid phase (LP) epitaxial growth techniques however, has proved to be quite difficult and time consuming. Much additional effort is needed to improve performance and reproducibility of these devices in the 30-90 GHz range.

The inability to precisely control the doping profile from one iteration to the next using CVD or LP epitaxial growth techniques creates formidable problems in the design, development and production of millimeter wave devices. The MBE materials growth technique, on the other hand, allows tight control of layer thickness and impurity profile and is capable of rapid changes in impurity type. Perhaps most importantly, MBE is reproducible.

Prior to the development of MBE, it was difficult to

correlate experimental results with theoretical computer predictions to optimize and to determine fundamental limitations because of the non-reproducibility and inadequate control of the CVD methods evices with closely controlled doping profiles and more abrupt transitions should yield a more deterministic model with which to correlate results and improve performance.

OBJECTIVES

The overall objective of this program was to demonstrate the feasibility of utilizing MBE growth techniques to produce improved and reproducible, highly efficient millimeter wave GaAs IMPATT devices. A further objective was to identify the high-frequency limits of such devices and the fundamental physical and material parameters contributing thereto.

The research reported on herein focused on improved doping profiles for higher performance millimeter wave IMPATT structures and involved both theoretical and experimental efforts. Specific areas investigated were:

- o theoretical studies of millimeter wave IMPATT structures,
- o MBE GaAs epitaxial growth,
- o fabrication of devices,
- o RF testing of devices, and
- o correlation of tests with theoretical models.

Specific tasks undertaken to accomplish the program objectives will be discussed in detail in subsequent sections. Briefly, the tasks involved theoretical and experimental investigations leading to potential improvements in millimeter

wave GaAs IMPATTs via doping profiles consistent with MBE technology. The profiles investigated were high-low and low-high-low single-drift structures and flat-Read and Read-Read double-drift structures proportioned to operate in the 35-40 GHz frequency range. MBE was used to prepare materials with these impurity profiles and devices were fabricated for RF testing. These steps were then repeated to find a design yielding maximum efficiency and maximum power within the above frequency range.

SECTION II

MOLECULAR BEAM EPITAXY

During the past few decades a great deal of effort has been devoted to the growth of epitaxial semiconductor layers. Many techniques have been tried: vacuum evaporation, molecular beam epitaxy, sputtering, liquid phase epitaxy, pyrolytic deposition, and halide transport. Varying degrees of successful material growth have been experienced with these techniques. The versatility and extremely precise control of layer thickness and doping available with molecular beam epitaxy make it a natural choice for millimeter wave devices where the material quality and doping profile are particularly stringent.

Molecular beam epitaxy (MBE) is an ultra high vacuum deposition technique that has demonstrated significant success in the preparation of complex layers of elemental, III-V, IV-VI, and II-VI semiconductors. This semiconductor growth process has rapidly matured in the last few years to the point that useful devices are being demonstrated including GaAs FETs, IMPATTs, and millimeter wave mixer diodes. Significant advantages which MBE provides over LP and CVD are uniformity, extremely precise control in layer thickness and doping, low epitaxial temperatures which minimize thermal diffusion effects, masking flexibility, and versatility in selecting the chemical composition of the deposited epilayer.

The growth of epitaxial semiconductors by MBE involves the condensation of beams of atoms or molecules upon a single crystal substrate. A schematic diagram of an MBE system is given in Figure 1. Since typical growth rates are on the order of 3 Å sec^{-1}, very abrupt changes in composition and/or doping are achieved by selectively shuttering molecular beams projected from individually heated ovens containing component elements and doping species. The growth process is generally carried out under ultra high vacuum (UHV) conditions at relatively low substrate temperatures. The UHV environment facilitates analytical surface characterization including Auger, low energy electron diffraction, and reflection high energy electron diffraction. The low substrate temperature minimizes undesirable thermal diffusion at interfaces where dopants and compositions change abruptly.

An improved MBE system was designed and assembled (under internal funding) for use during this program. The growth chamber of this system was significantly smaller than its predecessor, which should improve the pump-down and bake-out capability and, hopefully, lower the residual background doping level. The system contained six source furnaces and shutters, thereby allowing the growth of double-drift Read-Read type devices. The source shutters were redesigned to be more positive acting than those contained in the previous system.

Since the geometry of the new system was somewhat different and the source ovens were significantly different from our other systems, new growth parameters had to be established. The growth

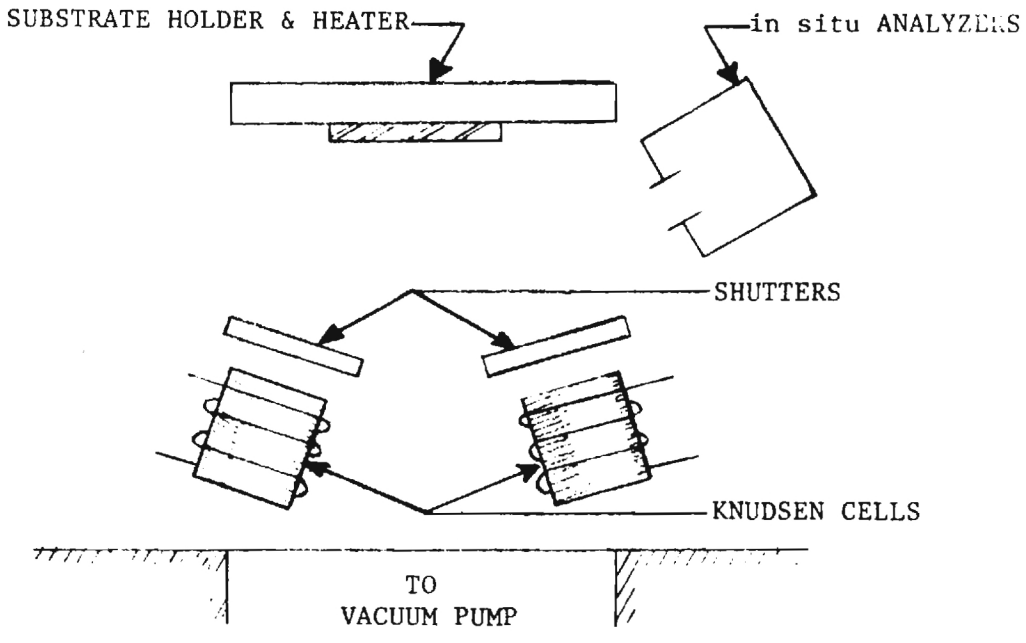

Figure 1. Molecular Beam Epitaxy System.

rate of GaAs was determined by the Ga flux which was controlled by measuring the pressure change with the Ga source shutter open and closed. An ion gauge mounted directly behind the substrate position was used to measure the source fluxes before and after growth. The Ga flux control parameter and the growth rate are shown in Figure 2.

The Si source (n-type dopant) and the Be source (p-type dopant) calibration curves used to grow the IMPATT profiles during the major portion of the program are shown in Figure 3. The impurity concentrations of the test samples were obtained from Hall mobility and capacitance versus voltage data. The temperatures during growth were measured with thermocouples located within the source ovens.

During the course of the program, it became increasingly apparent that one or both of these impurity dopant calibration curves were inaccurate. Consequently, a number of samples were analyzed by SIMS. The SIMS results confirmed the n-doped calibration curves but disagreed with the p-doped layers. This discrepency is discussed in detail in Section IV and VII.

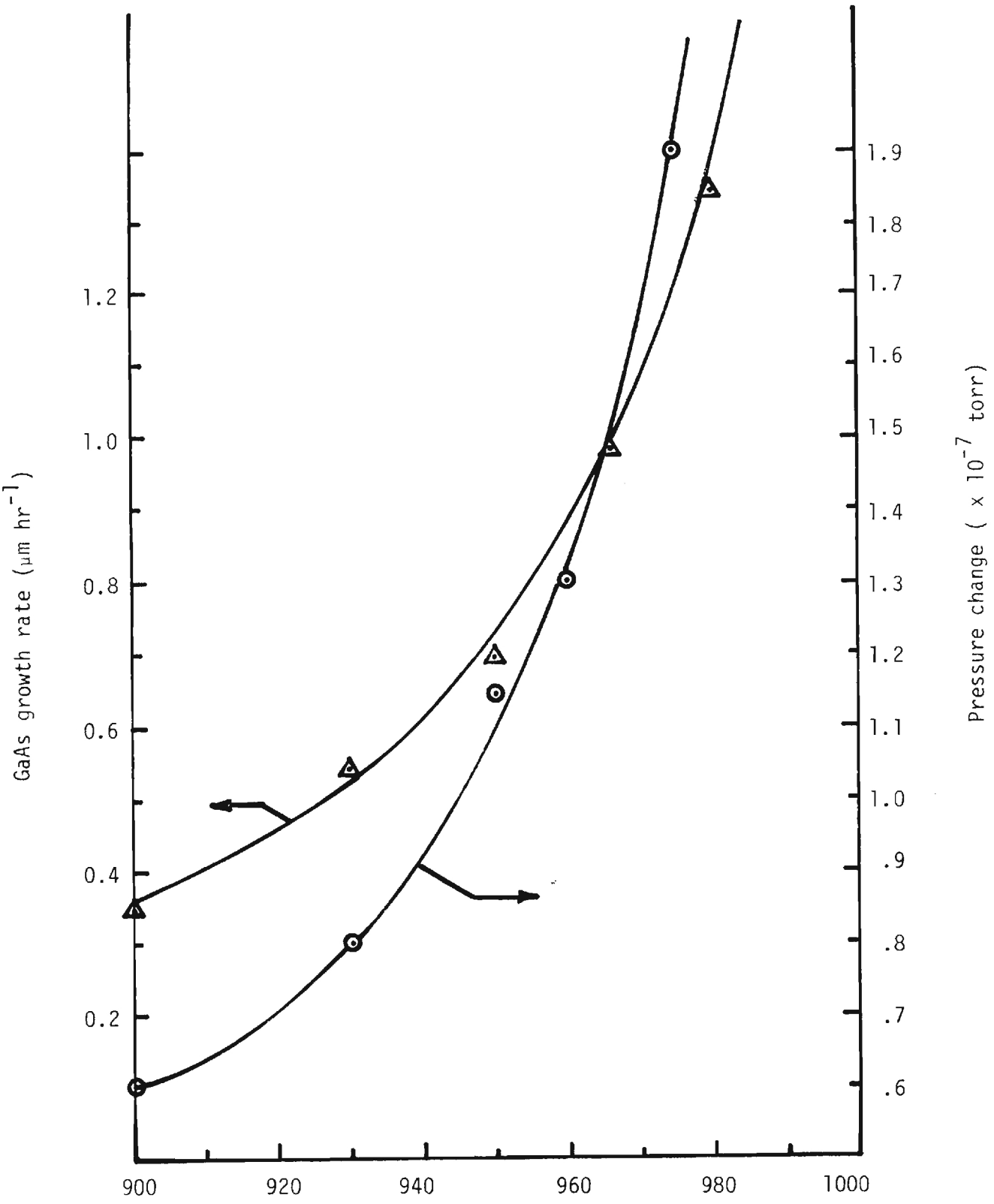

Figure 2. Ga control set point ^{o}C System III (PBN).

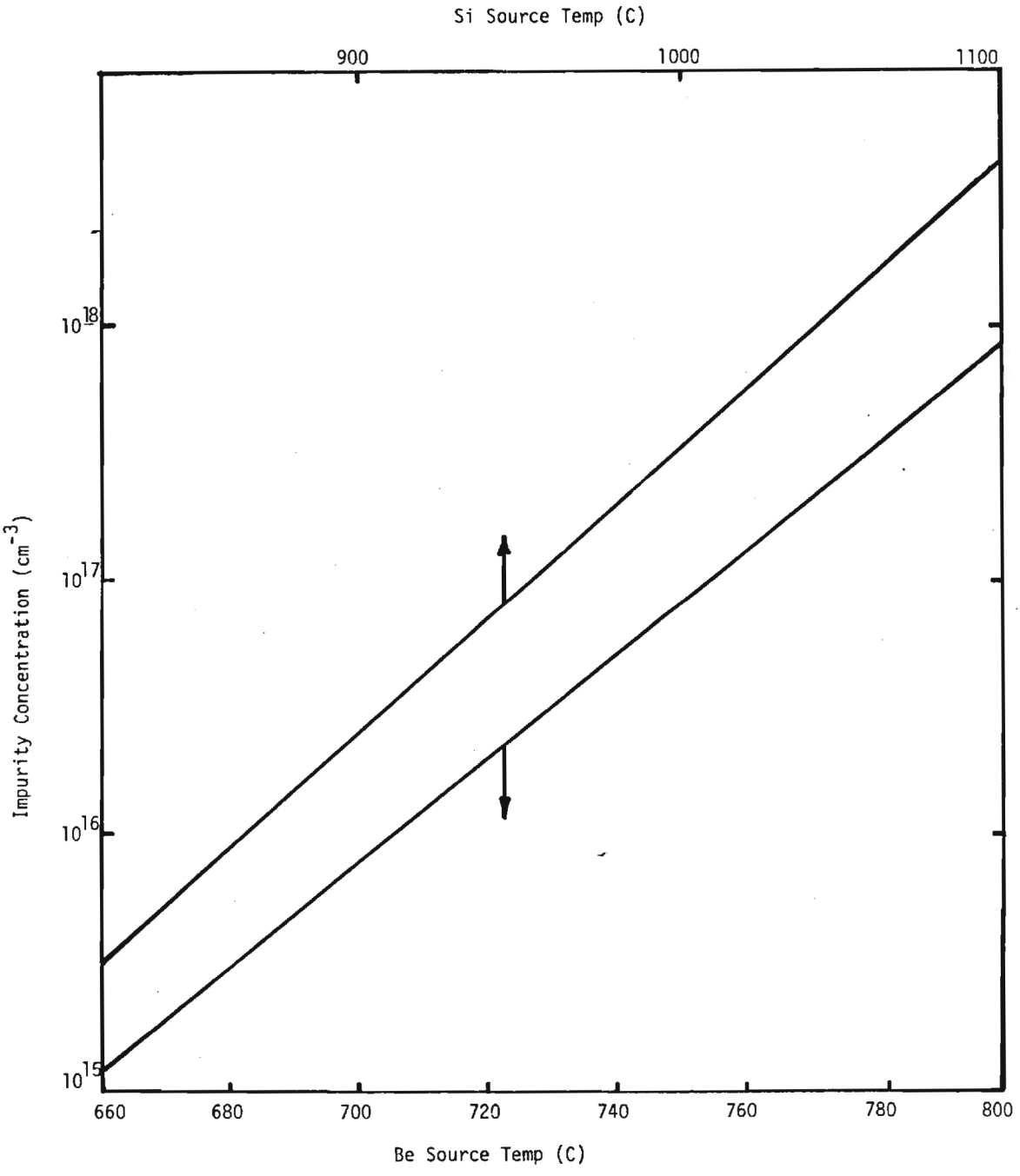

Figure 3. Calibration Curves for Be and Si Sources.

SECTION III

DEVICE DESIGN

IMPATT design necessitated a thorough understanding of the factors effecting IMPATT operation. An accurate mathematical description of IMPATT operation, however, requires a highly complicated model and a precise knowledge of the structural and the material parameters. The more general computer simulations involve methods in which the equations governing IMPATT operation are solved numerically without introducing any simplifying assumptions. This usually involves finite difference equations in which the solution starts with initial conditions and proceeds through the transient to a final steady - state solution. Fourier analysis of the steady-state wave forms then leads to output power, efficiency, and admittance data. Simulations of this type are far too costly for use in general device design because of the many structural and material parameters involved. Furthermore, disputes still remain about the values of drift velocities and ionization rates of GaAs at high-field levels, which add further to the uncertainty of the model. Because of the many inherent uncertainties and the expense of the more general solutions, most device developers resort to a semi-emperical design approach based on approximate models. The design approach and the models used during this program are described below.

In general, an IMPATT device is a semiconductor diode which operates in the reverse breakdown region. Under reverse bias, the

electric field is such that majority carriers are forced away or depleted from the junction area, forming a depletion region. When the electric field in the vicinity of the junction reaches a certain level, avalanche multiplication occurs, creating hole electron pairs which drift through the remainder of the depletion region. To help visualize IMPATT operation and the factors effecting efficiency, the active region of the diode can be separated into two distinct parts: a part in which mobile carriers (holes and electrons) are generated through impact ionization and the remaining part in which the carriers drift at saturated velocity. Read has shown that this device can generate power (or act as a negative resistor) at microwave frequencies.

The negative resistance can be attributed to two mechanisms. In the avalanche region, the generation of carriers is proportional to the density of carriers and to the electric field. This results in the current density generated within the avalanche region lagging the RF field, or terminal voltage, by 90^{o}. A further 90^{o} phase lag between the terminal current and terminal voltage is introduced via the drift of carriers through the drift region(s).

The dc to RF energy conversion occurs within the drift region via the interaction of drifting carriers with the electric field. Although necessary for the generation of carriers, the avalanche region does not contribute to the energy conversion processes. This "idealized" model leads to a simple approximation for the efficiency of an IMPATT device in terms of the dc voltage

across the avalanche region V_a and the voltage across the drift region V_d, i.e.

$$\eta = \frac{1}{\pi} \frac{V_d}{V_d + V_a} .$$

Despite it's simplicity, this expression is being used extensively here and at other laboratories as a guide in device development. The voltages across the avalanche and drift regions are obtained from a <u>static</u> solution of the ionization integral equation and Poison's equation.

Another approach which was used to help select initial target profiles utilized a large-signal quasi-static IMPATT computer program based on the analytic formulation of Kuvas and Lee (1). An existing computer program was modified to include double-drift devices with arbitrary profiles. In brief the large signal solution begins with a dc solution at the desired operating current. The electric field intensity and the ratio of hole-to-electron particle current density calculated for the dc case are assumed to remain unchanged in the large-signal case (2). A copy of this program, called QSTATIC, is listed in Appendix A.

The efficiency of a number of potential single-drift and double-drift devices were calculated using these two approaches. Typical devices are shown in Figures 4 and 5 with selected device structures and calculated efficiencies tabulated below. The distances associated with each device are measured from the

junction. The quasi-static efficiencies were calculated at 40 GHz assuming an RF voltage of 60% of the dc voltage.

Single Drift Devices

Flat profile:

doping density - 9.6×10^{16} cm^{-3}

efficiency - 12.9% (static)

12.1% (quasi-static)

High-low:

doping density - 30.0×10^{16} cm^{-3}

6.7×10^{16} cm^{-3}

interface - .13 microns

efficiency - 17.5% (static)

19.2% (quasi-static)

Low-high-low:

doping density - 6.7×10^{16} cm^{-3}

69.0×10^{16} cm^{-3}

6.7×10^{16} cm^{-3}

spike position - 0.9 microns

spike width - 02 microns

efficiency - 16.9% (static)

- 17.9% (quasi-static)

Double Drift Devices

Hybrid-Read: (p-side)

doping density - 8.0×10^{16} cm^{-3}

(n-side)

doping density - 6.0×10^{16} cm^{-3}

- 100.0×10^{16} cm^{-3}

- 2.0×10^{16} cm^{-3}

spike position - .16 microns

spike width - .02 microns

efficiency - 14.7% (static)

- 15.0% (quasi-static)

Read-Read: (p-side)

doping density - 20.0×10^{16} cm^{-3}

- 60.0×10^{16} cm^{-3}

spike position - .07 microns

spike width - .02 microns

(n-side)

doping density - 6.0×10^{16} cm^{-3}

- 125.0×10^{16} cm^{-3}

- $.6 \times 10^{16}$ cm^{-3}

spike position - .07 microns

spike width - .02 microns

efficiency - 23.9% (static)

- 21.9% (quasi-static)

These profiles were chosen during the first quarter of the program and were to serve as targets during initial growth runs.

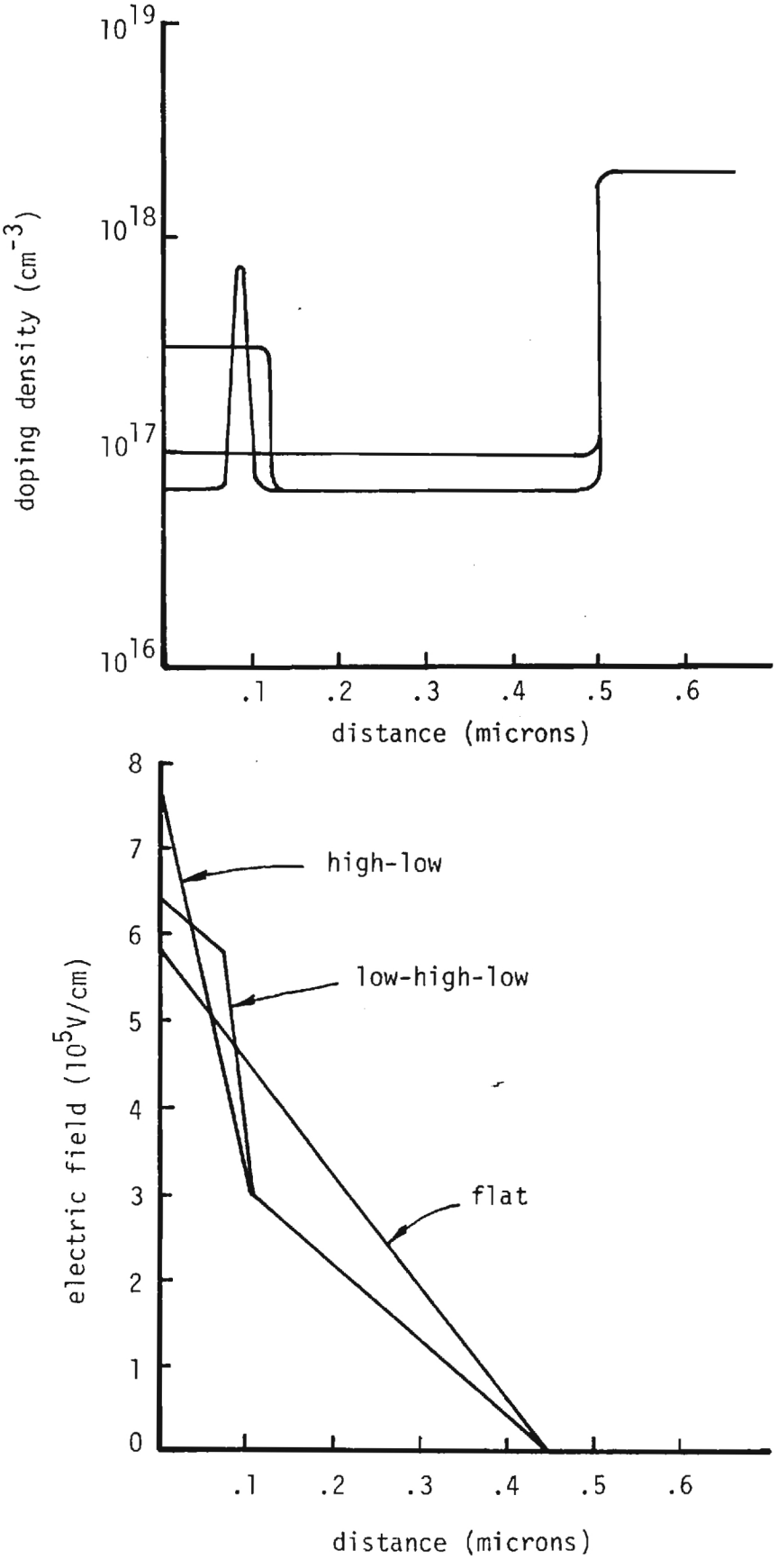

Figure 4. Single-drift millimeter wave IMPATT doping profiles and electric field intensity

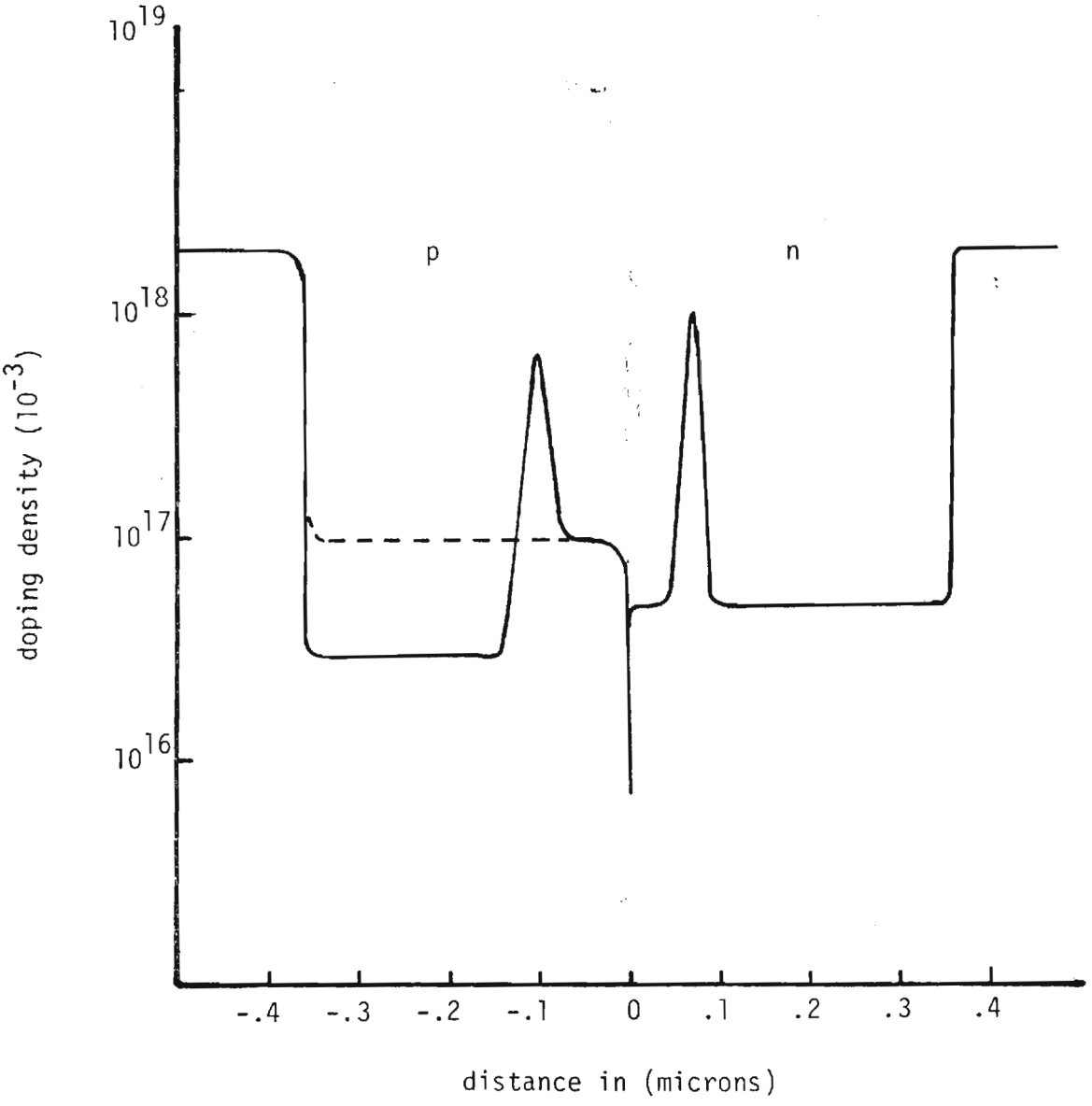

Figure 5. Double-drift millimeter wave IMPATT doping profiles.

They are based partially on actual designs as reported by workers in other laboratories and partially on computer simulations using QSTATIC. Computer simulations of the RF characteristics of millimeter wave IMPATTs are dependent on certain material parameters such as drift velocities and ionization rates for holes and electrons. Unfortunately there is still considerable uncertainly in these parameters, especially at the high electric fields where the above devices operate.

The initial plans were to grow a single-drift Schottky device first. Low-high-low single-drift devices would then be attempted since they are relatively easy to profile and would be a good indication of the ability to grow a particular structure. Hybrid-Read profiles were to be grown next. This structure would require the growth of both n and p-type material and would require a more elaborate profile evaluation. Following this, Read-Read structures similar to the one described above were to be grown and variations there of were to be optimized using a semi-emperical approach.

Concurrently with the growth and testing of these devices, attempts were to be made to refine the computer evaluations so that they would be more helpful in guiding further development.

Because of delays incurred due to system debugging however, only one single-drift device run was attempted. This material, an n-type Schottky structure, was grown primarily to confirm the growth calibration curves. Most of the subsequent runs concentrated on double-drift hybrid-Read type structures in which

the spike was contained within the n-type region.

SECTION IV

MATERIAL GROWTH

All material growth runs used highly conducting, silicon doped substrates purchased from Laser Diode Laboratories. They were polished by the supplier and cleaned prior to loading by a procedure that has been used successfully for many years in this laboratory for the growth of CVD and MBE epitaxial layers.

The cleaning procedure used is listed in Table I.

Table I. GaAs Substrate Cleaning Procedure

1. Vapor degrease in boiling trichlorethylene vapor.
2. While still in tri vapor, rinse with methanol and keep covered with methanol until blown off with dry nitrogen.
3. Each 1 minute in H_2SO_4:H_2O_2:H_2O, 5:1:1 and rinse in hot DI water.
4. Rinse in methanol and keep wet until Br etch.
5. Etch 1 minute in Br:methanol 1:50.
6. Rinse in methanol.
7. Rinse in hot DI water.
8. Blow dry with N_2.

Figure 6 depicts the hybrid-Read profile chosen for initial growth of double-drift device material. This profile is based on material previously grown by Raytheon using CVD epi-reactors. When processed into IMPATTs, single chip packaged devices with similar structures have nominally delivered 1.5 watts at 35 GHz with an efficiency of 15%. Breakdown voltages at 1 mA were

typically 17-18 volts.

The growth schedule for the profile shown in Figure 6, using the calibration curves of Figure 3 and a growth rate of 1 micron per hour, is shown in Table II.

After growth, the total thickness of the grown layers was measured using a step-profiler (profiling across a region partially masked by the substrate holder) and was found to be 2.05 μm for one sample and 2.15 μm for the other. Since these were in excellent agreement with the 2.0 μm target thickness, the materials were processed for further tests. This processing consisted of forming ohmic contacts on both the substrate and epitaxial sides of the wafer. Six mil mesas were then formed on the epitaxial side allowing breakdown voltages to be measured. All devices showed sharp breakdown characteristics with voltages at 1 mA between 16.5 and 17.5 volts. The fact that these values compare well with calculations and measured breakdown voltages of devices with similar profiles was very encouraging.

Because of the close agreement in both thicknesses and breakdown voltages, this material was processed into IMPATTs using a procedure developed on a previous IMPATT program. This is a rather time consuming procedure involving several delicate steps. Each step of the process was performed with great care and precision and the dc characteristics of the devices were always very uniform.

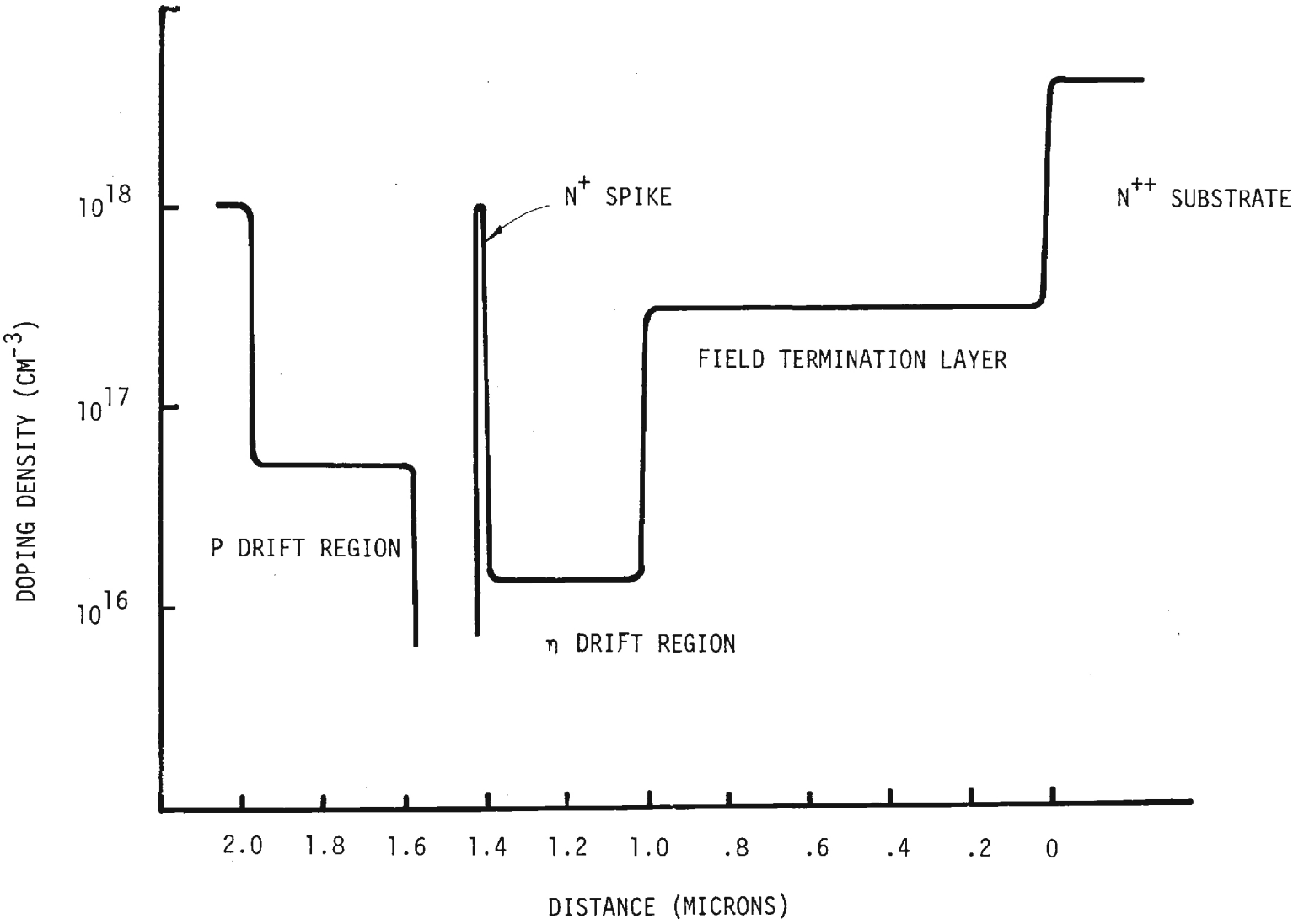

Figure 6. Doping density profile of double drift hybrid structure.

TABLE II. GROWTH SCHEDULE

SAMPLE NO. E 0329 -III DATE/OPERATOR EM/JL

RUN OBJECTIVE: DOUBLE DRIFT IMPATT

SYSTEM MODIFICATIONS:

SUBSTRATE: TYPE GaAs LOT A1457P DOPING Si ORIENTATION 2° off [100]

PUMP DOWN DETAILS:

BACKGROUND PRESSURE: $1. \times 10^{-8}$ Torr

$\Delta P]_{GA}$ $4. \times 10^{-7}$ Torr

$\Delta P]_{As}$ 1.6×10^{-6} Torr

SHUTTER	OPEN	SHUT
Ga Oven		
___ Oven		
___ Oven		
___ Oven		
___ Oven		

GROWTH CONDITIONS/RUN PROFILE						
Time 8:36	60 min	24 min	1 min 12 sec	9 min 30 sec	20 min	6 min
Ga Oven Cont/Temp(°C)	990	OPEN				
#1 Voltage (V)	18.5					
Current (A)	7.3					
Si Oven Cont/Temp(°C)	1000	880	1060	off		
#2 Voltage (V)	18					
Current (A)	7.0					
Be Oven Cont/Temp(°C)	200	CLOSED			740	880
#4 Voltage (V)						
Current (A)						
As Oven Cont/Temp(°C)	296	OPEN				
#3 Voltage (V)	3					
Current (A)	2.4					
___ Oven Cont/Temp(°C)						
Voltage (V)						
Current (A)						
Substrate Cont/Temp(°C)	580					
Voltage (V)	16.3					
Current (A)	2.8					
Ionization Gauge (Torr)	3×10^{-7}					

SECTION V

PROFILE EVALUATION

INTRODUCTION

At the outset of the program, and accurate evaluation of the impurity concentration of the grown material was recognized as a critical task in the development of millimeter wave IMPATT devices. To set up an automated computer controlled system to measure such profiles, as has been done by some large volume manufacturers, was beyond the scope of the present program. The automated equipment measures C-V data for double drift material and converts this data to an impurity concentration vs depletion width. At this step, the measurement yields an "effective" doping profile which does not resemble the actual profile throughout the composite material. By step etching down through the pn boundary and forming a Schottky barrier at the interface, the profile of one side can be determined by a straight forward calculation. It is then possible to infer from the two sets of data the doping profile of the side etched away.

Rather than resorting to that type of measurement which requires a large amount of data and hence automatic equipment, the plans were to interpret the measured impurity concentrations. This section contains a discussion of effective impurity concentrations for double drift devices as obtained from C-V data. Several examples of effective doping concentrations N_E vs depletion width W for typical IMPATT double drift structures are

given. The problems encountered in interpreting these data are also discussed. The profile of selected devices and test samples as obtained from Secondary Ion Mass Spectrometry (SIMS) measurements are also given.

Although profile measurements for single-drift devices are considered straight forward, the conventional techniques do not provide a complete profile description within the zero bias depletion region. This problem becomes more acute for millimeter wave low-high-low (spike) devices where the zero bias depletion may include the spike (highly doped region). In addition, the devices often enter low-level breakdown before the active or operating region is completely depleted. Step etching is often used to provide a profile description throughout the remaining region.

Establishing the doping profile of the double-drift device is considerably more complicated. In general, conventional techniques yields an effective concentration N_E and total depletion width W in terms of a change in capacitance, dC, with a change in applied voltage dV, as given by

$$N_E(W) = -\frac{C^3}{q\epsilon A^2} \cdot \frac{1}{dC/dV} \quad \text{and} \tag{2}$$

$$W = \epsilon A/C, \text{ where}$$

$$\frac{1}{N_E(W)} = \frac{1}{N_A(y_p)} + \frac{1}{N_D(X_n)}, \tag{3}$$

$$W = y_p + X_n, \text{ and}$$

N_A and N_D are the net acceptor and donor concentrations at the edges of the depletion region (y_p, X_n) resulting from the applied voltage V.

These equations are a consequence of the more general equations given by

$$V + V_b = \frac{q}{\varepsilon} \left\{ \int_o^{y_p} \left[\int_o^{y} N_A(y)dy \right] dy + \int_o^{x_n} \left[\int_o^{X} N_D(X)dx \right] dx \right\} \qquad (4)$$

and

$$\int_o^{y_p} N_A(y)dy = \int_o^{x_n} N_D(X)dx. \qquad (5)$$

which of course, result from integrating Poisons equations twice and invoking conservation of charge. For a given doping profile $N_A(y)$ and $N_D(X)$, an applied voltage V will result in a depletion width $W = y_p + X_n$ and a corresponding capacitance C.

As stated previously, the conventional technique of determining doping profile directly from CV measurements yields an effective doping profile which does not represent the true profile throughout the composite material. A computer program based on the above equations was developed for interpreting CV data and for reconstructing doping profiles. This computer program (listed as CV TEXT in Appendix B) can also simulate CV

data of double-drift devices of arbitrary doping profile.

Figures 7 and 9 show the effective profile, as obtained from simulated CV data, of typical hybrid-Read and Read-Read devices where actual profiles are shown in Figures 8 and 10.

Note the unusually wide rectangular "spike" shown in the "effective" doping profile of the hybrid-Read device. For the uniformty doped p-region, the total depletion width changes as $W = (1 + N_D(X)/N_A)X$ which causes the width of the actual spike of thickness and doping N_D to show up as a spike of thickness $(1 + N_D/N_A)d$ and doping $N_DN_A/(N_D + N_A)$ in the effective profile. For practical cases where both p and n regions may have complicated profiles (as in the Read-Read device), the effective doping can be quite complicated. Also note the arrows shown in the Figures. These represent the approximate extent of the zero bias depletion region. Little information on profile can be obtained from CV data for this region. A slight extension of the profile towards the junction can be obtained by applying slight positive bias. No information on $N_A(y)$ individually can be deduced from the effective doping distribution without first knowing the distribution of one side. One approach helpful in confirming whether or not a particular target profile had been grown would be to compare calculated values of $N_E(W)$ based on the target profile with values of $N_E(W)$ obtained from CV data measured on the grown material. If agreement is good, one can be more confident in the profile grown. One should be aware, however, that the effect profile of a double-drift device is not

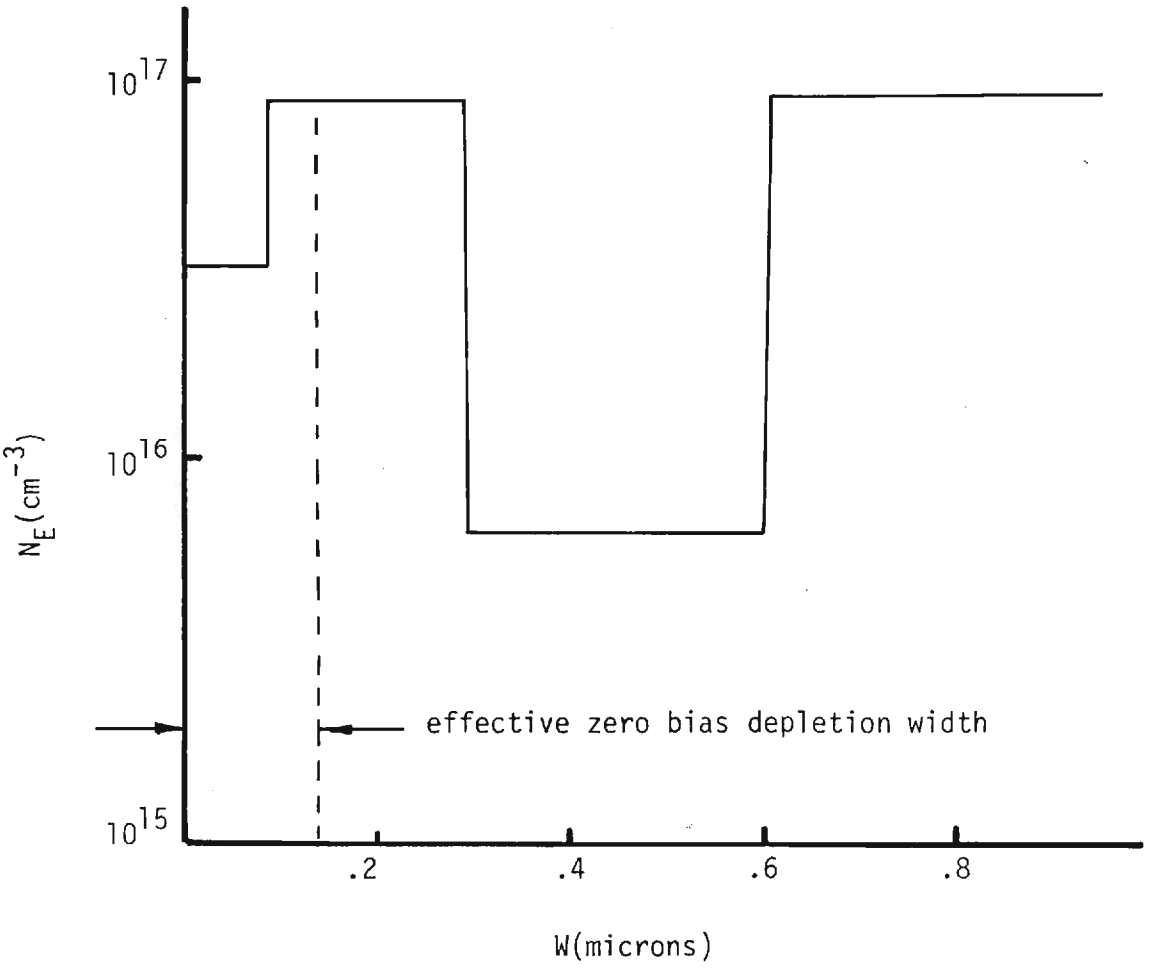

Figure 7. Effective Profile of Hybrid-Read Double-Drift Device

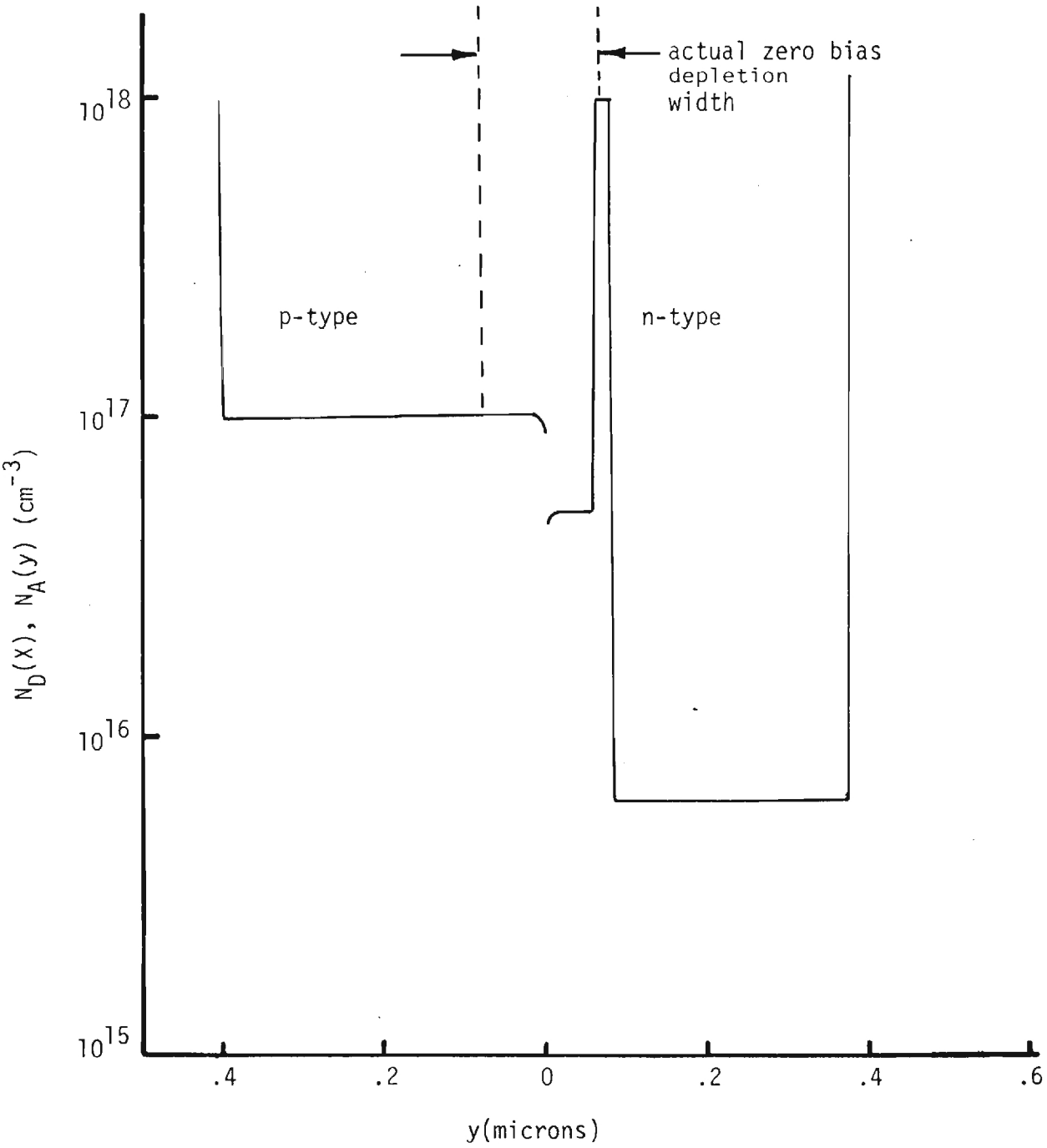

Figure 8. Actual Profile of Hybrid-Read Double-Drift Device

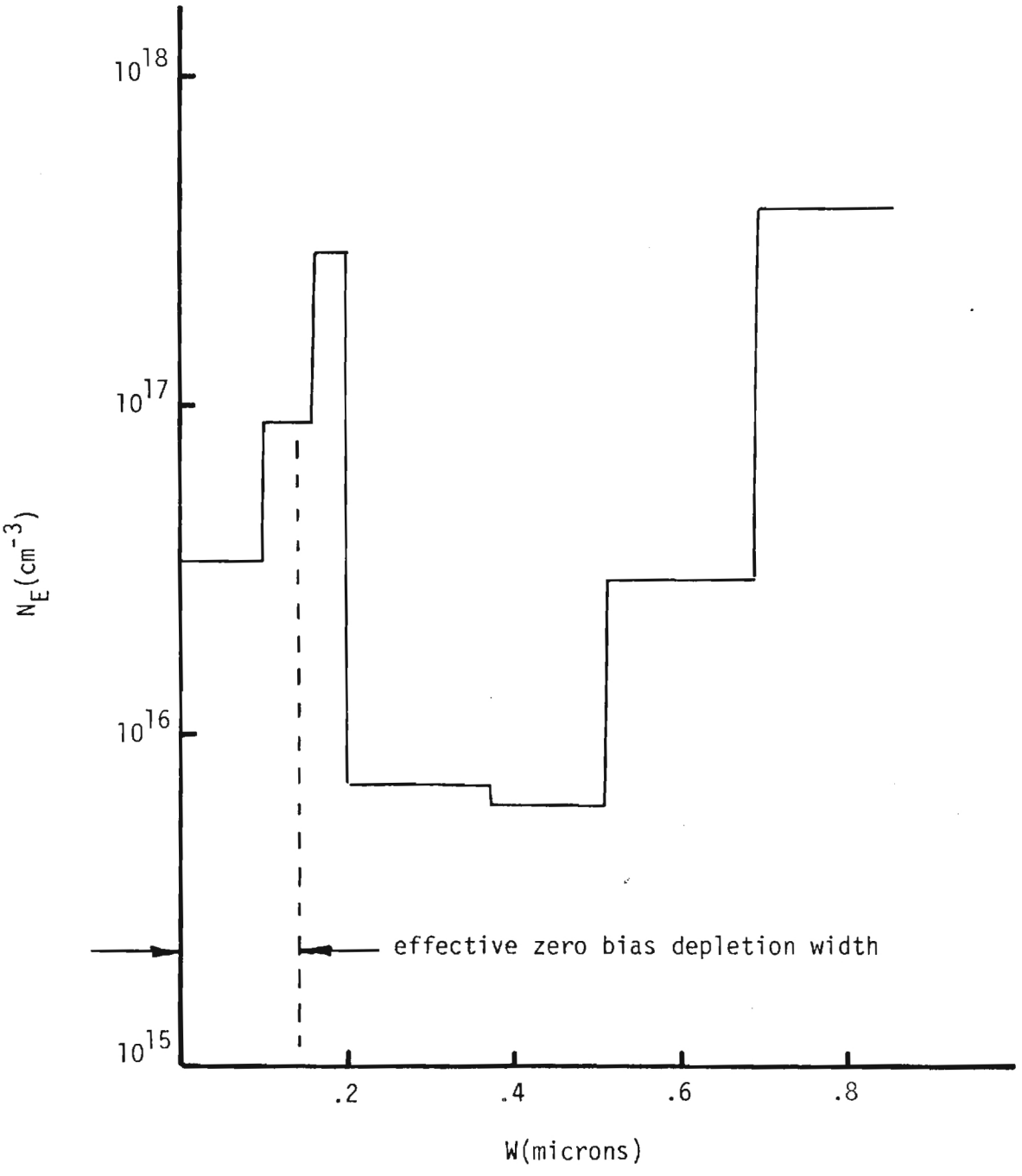

Figure 9. Effective Profile of Read-Read Double-Drift Device

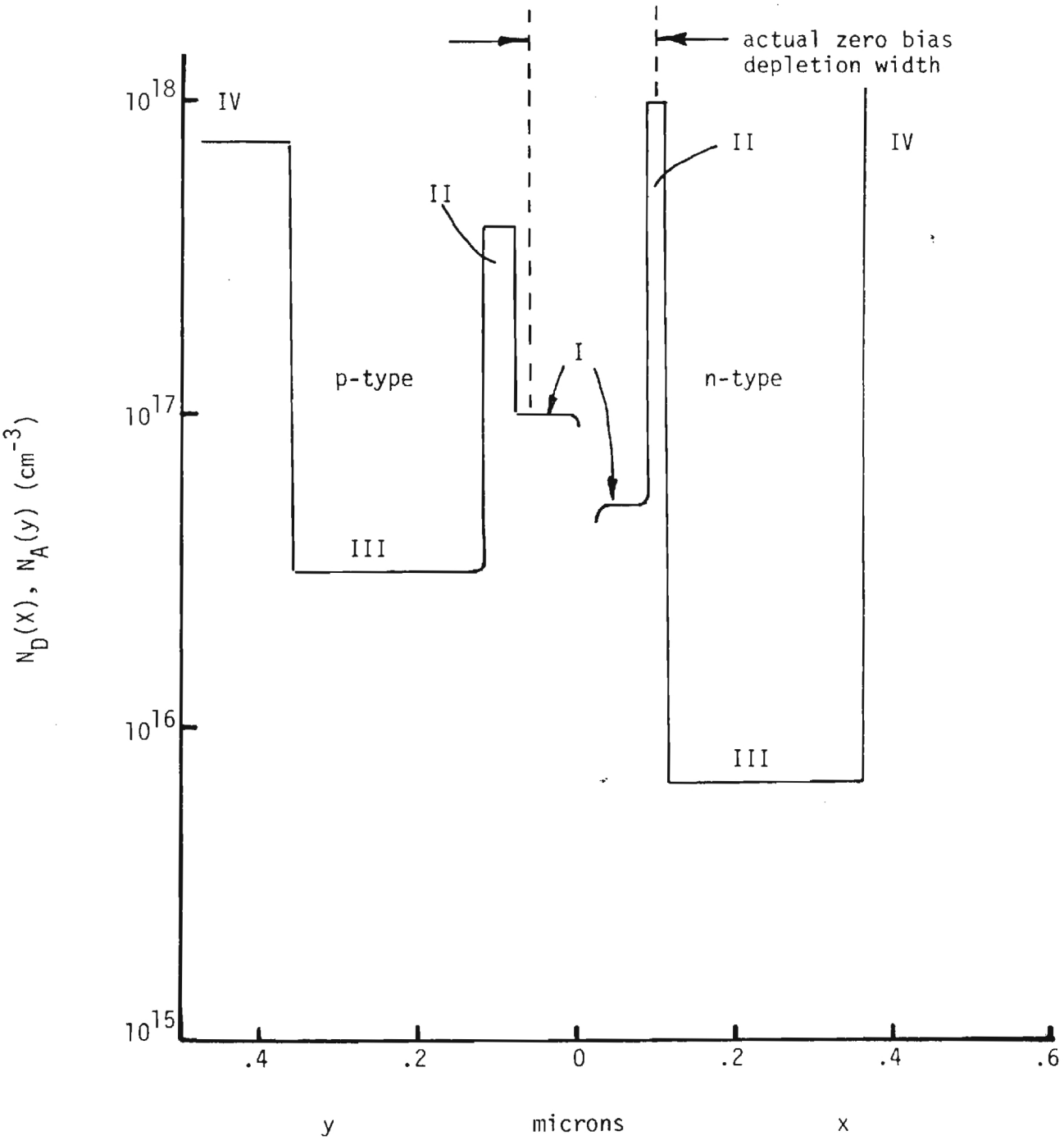

Figure 10. Actual Profile of Read-Read Double-Drift Device

unique and that an infinite combination of $N_A(y)$ and $N_D(x)$ can theoretically give the same $N_E(W)$. The task then is to determine uniquely $N_A(y)$ and $N_D(X)$ from measured C-V data.

There are two methods commonly used in reconstructing the doping profiles of double-drift devices. The first method involves etching a series of steps into both the p and n region, forming Schottky junctions at the various etch levels, and then evaluating the doping profile about those levels in the conventional manner. Unfortunately, this requires Schottky junctions on both p and n type material. In addition, the thickness of the active regions of millimeter wave IMPATTs are such that limited information can be obtained on the p-side because of the close proximity of the p-type Schottky with the p-n junction[3].

The other method involves etching just through the pn interface, forming a Schottky junction at that position, and evaluating the remaining layer in the conventional manner. The profile of the other layer can then, in theory, be uniquely determined by using integrated charge expressions[3]. Equation (5) can be rewritten as

$$E_Q\begin{pmatrix} X \\ y \\ W \end{pmatrix} = \frac{q}{\varepsilon}\int_0^X N_D(X)dx = \frac{q}{\varepsilon}\int_0^X N_A(y)dy = \frac{q}{\varepsilon}\int_0^y N_{eff}(W)dx \qquad (6)$$

The field at any point in terms of integrated charge is $E(y) = E_{max} - E_Q(y)$. The integrated charge expression can be written and generalized to

$$E_Q(z) = \frac{q}{\varepsilon}\int_0^z N(z)dz + \frac{1}{\varepsilon A}\int_0^V CdV \qquad (7)$$

which shows that the field in the swept out region can be expressed as a function of distance z and can be obtained (except in the zero bias depletion region, z_o) from C-V measurements. By treating E_Q as an independent variable and distance z (either x, y or z) as the dependent variable, then $Y(E_Q) = W(E_Q) - X(E_Q)$ as depicted graphically in Figure 11. The Roman numerals denote the regions (with subscripts L for left and R for right) that the electric field sweeps through as E_Q increases. The doping profile $N_D(y)$ can theoretically be determined from $E_Q(y)$ using equation (6). In actual practice, however, the data about the origin (within the zero bias depletion width) can not be determined. Furthermore, the Schottky junction used to determine the profile of one side cannot always be placed just within the side. Both introduce an uncertainty in the proper orientation of the $W(E_Q)$ curve with respect to the $X(E_Q)$ curve. This can cause significant errors in the $Y(E_Q)$ curve and hence in the reconstructed doping profile for the remaining side.

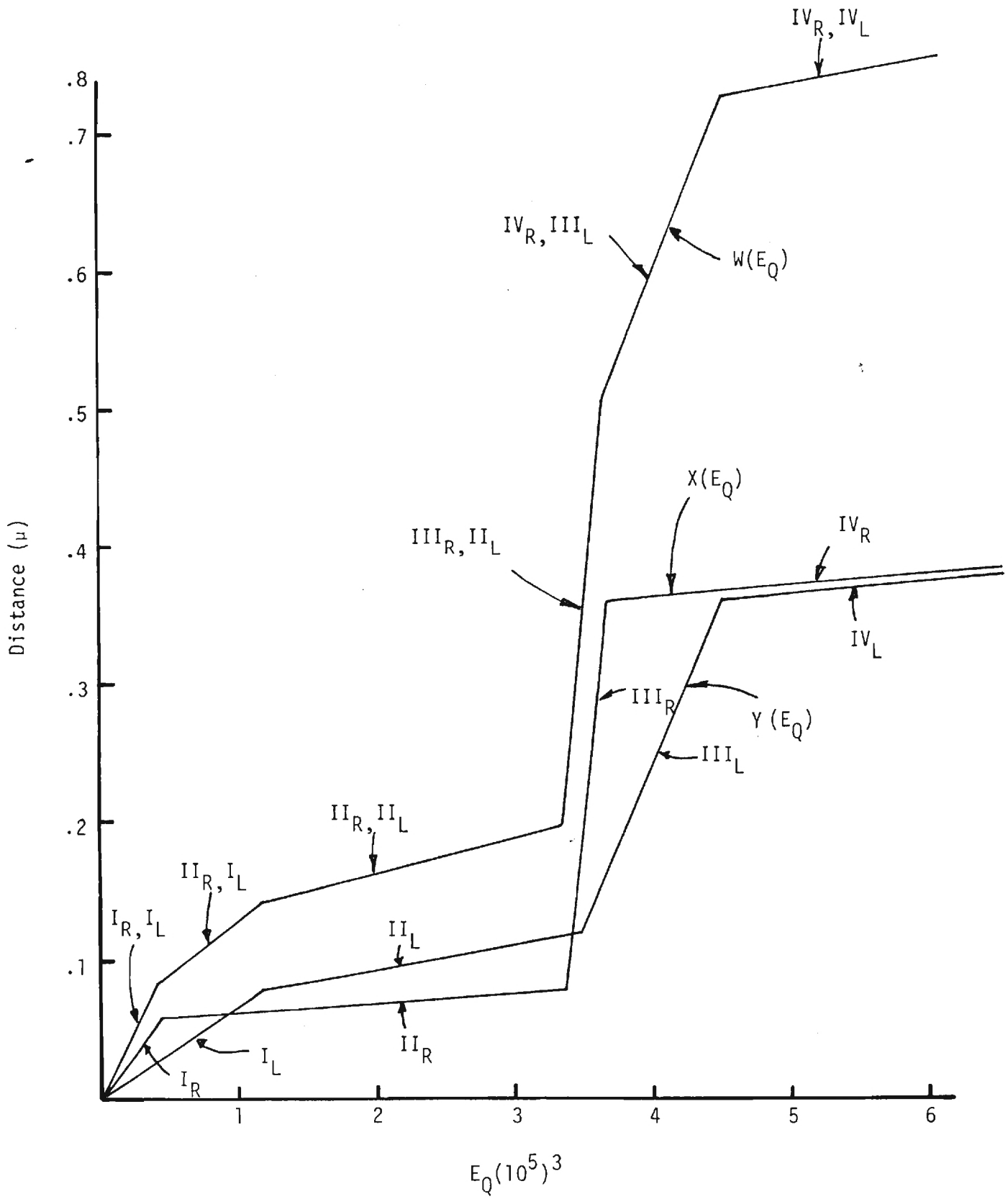

Figure 11. Integrated Charge Technique for reconstructing profile of one side knowing composite profile and profile of other side.

which shows that the field in the swept out region can be expressed as a function of distance z and can be obtained (except in the zero bias depletion region, z_o) from C-V measurements. By treating E_Q as an independent variable and distance z (either x, y or z) as the dependent variable, then $Y(E_Q) = W(E_Q) - X(E_Q)$ as depicted graphically in Figure 11. The Roman numerals denote the regions (with subscripts L for left and R for right) that the electric field sweeps through as E_Q increases. The doping profile $N_D(y)$ can theoretically be determined from $E_Q(y)$ using equation (6). In actual practice, however, the data about the origin (within the zero bias depletion width) can not be determined. Furthermore, the Schottky junction used to determine the profile of one side cannot always be placed just within the side. Both introduce an uncertainty in the proper orientation of the $W(E_Q)$ curve with respect to the $X(E_Q)$ curve. This can cause significant errors in the $Y(E_Q)$ curve and hence in the reconstructed doping profile for the remaining side.

A test was made to determine if the scanning electron microscope (SEM), could be used to orient the two curves. This instrument was used extensively in other IMPATT programs conducted at Georgia Tech to assess device geometry and to perform failure analysis. One of these programs (AFAL-TR-78-63) utilized the SEM for depletion width evaluation using the voltage contrast (V.C.) mode. This task was unique in that most prior V.C. work had been performed on planar device geometries while the tests on IMPATTs require contrast resolution in the mesa-height direction.

One of these tests was repeated on this program to determine if the technique could be used to gain more information on the doping profile of double-drift devices. The results of this test is shown in Figure 12 as a composite of the series of photographs of a flat profile double-drift X-band device under different bias conditions. These photographs were taken using both the usual V.C. mode and specimen current mode. The middle band shows the depletion region as it widens with an increase in reverse bias. This image is formed from the specimen current which is caused by charge current multiplication resulting from the impingement of the electron beam within the depletion region.

Note the position of the junction shown as the relatively narrow line for .71 volts positive bias where the depletion region has narrowed considerably. It is also worthwhile to note the fuzziness and striations in the vicinity of the junction at low bias levels. The fuzziness is thought to be due to charge

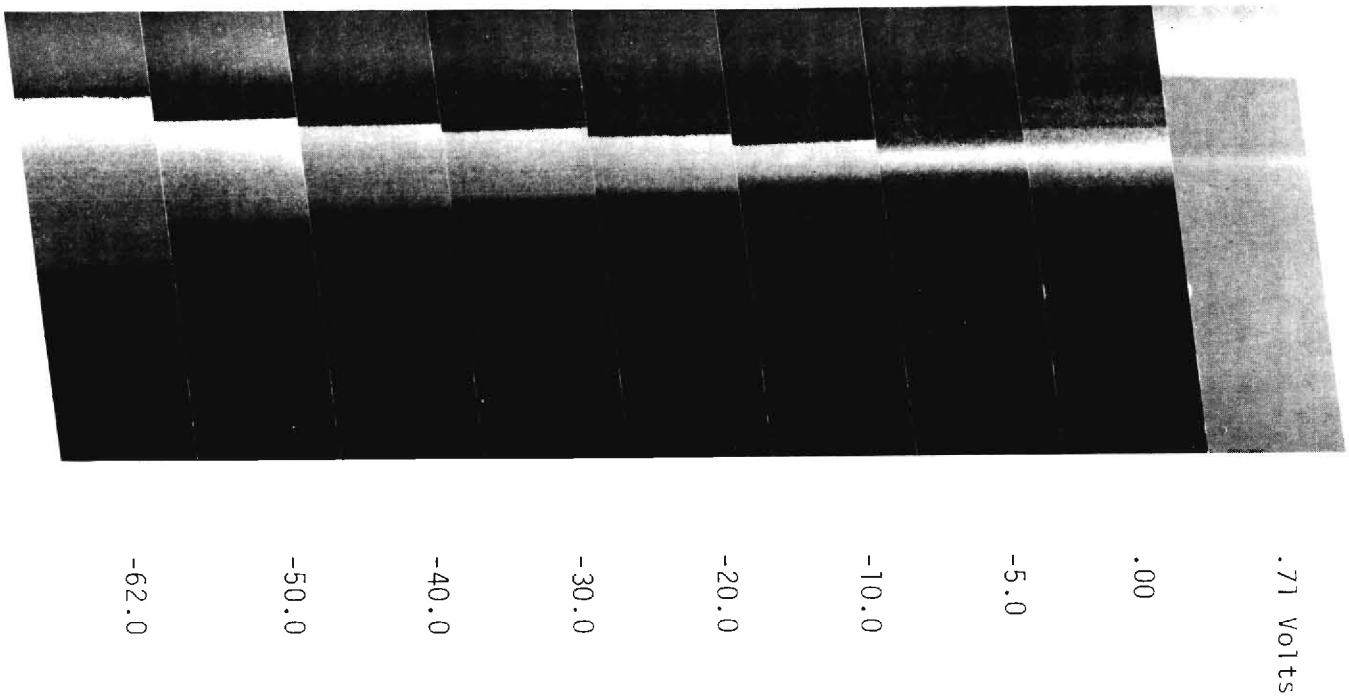

Figure 12. Voltage contrast of flat double-drift IMPATT.

accumulation at the surface (charging from the beam). Increasing the voltage in either direction removes this charge. The striations are though to be due to nonuniform charging caused by nonuniform doping within the pn transition region. These tests showed that the position of the spike and the widths of the drift regions could perhaps be determined from contrast analysis when abrupt transitions are involved. A quantitative evaluation of the impurity concentrations of the various layers by such tests, however, seems doubtful. Spike positions and drift region widths depend upon growth rates, a quantity which proved to be controllable and repeatable. Since accurate impurity concentration could not be determined accurately from these tests, they were discontinued.

The hybrid-Read structure initially grown and tested was the E0329-III wafer whose target profile is reproduced in Figure 13. The spike of this structure contained approximately 2×10^{12} Coulombs cm^{-2} and was nominally .16 microns from the junction. These devices had very sharp breakdown characteristics with breakdown voltages between 17.5 and 18.5 volts at 1 mA. The maximum output power obtained was about 20 mW when biased to approximately 200 mA. The E0329-III MBE grown profile was based on material previously grown by Raytheon using CVD epi-reactors and which nominally delivered 1.5 watts at 35 GHz with an efficiency of 15%. The breakdown voltages of the E0329-III MBE devices and the CVD devices on which this material was based were in good agreement yet the output powers differed by orders

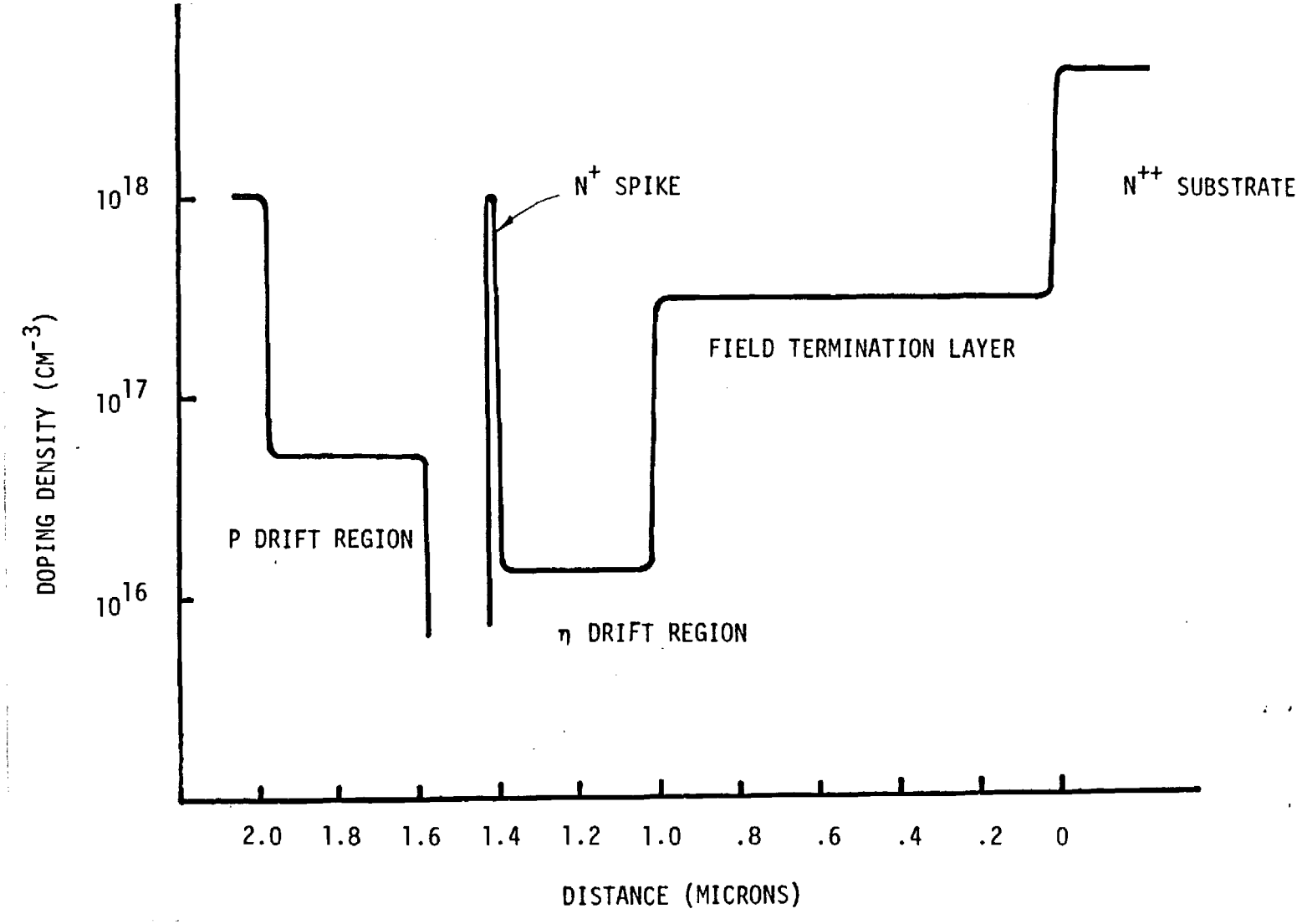

Figure 13. E0329-III Target Structure.

of magnitude.

Measurements were made in an attempt to determine the reasons for the vast difference in output power between the devices. Figure 14 shows the composite profiles of two Georgia Tech (GT) MBE devices and two CVD devices on which the GT profile was based. Also shown is a theoretical composite profile based on a rectilinear profile of Figure 13. It should be kept in mind that the impurity concentration shown is an effective value which, as discussed previously, is related to the impurity concentration on both sides of the junction by $1/N_{eff} = 1/N_A + 1/N_D$ and the depth is the total distance depleted on both sides of the junction. The accuracy of a profile measurement depends upon accurately knowing the device area. Since measured or calculated impurity concentration is inversely proportional to the square of the area and the depth is directly proportional to the area, any error in device area will shift the measured profile along a line with slope of -2. Since one of the Georgia Tech profiles shifted along a line with slope of -2 (indicated on the Figure 14) coincides with the other profile, the profile of the two devices (impurity concentration and depth) are probably very similar and the indicated difference is more likely a difference in their areas. All four devices had been etched in the package which prevented an accurate determination of device area. If the lower GT profile were shifted up to the higher one, all four devices would show essentially the same depth relationship but with significant differences between impurity

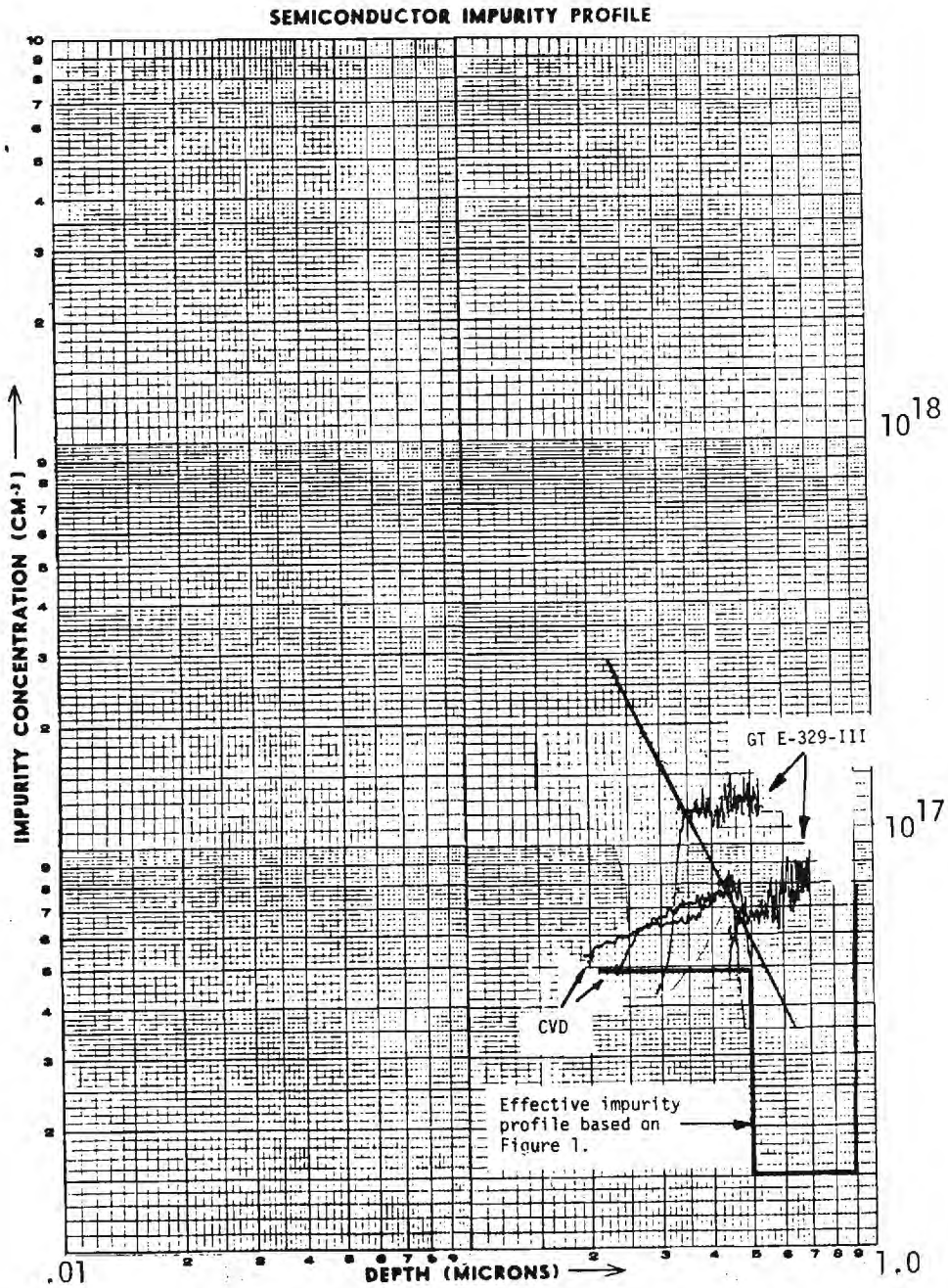

Figure 14. E0329-III Measured profile, CVD Measured profile, and calculated profile of target structure.

concentrations. The zero bias depletion edge does not extend into the spike for the MBE grown material whereas it appears to extend into this region for the CVD material. For most of the profile (near horizontal portion), one depletion edge moves through the uniformly doped p region and the other edge moves through the highly doped spike region. For the CVD grown device, the depletion edge moves out of the spike region and into the n-type drift region for an applied bias of about 14 volts. For the MBE grown device, the depletion edge remains in the spike region even up to the breakdown voltage of about 18 volts.

These differences in performance were thought to be due to excess charge contained between the junction and spike-drift interface region. Decreasing this charge (decreasing the impurity concentration) would result in a smaller change in electric field in this region and deplete more of the n-type drift region. That portion of the drift region not depleted would introduce loss and consequently decrease output power and efficiency. This is a possible explanation for the low output power of the MBE grown devices.

There was also a significant difference in the dc bias capability of the two devices. The MBE grown chips burned out at about 200 mA bias whereas the CVD chips would withstand bias currents typically greater than 600 mA. Figure 15 compares the reverse I-V characteristics of these devices. The slope of the I-V curve is equal to $1/R_{TH} + 1/R_{SC}$ where R_{TH} is the thermal resistance and R_{SC} is the space charge resistance. Note that the

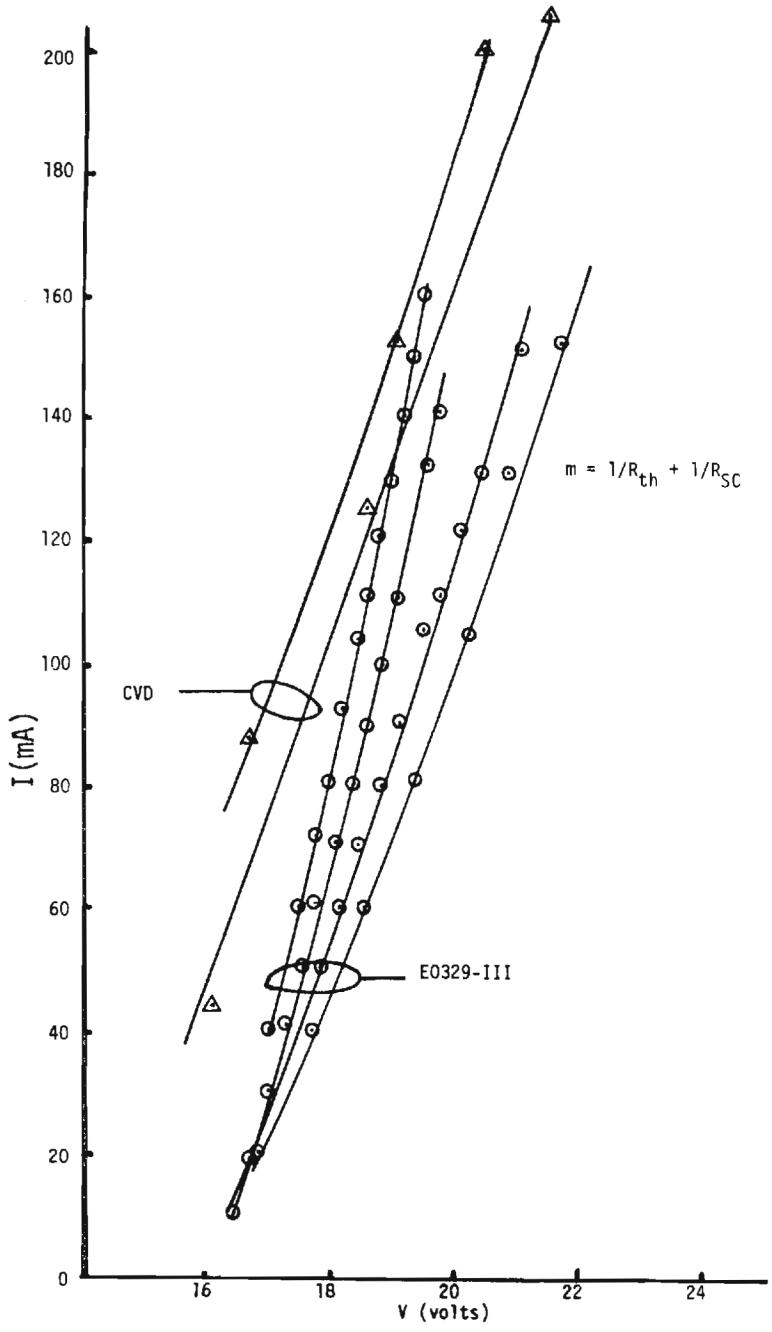

Figure 15. Reverse I-V Characteristics of Selected Devices.

slopes of the I-V curves for the MBE devices are equal to or greater than those for the CVD devices. Although not conclusive, this test indicates that the MBE devices are heat sunk as well as the CVD devices.

A single drift structure (E0401-III) was grown having the same doping profile as the n-side of wafer E0329-III. Measured profiles of chips from this material are shown in Figure 16. Again a rectilinear plot of the idealized target profile is shown for comparison. The actual profiles shown (not the same chip) were measured on an automatic profiler and on a C-V bridge. There is an obvious discrepancy in the measured drift width (.15 to .20 microns) and the desired drift width (.40 microns). At the time the measurements were made it was thought that the discrepancy was due to premature or soft breakdown characteristics of the Schottky junctions since the sample measured on the automatic profiler did have a softer breakdown than the other sample. The cluster of points about the doping of the field termination layer (3×10^{17}) displaced approximately .2 microns (12 min growth time) is not understood. It is not likely due to an uncertainty in device area nor is it likely due to a 12 min delay in operating the source shutter since the growth rate was well under control. No devices were processed from this material. It was grown mainly as a check on the growth of the n-type region of E0329-III.

The next double drift IMPATT materials (E0511-III and E0512-III) grown were similar to the E0329-III except that the peak

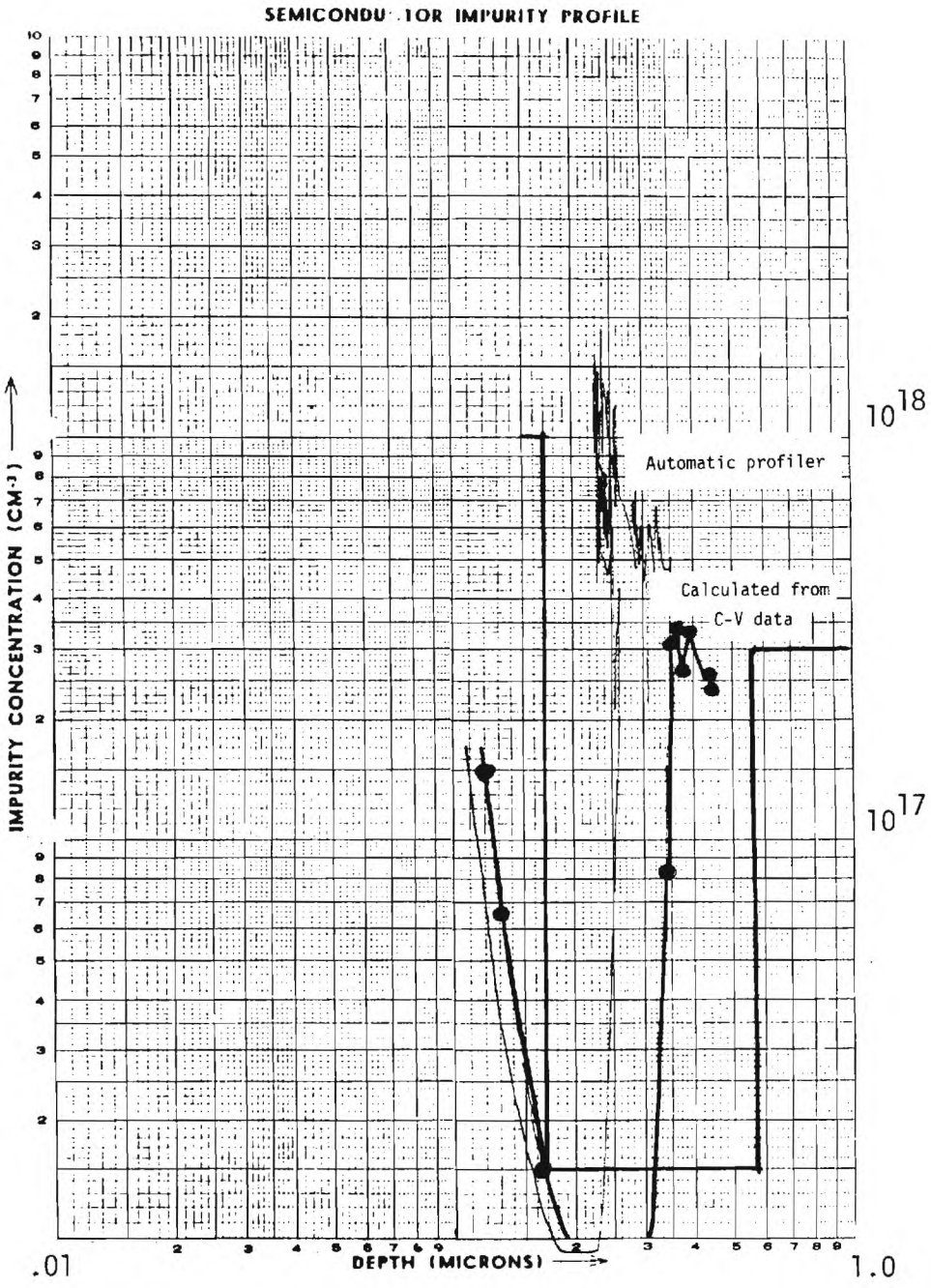

Figure 16. E0401-III-2 Measured profiles and calculated profile of target structure.

impurity concentration in the spike was decreased from 1 x 10^{18} to .8 x 10^{18}, the impurity concentration in the p-drift region was increased to 8 x 10^{16}, and the doping between junction and spike was increased to 6 x 10^{16}. The measured impurity concentration versus depth for this material is shown in Figure 17. Also shown for comparison is a calculated profile based on an ideal rectilinear model. Note that the spike is still not depleted. The effective impurity concentration during the spike "sweep out" should be slightly lower than the doping in the p-region. This profile and the preceeding one suggests that the p-type doping may already be larger than that intended.

Material E0512-III was processed and tested as IMPATTs. One device yielded an output power to 41 mw at 34.6 GHz when biased to 235 mA. All of the other devices tested burned out at current levels less than 235 mA with output powers in the 25-30 mW range.

Since most of the profile measurements and RF tests performed at this point suggested that the n-type drift region may not be depleting prior to breakdown, the spike width was decreased to 100A (the growth time for the spike was halved) for the next growth run. In other respects this device was similar to E0512-III. Several devices from this run oscillated at 36 GHz with output powers between 100 and 140mw. Again, however, the diodes burned out at current levels less than 250 mA.

The next growth run completely eliminated the spike. The structure was a double drift flat-flat profile in which the impurity concentrations and the depths of both type materials

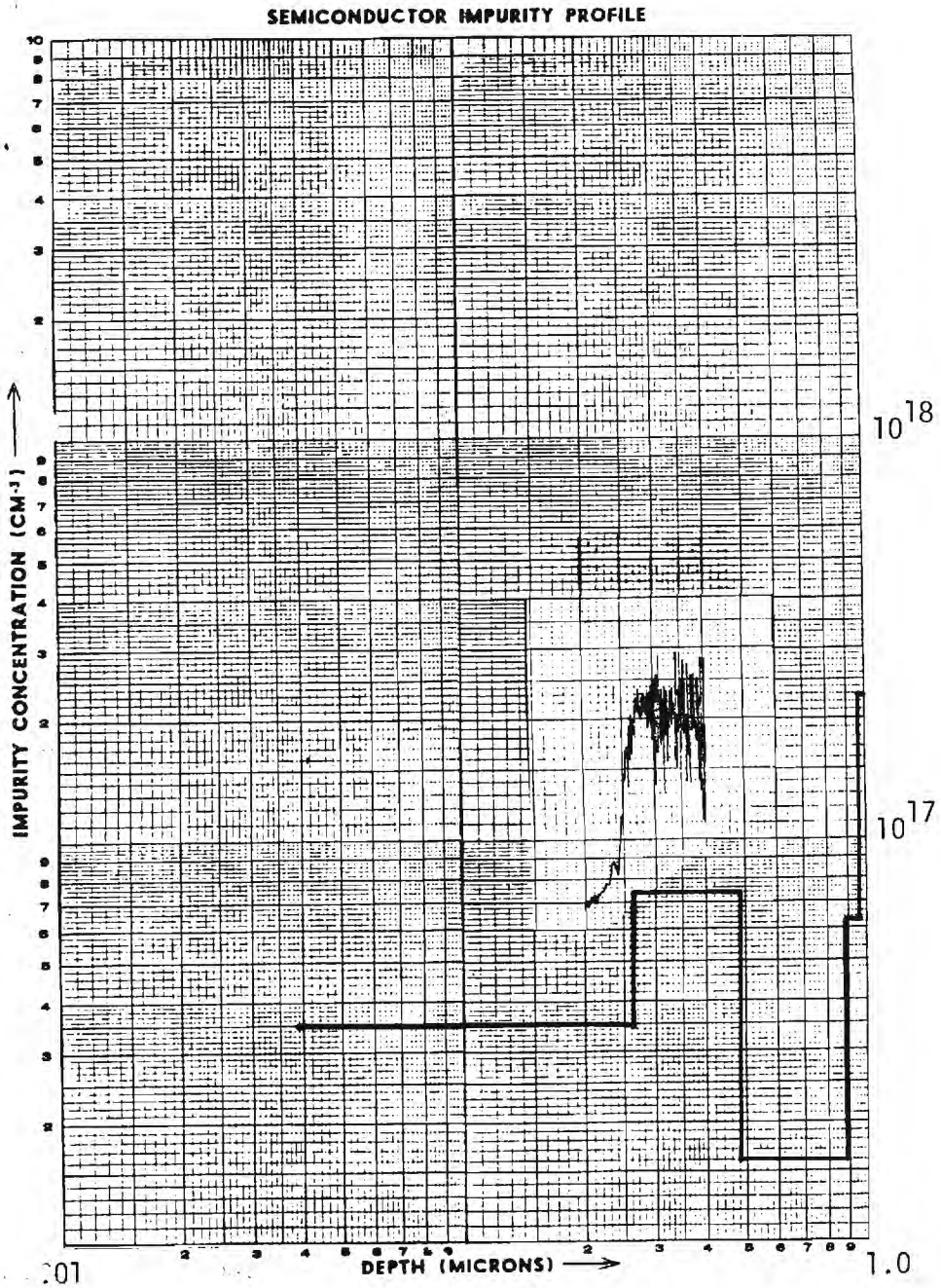

Figure 17. E0512-III measured profile and calculated profile of target structure.

were chosen to be fully depleted at a peak electric field of 5.0 x 10^5 V/cm. Each region was doped to 7 x $10^{16}cm^{-3}$ over a distance of .5 x 10^{-4}cm. Although this structure was grown primarily to check the system calibration, the material was processed and tested as IMPATTs. Maximum output power obtained with these devices was 21 mW at dc bias currents up to 219 mA. The devices operated at about 31 GHz. All devices tested burned out at current levels less than 219 mA.

As stated, the flat profile double drift devices were grown primarily to check system calibration. Since both p and n-type impurity concentrations were to be 7 x $10^{16}cm^{-3}$, the effective concentration should measure 3.5 x $10^{16}cm^{-3}$, and the total depletion depth should measure 1.0 x 10^{-4} cm prior to breakdown.

Samples from material E0329-III were sent to Raytheon, for the purpose of analyzing the impurity concentration. This company has devoted considerable effort and funds to set up an automated digital profilometer which is controlled by an Intel 8080 microprocessor based digital computer. The measurements entails step-etching the structure, forming Schottky junctions at each step, and calculating impurity concentration from C-V measurements. The results of this analysis is shown in figure 18 along with the idealized rectilinear profile.

The first measurement was made with the Schottky placed on the p^+ contact layer (XI = 0). The zero bias depletion width was Xo = 0.104 microns which allowed the impurity concentration of part of the p^+p transition layer to be obtained (curve 1). After

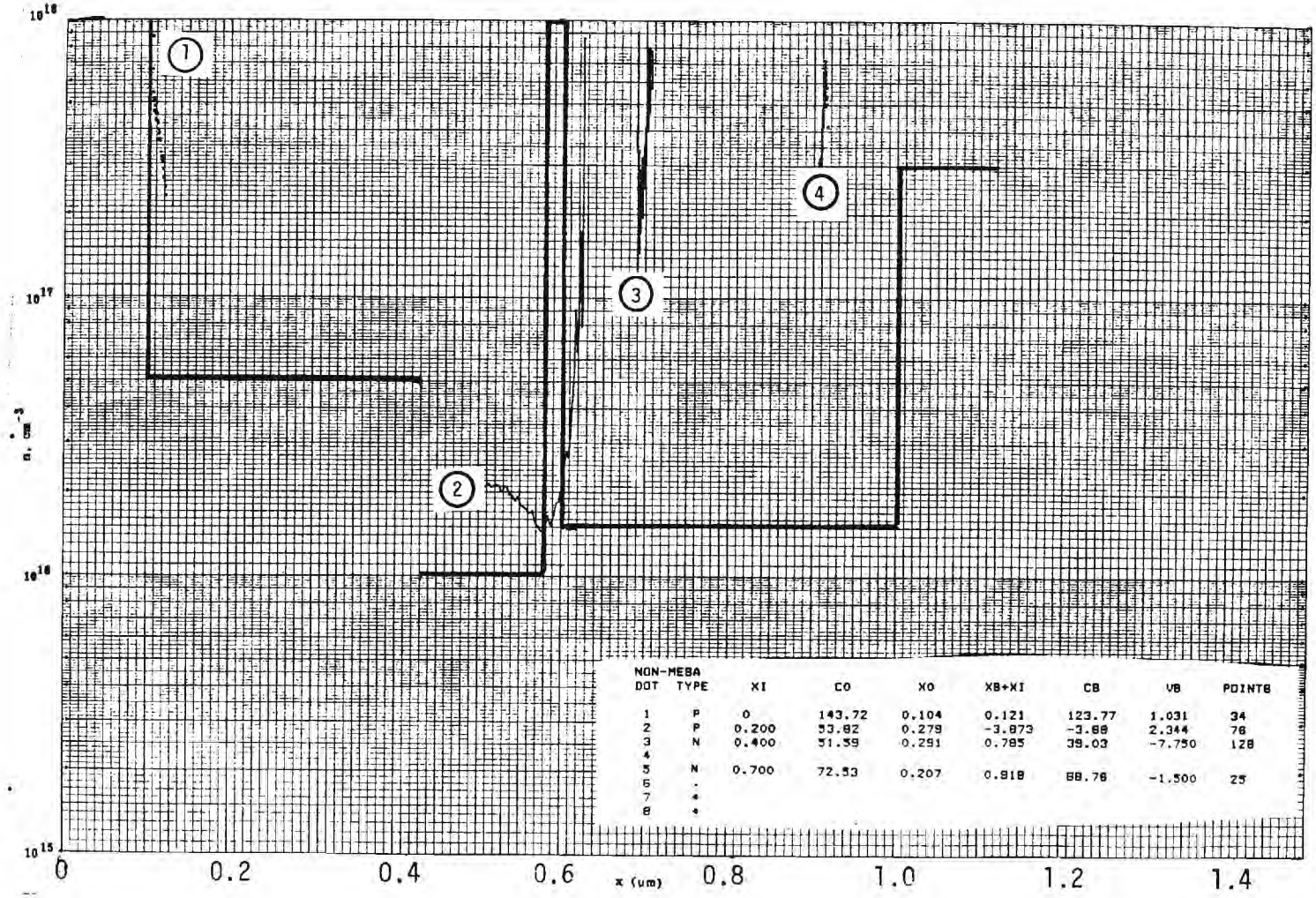

Figure 18. E0329-III measured profiles at selected etch depths.

etching 0.200 microns, the zero bias depletion edge extended through the p-n junction making any conclusions from the data thereby obtained subject to error (curve 2). The second etch (.400 microns from original surface) was close to the junction and identified as n-type material. From there the zero bias depletion edge extended to .291 microns where the results of C-V data reduction indicated a relatively high impurity concentration (curve 3) approximately .1 micron further into the n-drift region than where the spike was thought to be. The fifth etch went to .7 microns and showed a zero bias depletion depth of .207 microns. C-V data indicated an abrupt interface at this position of relatively high doping. This is thought to be the interface between the n-drift region and the field termination layer. The drift termination interface seems to be displaced into the drift region by about .1 micron, consistent with Figures 16 and 18.

Figure 19 shows the composite or effective impurity concentration measured by Raytheon. The near horizontal trace is thought to results when one edge of the depletion remains in the highly doped spike while the other edge sweeps through the p-type drift layer. The deduced p-type impurity concentration from this plot is more consistent with the growth target of $5 \times 10^{16} cm^{-3}$ but is not consistent with an actual higher impurity concentration implied from Figure 14, 16 and 18.

Material from the E0512-III double drift IMPATT run was sent to Charles Evans and Associates for evaluation of the Si and Be impurity concentration profiles. When this data was returned it

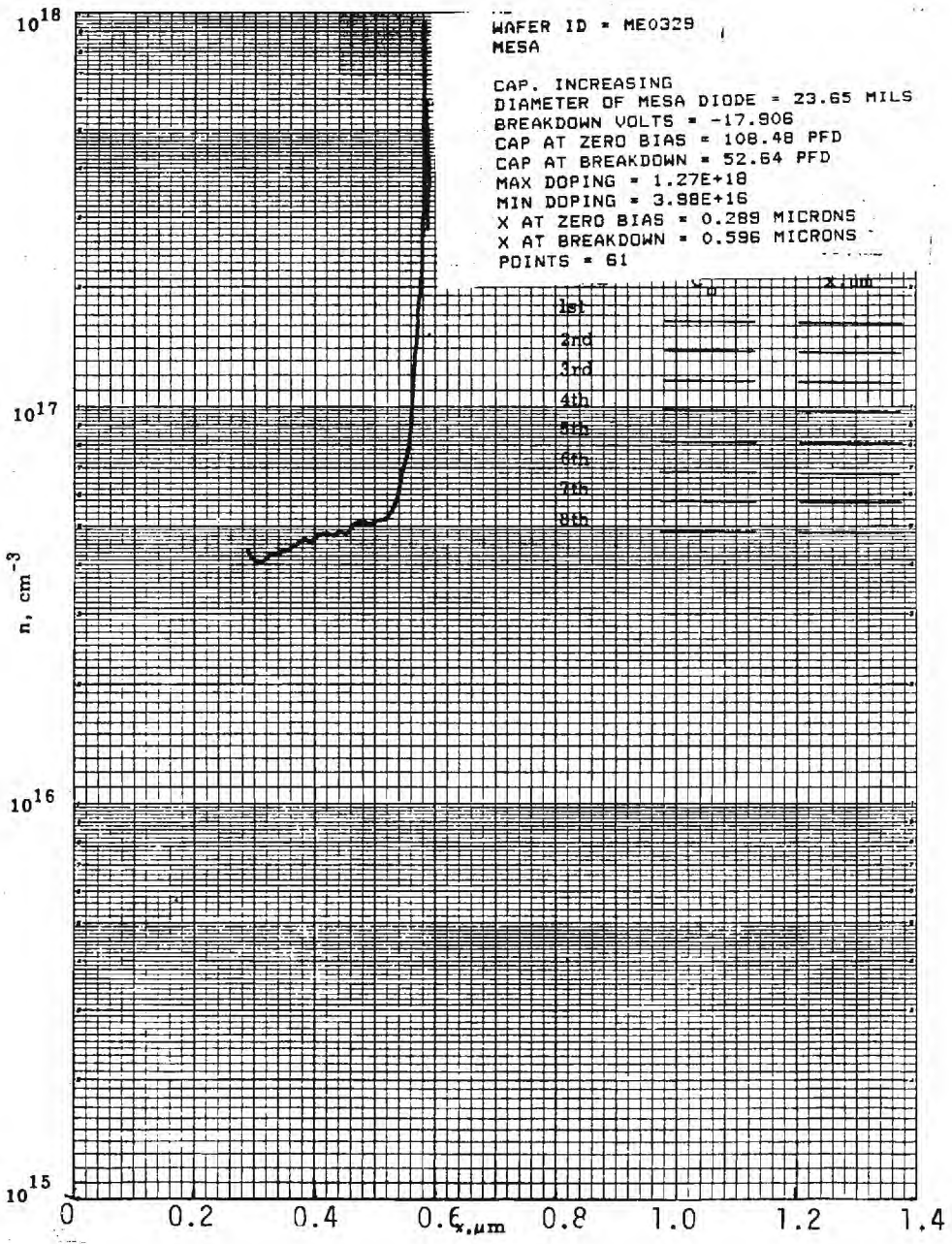

Figure 19. E0329-III measured effective profile of composite material.

was immediately obvious from he Be profile that the Ga source was contaminated with Be. The level of contamination was such that the Ga source was contributing 1.2×10^{17} cm^{-3} Be doping at all times during growth. All materials grown on the program after this run were certainly similarly contaminated. Also, since it is not known how or when the contamination occurred, there is a distinct possibility that all the layers grown for this program to that point were contaminated.

Figure 20 shows the SIMS depth profile for Si and Be as obtained on sample E0512-III. The SIMS analyst claims an uncertainty of 7% in depth and a factor of two in concentration. For comparison, the target profile is drawn on the experimental data. For one familiar with MBE growth procedures, it is immediately obvious from the data in figure 20 that the Ga source is contributing a Be doping of 1.2×10^{17} cm^{-3}.

The growth rate of GaAs MBE is determined by the Ga flux. Thus, for precise control of layer thickness and doping concentration, the Ga flux is calibrated before the start of each run. An ion gauge placed 1-2 cm behind the sample growth position is used to measure the Ga and As flux before the sample is introduced. Precise control of the flux is obtained by adjusting the source temperature until the desired pressure change is observed when the source shutter is opened and closed. After calibration, the Ga temperature is reduced $50^{o}C$ and held until the As flux is calibrated and growth is initiated. A full As flux is always used when the substrates are heated to temperature, and

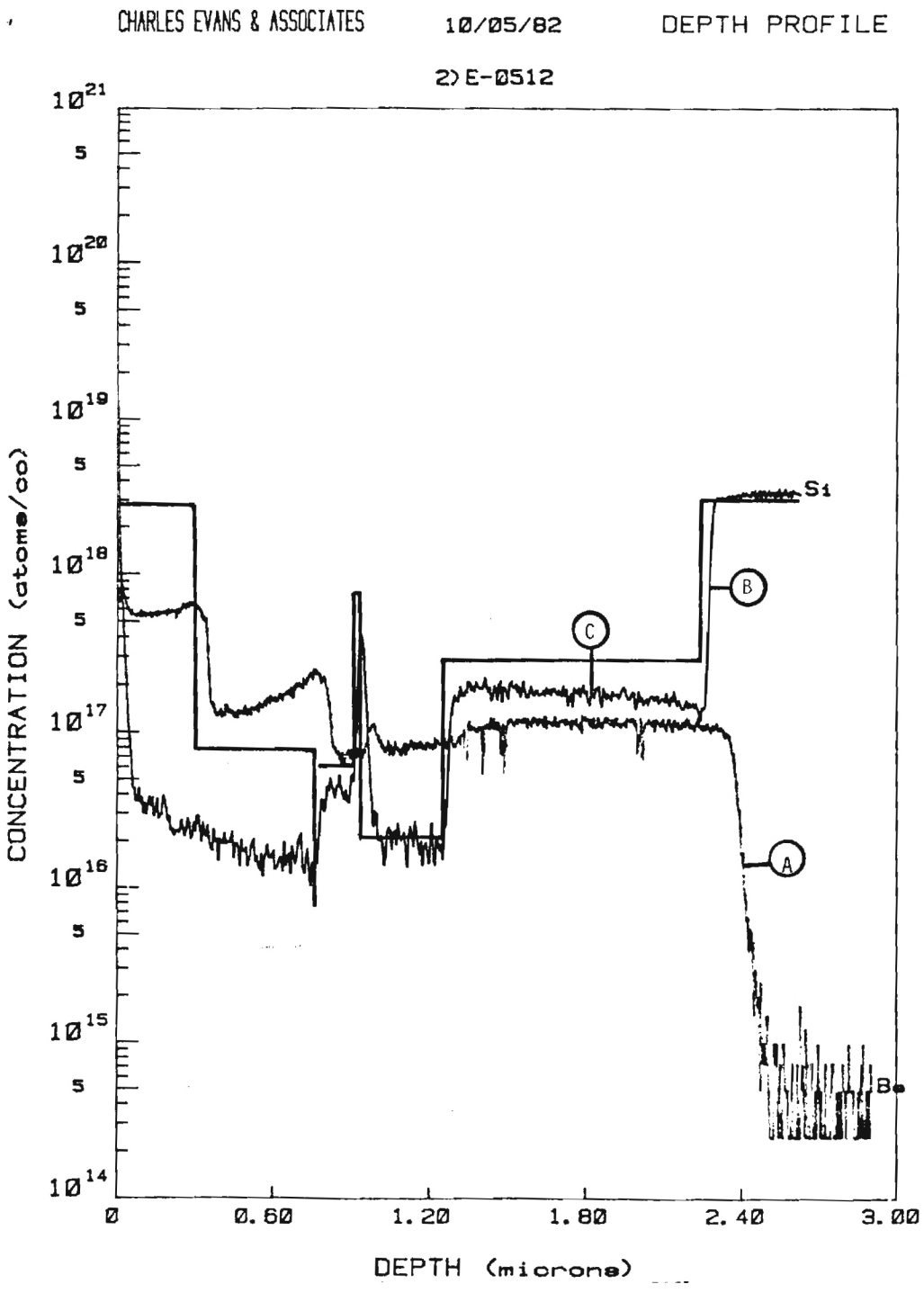

Figure 20. SIMS Profile for Si and Be in layer E0512.

growth is initiated by opening the Ga source shutter and increasing the temperature to the calibrated set point. This procedure is necessary in order to avoid an initial high Ga flux that occurs when the shutter is opened and the source has been held closed at the calibrated temperature for more than 30-40 seconds. It also avoids excess Ga deposit on the back of the shutter which can drop off and contaminate the heater coils.

At position A marked in figure 20, the increase in Be doping corresponding to the increase in Ga temperature when growth is initiated can be seen. This is the obvious indication of Ga source contamination. The only other action taken at this time during growth is the opening of the Si source shutter, and when the temperature of the Si source is changed at latter times during growth, no corresponding change in Be doping is observed.

Positions A on the Be curve and B on the Si curve in figure 20 must necessarily be at the same depth in the layer at any one position on the sample since both indicate the start of the growth. The depth discrepancy may be due to the fact that the profiles where taken at different positions on the sample. In any case it is within the 7% uncertainty. There is good agreement between the experimental data and the target profile for Si. The field termination layer at C in figure 20 is low but within the concentration uncertainty quoted by the SIMS analyst. The doping level, thickness of the drift region and the position of the spike are excellent. If the target profile is correct, a single drift device with identical Si profile should perform very well.

There is a gradual increase in Si doping from 0.7 m depth to the surface that would be disturbing since the Si source is closed and off during this growth but no such effect is seen in the second SIMS profile shown in figure 21.

In order to correct the problems discussed above, the Si and Ga source materials were discarded and the empty ovens baked out at 1400°C in a separate vacuum system. Also, the Be oven was moved to a position less likely to cause contamination problems. After replacing the source ovens and refilling them with new materials, a calibration layer was grown specifically for SIMS analysis.

The Si depth profile for the calibration run is shown in figure 21 and again the Si data shows excellent control. The target concentrations and layer thicknesses are very close and the background concentration is 3-5 x 10^{15} cm^{-3} when doping at 10^{17} cm^{-3} or less. When doping at 10^{18} cm^{-3} the background level is an order of magnitude higher. In both cases the Si background may possibly be reduced by changing from water cooling to LN_2 cooling in the source shroud.

The SIMS profile for Be in the calibration layer is shown in figure 22. The Be level is 50 to 100 times higher than the target profile, reaching a maximum of 2 x 10^{19} cm^{-3} near the surface. It is encouraging to know doping of this magnitude can be achieved with Be since it should facilitate the fabrication of ohmic contacts to p-type materials. However, the data in figure 22 are also 50-100 times higher than the data in figure 20 and the data

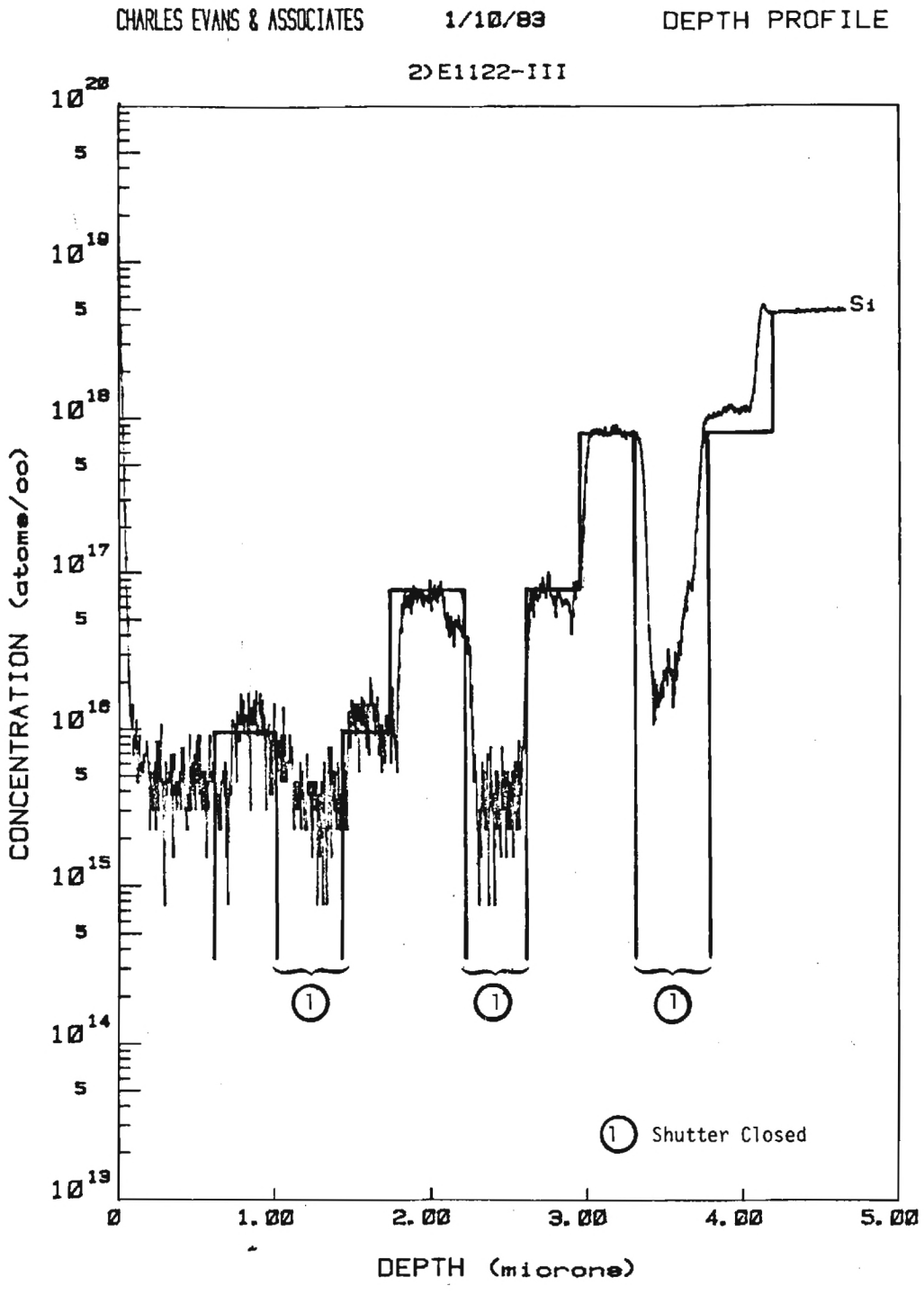

Figure 21. SIMS Profile for Si in calibration layer E1122.

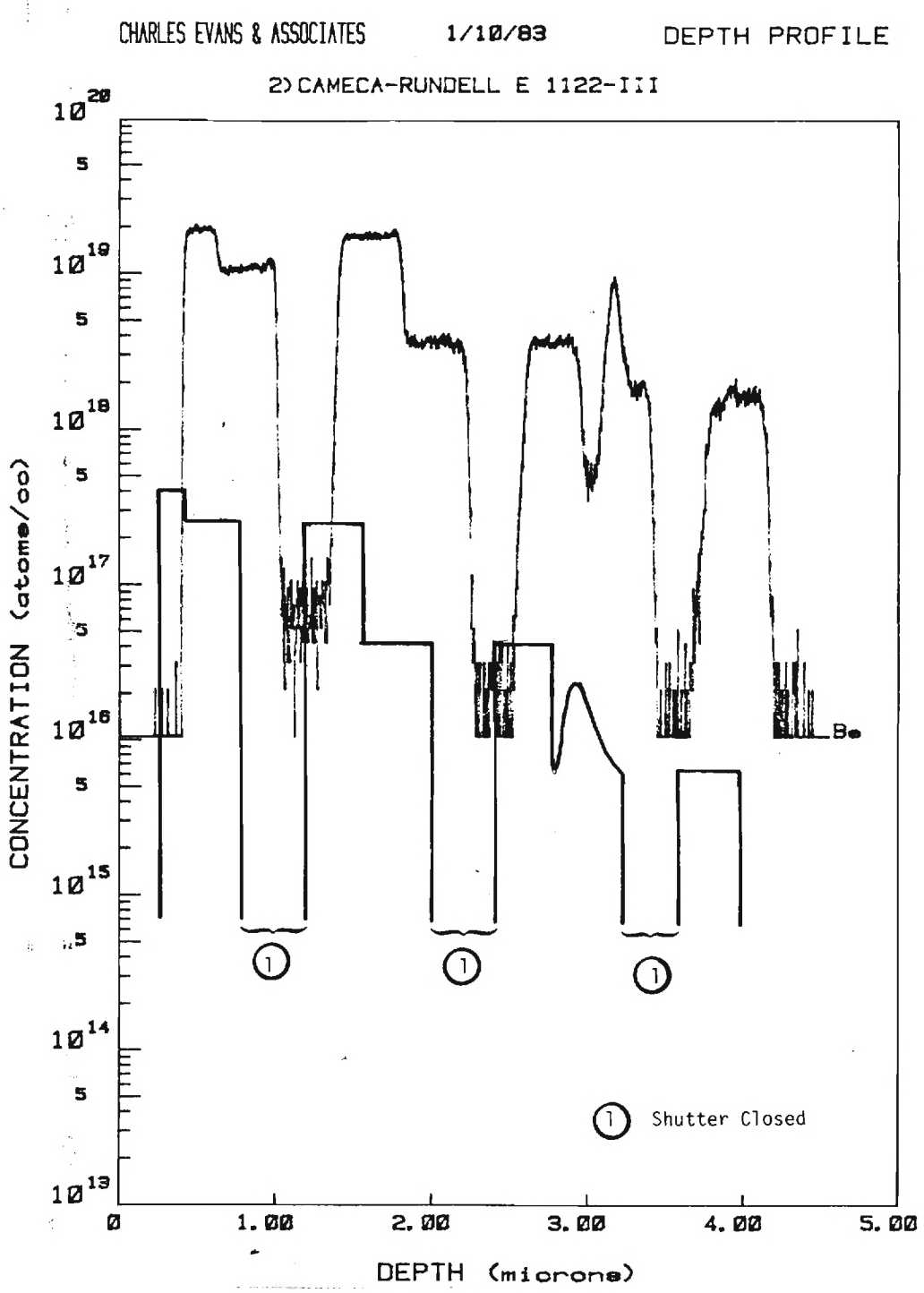

Figure 22. SIMS Profile for Be in calibration layer E1122.

obtained by Hall and C/V measurements at identical source temperatures. No explanation could be given for the discrepancy in the data for Be in the calibration layer.

The SIMS data for both samples show excellent control of the Si impurity level, excellent control of the layer thickness, and very sharp interfaces between layers. The control was such as to inspire confidence that good double drift IMPATT layers could be grown with the Georgia Tech MBE system.

After the Be source was recalibrated, another hybrid Read structure was grown. The target profile for this run (F0406) was similar to a previous run (E0512) in which a maximum output power of 41 mW had been obtained. An output power of 540 mW was obtained with material F0406 as discussed in the Rf section.

SECTION VI

DEVICE FABRICATION

Fabrication of diodes from epitaxial material consists of wafer thinning, metalization of both sides, and die delineation by etching. Figure 23 shows the GaAs thickness and metalization scheme used at Georgia Tech. Gold plated heat sinks were chosen to optimize heat sinking and to facilitate possible thermocompression chip bonding.

Ohmic contacts to both sides of the material are required as shown. Contact to the p^+ layer is accomplished by an RF sputter deposited trimetal system of PT-Ti-Au. The contact to the n^+ material is Au-GeNi, Au evaporated to the thicknesses indicated and then alloyed at 440°C for 20 seconds.

A flow chart of the complete fabrication procedure is shown in Figure 24. Many of these steps are standard; however, several steps are unique to high frequency IMPATT processing and will be described below.

GaAs thinning to less than 10 μm is performed to minimize undercutting of the back contact when etched. Thickness measurements requiring an accuracy on the order of 1 μm are difficult to make with conventional means. To facilitate this measurement, a dot pattern consisting of 7 mil diameter dots on 0.032 inch centers is delineated on the p side of the wafer. Holes are then etched 10 μm deep using methanol: hydrogen

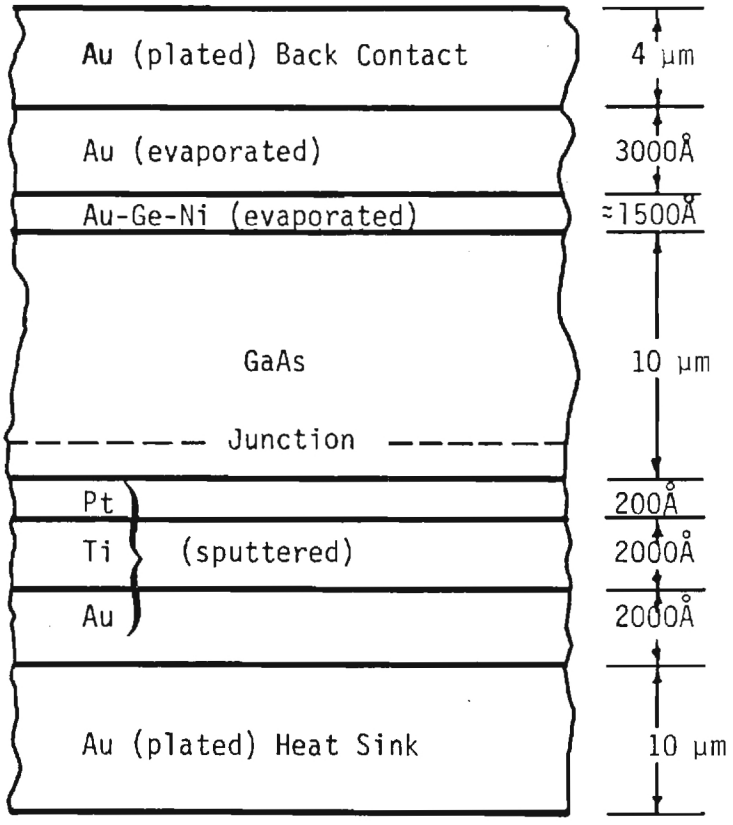

Figure 23. Material Structure for IMPATT Diodes.

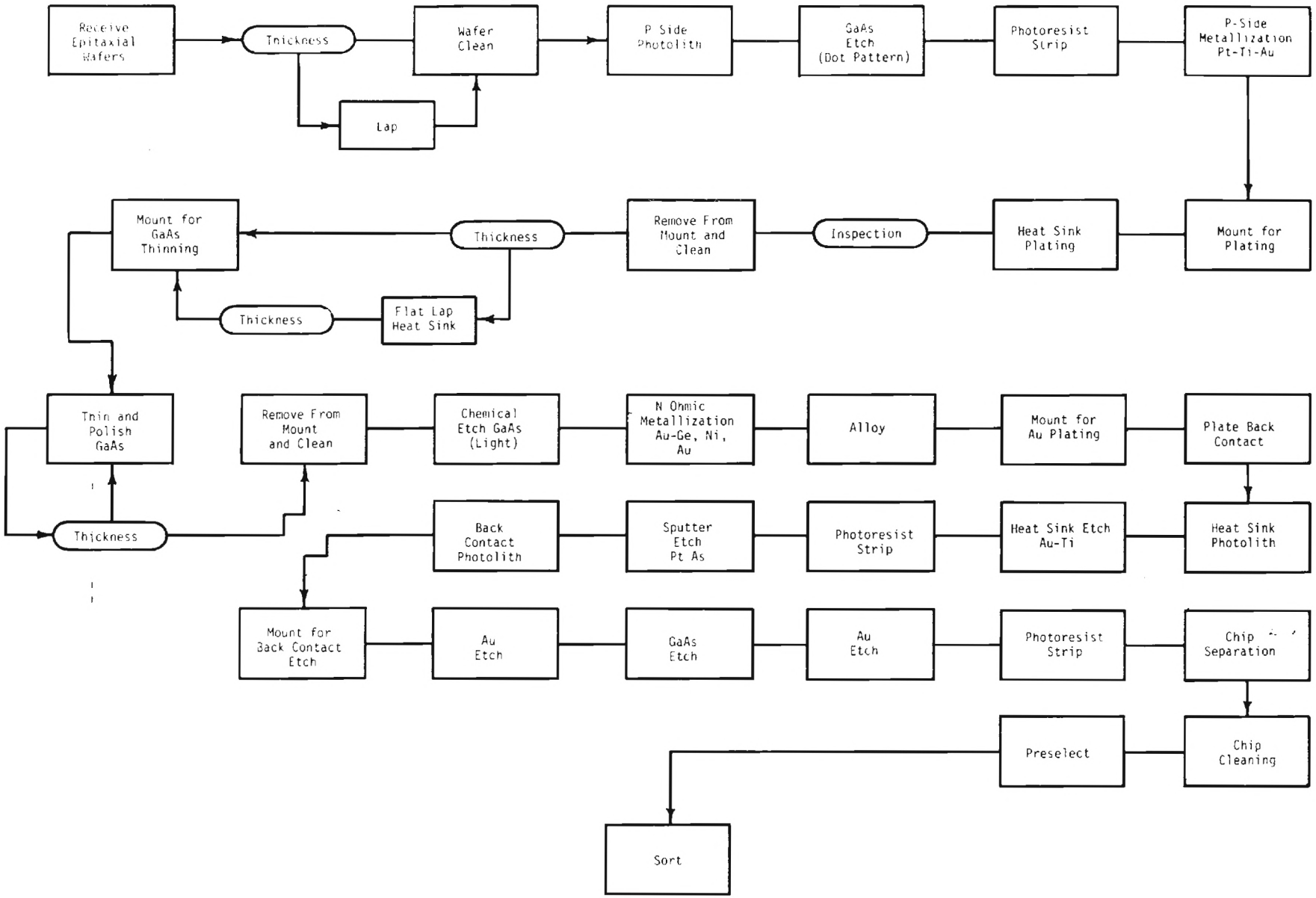

Figure 24.Process Flow Chart for Double Drift IMPATT Diodes

peroxide:phosphoric acid in the ratio 1:1:1. During the wafer thinning and polishing process, the appearance of the dots indicates completion of the process.

Target materials of 99.999% purity, mounted in a Perkin-Elmer, (model 2400) sputtering system were used to form the ohmic contact to the p^+ material. All targets were presputtered for 2 min at 500 watts prior to substrate metalization. Platinum was deposited for 1.5 min at 150 watts, titanium for 25 min at 500 watts, followed by gold for 4 min at 500 watts.

Gold plating to form the diode heat sink is the next processing step. Devices normally processed at Georgia Tech are typically greater than 1 mil in thickness. As a result, any stresses imposed on the GaAs by the plating have little effect on the mechanical stability of the wafer. With thickness less than 0.5 mil, thermal expansion mismatches often cause severe warping of the wafer.

Periodic reverse current (PR) plating is a recognized procedure for reducing stress in plated layers. This procedure, which is used extensively in copper and silver plating, also has the reported advantages of substantial leveling of the base surface and improved uniformity on irregularly shaped samples [4]. Periodic reverse plating is a process wherein the plated layer is deplated during a periodic time interval which is short compared to the time interval in the forward direction. Although this procedure is common for silver and copper plating, literature concerning gold deposition by this method is limited.

Reid and Goldie [5] indicate that PR plating of gold has been performed using a simple cyanide electrolyte with 25-40 g/l of gold and 10 g/l of free potassium cyanide at a temperature of 60-75°C. Current density was specified at 1-15 mA/cm^2 with anodic to cathodic time ratio of 15:2. No actual plating and deplating times were given.

PR current plating requires a means of periodically exchanging the connections to the plating bath anode and cathode. Georgia Tech has developed a circuit which periodically reverses the anode and cathode potential and maintains desired forward and reverse plating currents.

Forward and reverse times were adjusted at 35 seconds and 5 seconds, respectively, while the forward and reverse current densities were maintained at 3 mA/cm^2 and 2.25 mA/cm^2. Plating rate was measured to be approximately 3.5 microns per hour.

After plating, the material was lapped and polished. Slices, 13 mils thick were mounted on a lapping fixture and thinned to 4 mils using a Mazur horizontal-action lapping machine. Further thinning to 10 microns was accomplished by a chemical mechanical operation utilizing a Beuhler polishing wheel saturated with a 1:4 Clorox-water etching solution. The appearance of the gold dot pattern indicates a final wafer thickness of 10 microns.

Figure 25 is a scale drawing of the mesa structure and the heat sink arrangement used for this effort. The iron oxide mask set consists of two IMPATTs fabricated on a common 5 x 10 mil heat sink. Front to back alignment is accomplishment by optically

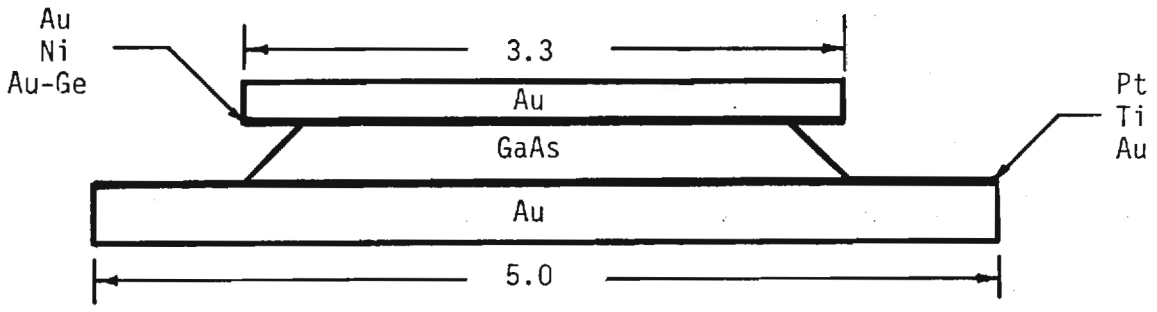

Dimensions in mils

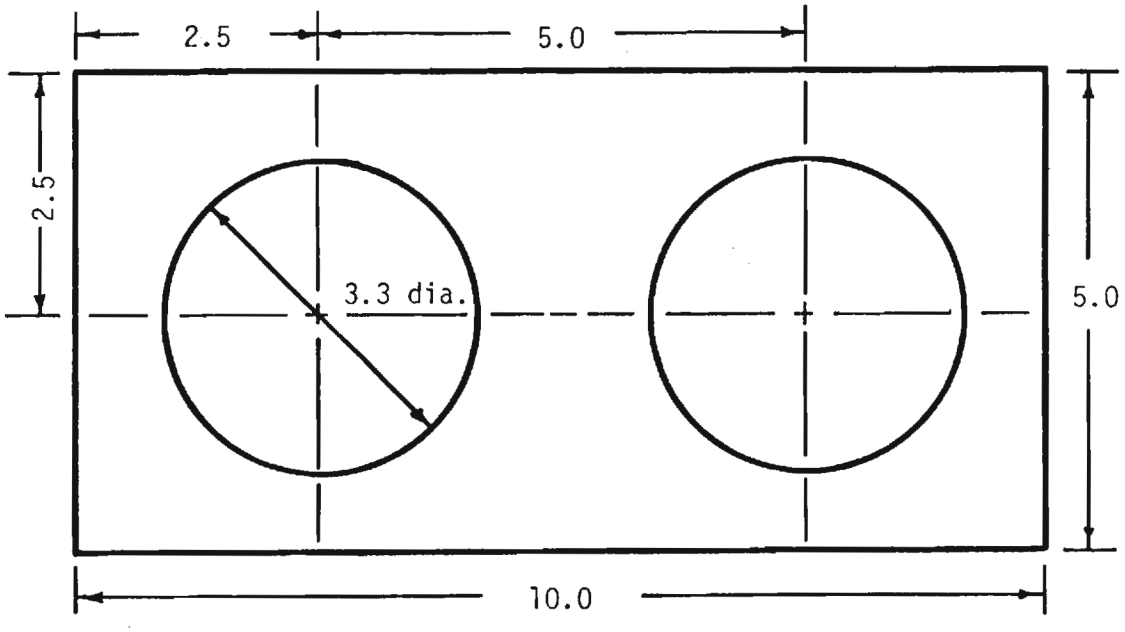

Figure 25. Mesa Structure and Heat Sink

aligning the heat sink-defined material to the heat sink mask and then aligning that assembly to the back contact mask.

Figure 26 shows SEM photographs of an actual mesa after completion of the processing steps. The jagged material around the heat sink edge is thought to be platinum which was not sufficiently removed prior to device separation. In some instances, this material can curl up and place a short between the heat sink and top contact (notice left chip). Most of the chips, however, showed essentially the same breakdown characteristics after processing as they did before.

The IMPATTs are then separated by cleaving thought the Au heat sink with a razor blade, stressed to 60 mA to eliminate those subject to premature burn out, and then mounted in standard EHF micropill package similar to that shown in Figure 27. Contact is made to the diode via a crossed wire connection. Each chip is then etched within the package until the overall capacitance is between .6 - .9 pF and RF tested using the equipment described in Section VII.

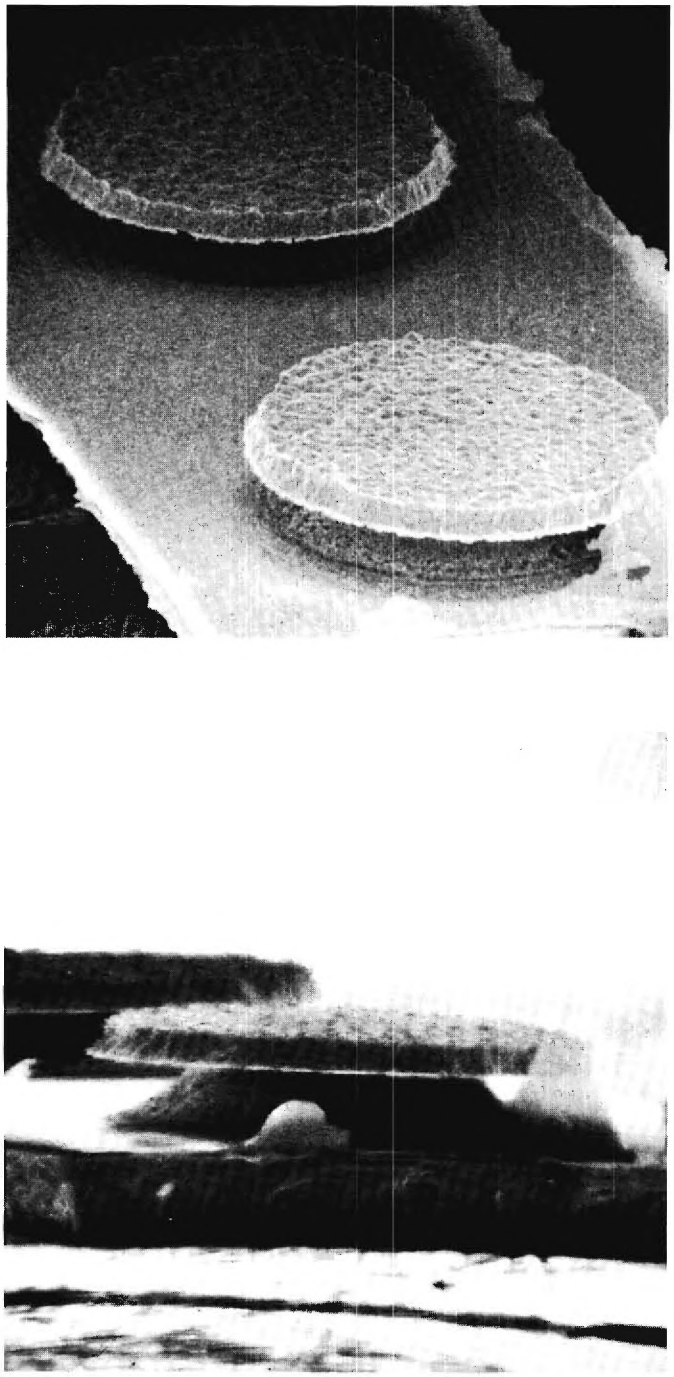

Figure 26. SEM photographs of IMPATT mesa.

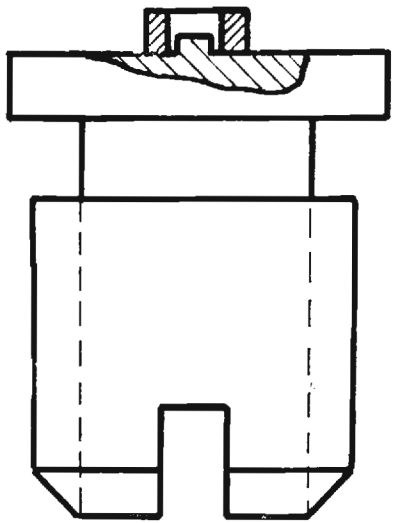

Standard Pedestal

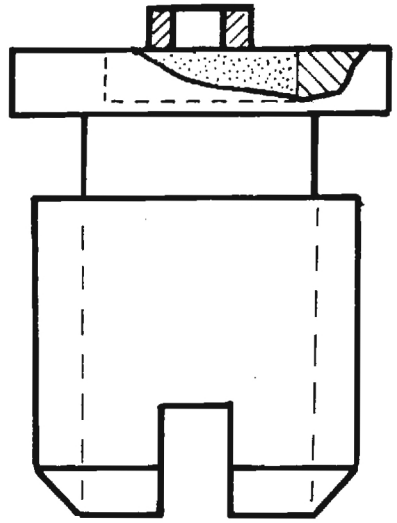

Embeded Diamond

Figure 27. Millimeter Wave IMPATT Packages.

SECTION VII

SPECIAL TEST FIXTURE AND EQUIPMENT

A special test set-up and several test fixtures were available during the program for evaluating IMPATTs between 26.5 and 40.0 GHz. Cross-sectional drawings if two typical fixtures are shown in Figure 28.

The Q-band structure proved to be the most versatile and was generally more adaptable for experimental purposes. The basic components of this fixture are the E-H tuner which is constructed within the main housing and employs teflon loaded dumbell shorts, the packaged diode which is mounted on a copper slug and positioned flush with the waveguide surface, the bias pin which contacts the diode and couples it to the waveguide, and the back short which is also constructed within the main housing and employees a teflon loaded waveguide short. Not shown is a low-pass filter constructed as a part of the outer conductor of the bias pin. The philosophy underlying this structure is simple in principle and easily understood. The portion of the center conductor within the waveguide acts as a post which couples the diode chip and mounting parasitics to the waveguide. The backshort, in principle, is adjusted to resonate the coupled impedance at the desired operating frequency. The E-H tuner is adjusted to provide the proper load impedance transformation to optimize output power at that frequency. The adjustments of the

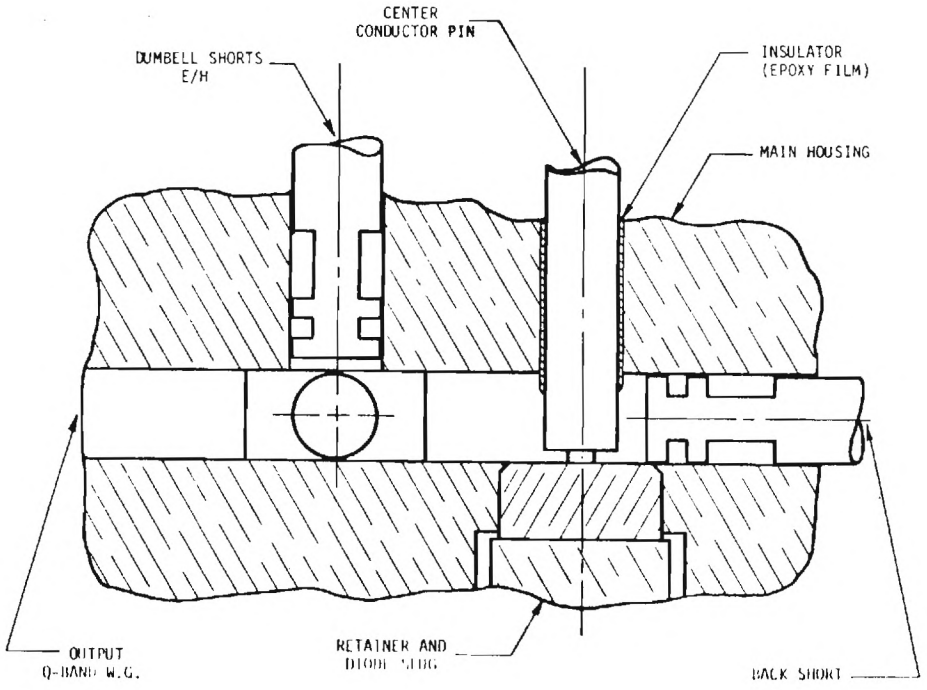

Figure 28a. Cross section of Q-Band Fixture.

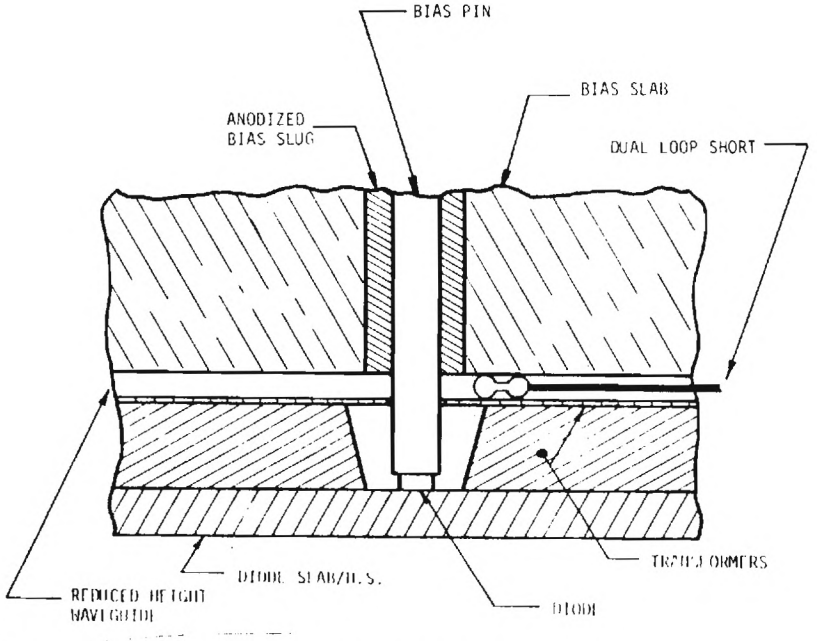

Figure 28b. Cross section of K_a-Band Test Fixture.

back short and E-H tuner are, of course, interrelated in practice and must be "tuned" concurrently.

The diameter of the center conductor is a circuit variable which effects oscillator performance. it has been found experimentally that a given diode will operate "best" with a certain size center conductor. Thus center conductors of various sizes have been constructed to optimize performance when testing diodes during development.

The K_a-band fixture was less versatile as a general evaluation tool. The basic components of this fixture are the reduced height waveguide section, the step transformer between the reduced height and full height waveguide (not shown), the tapered coaxial transformer, the diode mounted on the copper heat conducting slab, the iris transformer, the bias pin, and the back short. The reduced height transformer of this circuit serves the same function as the E-H tuner of the Q-band circuit. The transformation from the diode chip to the waveguide for this circuit is much more complicated and involves many more variables than does that for the other circuit. In addition, it has been observed that the K_a-band circuit works "best" when the diodes are embeded in an additional short section of low impedance line. These additional variables present problems when this circuit is used as a test fixture for the evaluation of diodes.

A special test set-up, purchased preassembled and precalibrated was used for evaluating diodes developed under the program. The overall equipment is shown in Figure 29. The set-up

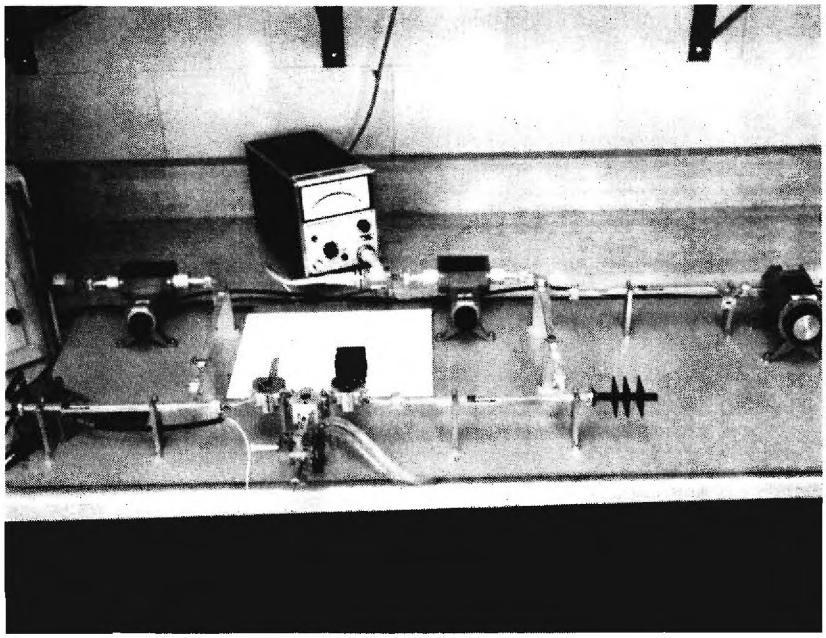

Figure 29. 26.5 to 40 GHz Dedicated Test Set-up.

is configured primarily for measurement of output power, spectrum and frequency, but also includes a five-port circulator assembly to allow injection locking experiments. The nominal set-up consists of .140" x .280" waveguide and covers the 26.5-40.0 GHz frequency range. Both of the oscillator circuits described above can be incorporated into the test set-up.

SECTION VIII

RE RESULTS

Although unknown at the time, the gallium source used to grow the IMPATT material become contaminated during the first part of the program and remained so during all but the latter few months. Sometime on or before 12 May 1982, the Ga source become contaminated with Be which effectively resulted in a high p-type background at the 10^{17} cm^{-3} level. This caused the intended lightly doped n-type drift layers to be p-type instead. Some of the hybrid-Read devices then showed three p-n junctions because of the added Be from the Ga source. After discovering the contamination, it was easy to understand the poor device performance obtained during much of the program and the difficulties encountered in the interpretation of impurity profile from C-V data.

Some of the earlier RF results are shown in Figure 30. These data are for a hybrid-Read device (E-0329) in which the spike was initially 200A wide with a peak impurity density contained within the spike was to be 2×10^{12} cm^{-2}. The RF results and breakdown voltage characteristics of device E0329 suggested that excess charge was contained between the junction and the n-type spike-drift interface. The other two devices, E0512 and E0622, represent structures in which the spike position was fixed and the amount of charge within the spike varied. The spike width of E0512 was kept at 200A and the impurity concentration reduced to

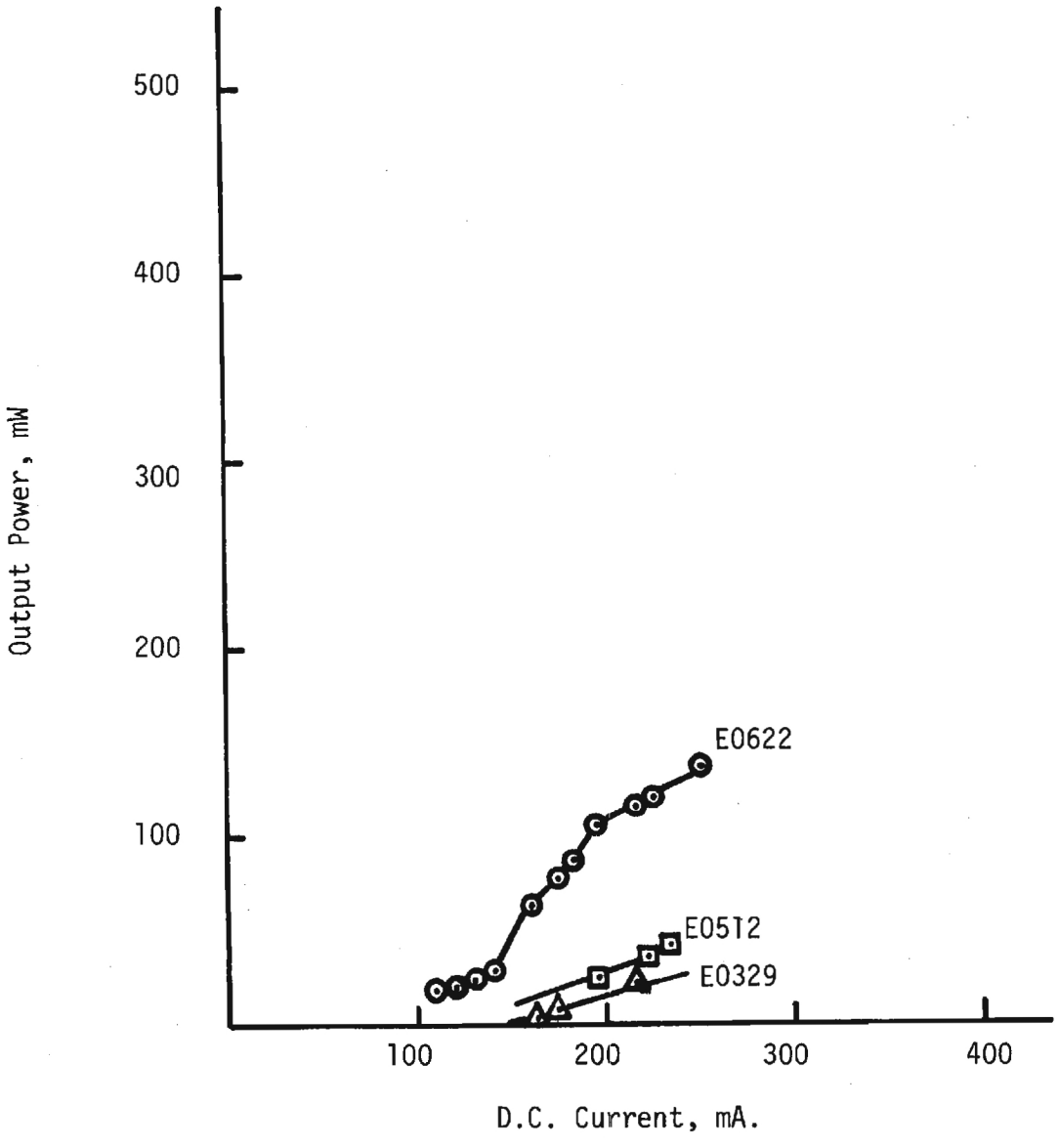

Figure 30. Early RF Results.

0.8×10^{18} cm^{-3}. The impurity concentration of the other device, E0622, was then kept at $.8 \times 10^{18}$ cm^{-3} and the spike width reduced to 100A. The RF output power progressively increased during this series of changes which suggested that the charge contained within the spike be reduced further.

Attempts to characterize the profile from C-V data, however, suggested that the system calibration may have changed. As a further check, a double drift flat-flat profile structure was grown. Attempts to evaluate its profile from C-V data suggested a much higher p-type concentration than that intended as discussed previously in Section V. The results of these attempts prompted the SIMS evaluation and the discovery that the system was and had been contaminated for a indefinite period of time.

After cleaning, reloading, and recalibrating the Si and Ga sources, another hybrid-Read structure was grown. The target profile for this run (F0406) was similar to a previous run (E0512) which yielded a maximum of 41 mW at 200 mA. Output power vs bias current for selected devices made from F0406 material is shown in Figure 31. One device gave 540 mW at 37.2 GHz when biased to 340 mA.

The data of Figure 31 actually represent the best results obtained from a group of 14 devices and illustrate an inherent problem we encountered in material optimization. Of the first 14 devices tested, only five yielded a output power greater than 200 mW. Of these two, only one yielded an output power greater than 350 mW. This single device, the last tested, yielded 540 mW which

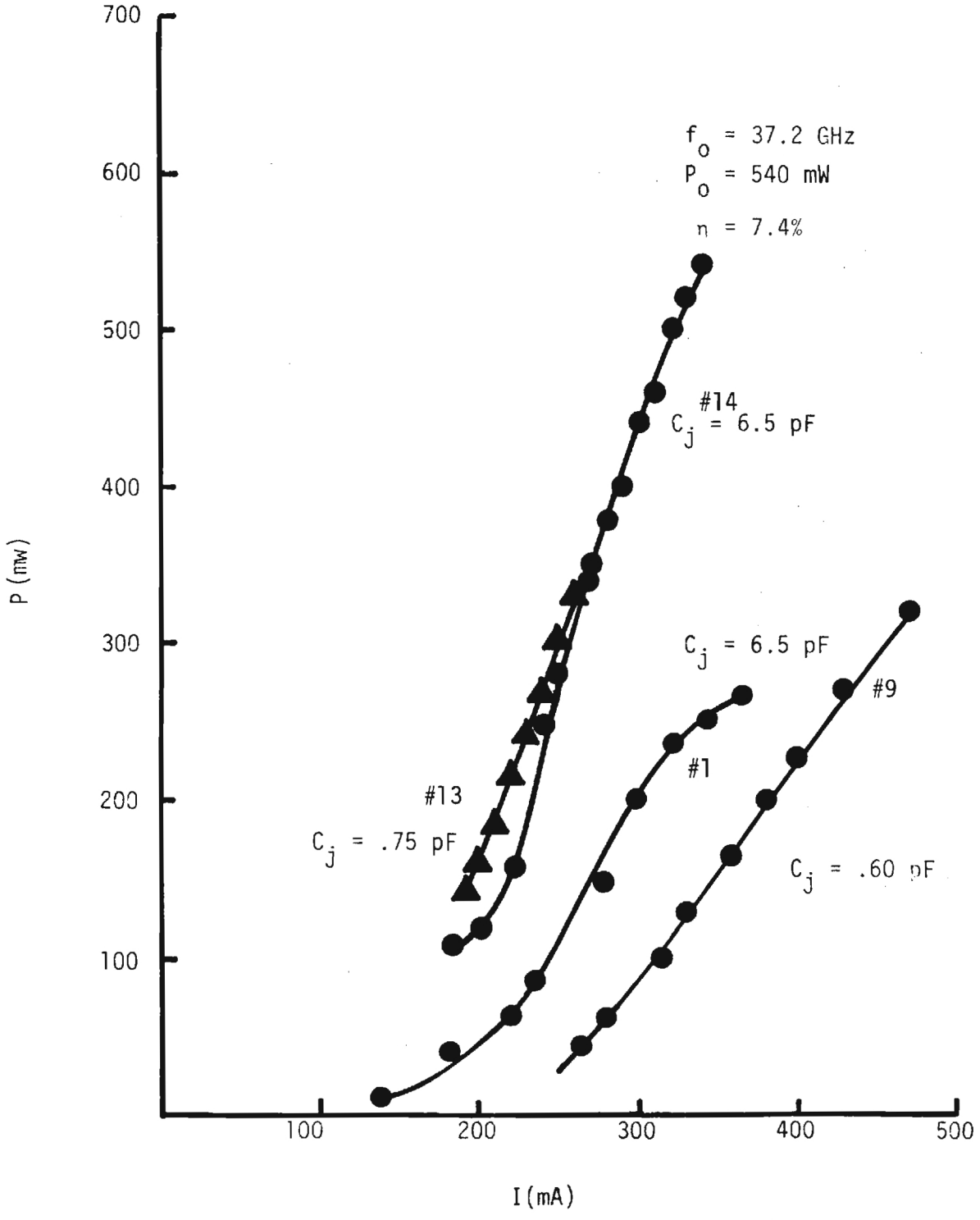

Figure 31. Experimental Data of Output Power vs Bias Current for F0406 devices.

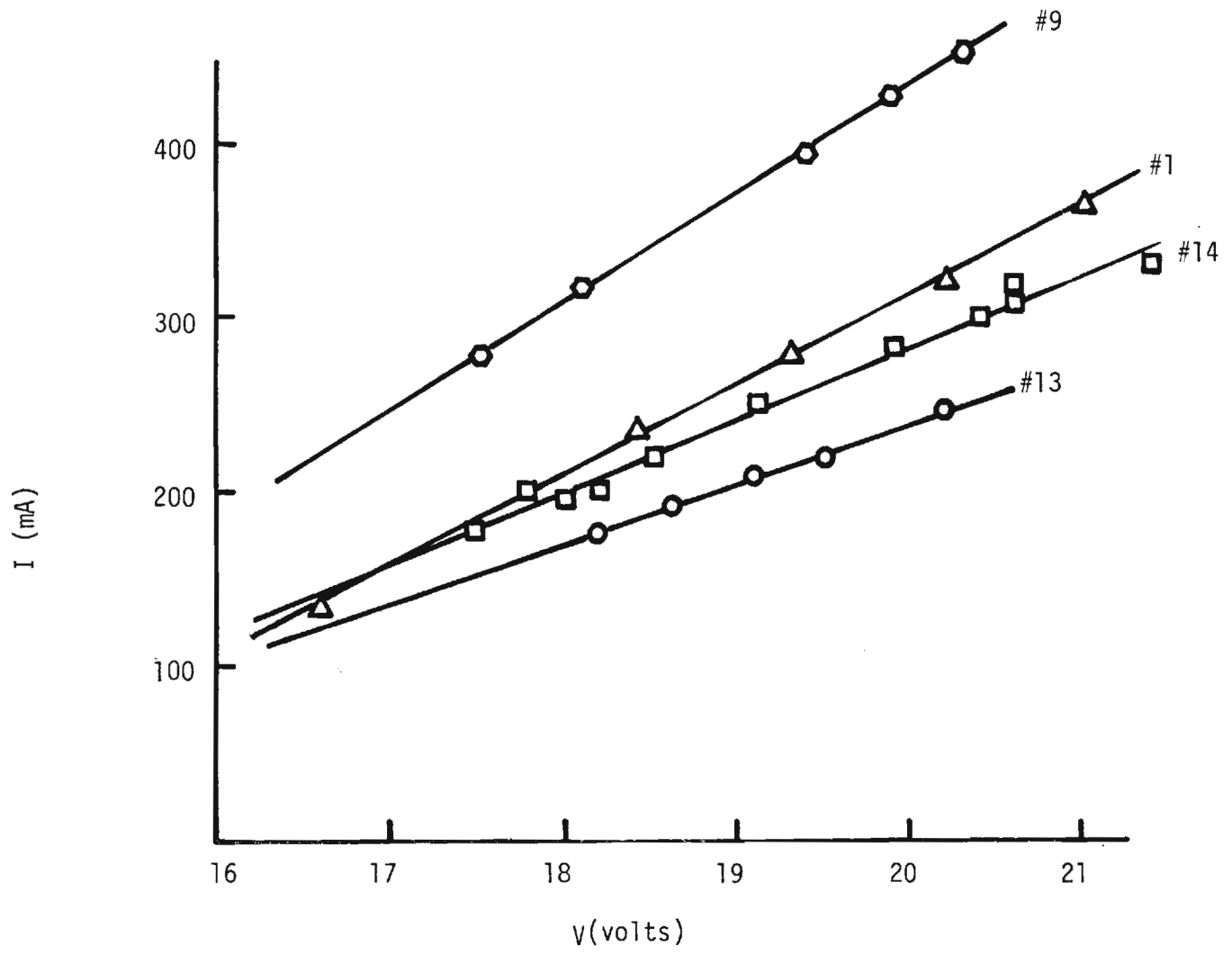

Figure 32. I-V Characteristics of F0406 Devices whose Output Power is shown in Figure 31.

is 50% more, than the next best. This raises the question: at what point does one stop testing devices from a particular run?

The breakdown voltage of packaged devices made from a particular material proved to be very consistent. For example, all breakdown voltages (at 1 mA) of the 14 devices made from F0406 material were 13.9 + .1 volts. Although every effort was made to mount each chip in a similar manner, the packaged devices were dissimilar in their RF and large current dc characteristics. The data plotted in Figure 32, shows the dc I-V characteristics for the F0406 devices whose output power is plotted in Figure 31. For negligible loss one would expect device #9 to have the lowest thermal resistance and #13 to have the highest since the slope of the I-V curve is equal to $1/R_{th} + 1/R_{SC}$ where R_{th} is the thermal resistance and R_{SC} is the space charge resistance (assumed constant). The output power characteristics of Figure 33, however, are inconsistant with the implied relative thermal resistances of Figure 32.

The differences between devices are probably due to those introduced during the chip mounting and contacting steps. The chip was soldered in a standard EHF pedestal package similar to that shown in Figure 27 using a solder preform and an RF induction heater. Preformed ribbons in the shape of a cross were then TC bonded to the top contact of the chip and the top contact of the metalized ceramic package. The best IMPATT devices available commercially use chips mounted on type 11A diamond embedded in a specially designed package. The chips, of beam lead

construction, are TC bonded to the metalized surface of the embedded diamond by a method which minimizes mechanical stress and leads to more uniform devices. In addition, the thermal resistance is significantly lower (can be as much as 50%) with the chip TC bonded to a well designed diamond heat sink.

Figure 33 illustrates what one might expect from the F0406 chips when mounted in a diamond package with a thermal resistance of about 28^{o}C/watt compared with what actually achieved with the standard pedestal mount with the thermal resistance of about 40^{o}C/W. As seen, this chip would be expected to produce approximately 825 mw when mounted on a diamond heatsink.

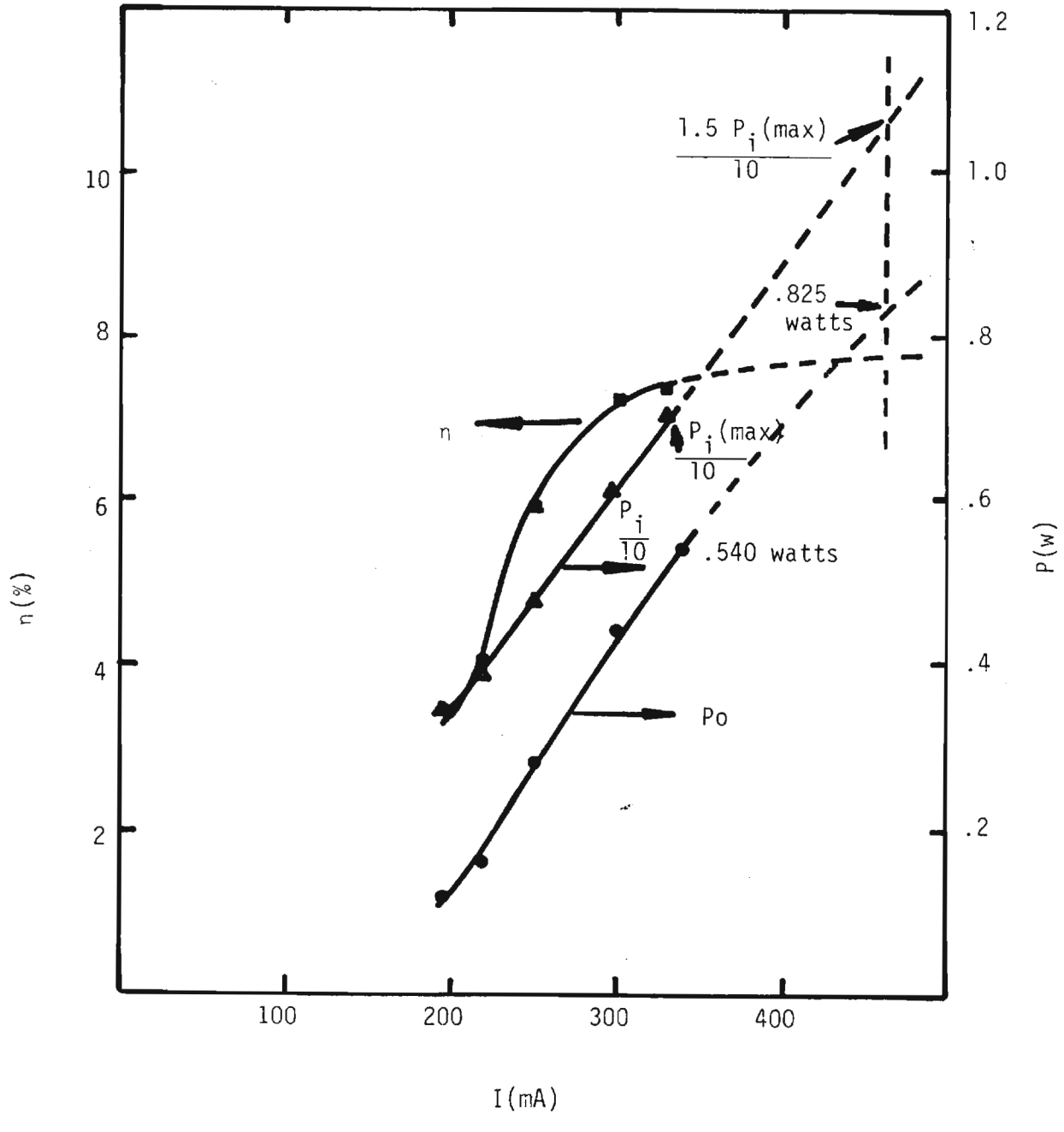

Figure 33. Expected Results using F0406 chips in Diamond Package.

SECTION IV

CONCLUSIONS AND RECOMMENDATIONS

The computer program QSTATIC included in appendix A can be used for computer simulations of the RF characteristics of millimeter wave IMPATTs. These computer simulations have been used to help establish a set of material parameters that optimize device performance. Unfortunately, many of the iterations of material growth, device fabrication and RF testing were performed on material that is now in doubt because of Be contamination of the Ga source.

The breakdown voltage of packaged devices and unpackaged chips from a particular run were always very consistent. Also, the consistency observed in the SIMS profiles of the Si doping indicate that the MBE material can be very well controlled to produce the desired profiles for millimeter IMPATT devices. This consistency conflicts with the wide range of RF and large current dc characteristics observed on even the best devices. We conclude, therefore, that the packaging methods used introduced wide variations in the devices even though the methods were applied consistently.

Any further work on MBE material for millimeter IMPATTs should include a heavy emphasis on the packaging problems of these devices. When the RF testing of the devices is used as the final and most important evaluation of the material, the device fabrication procedures must be eliminated as a parameter before

real confidence can be obtained in the material evaluation.

APPENDIX A

Computer Program QSTATIC

```
00100 PROGRAM QSTATIC(INPUT,OUTPUT,TAPE5=INPUT,TAPE6=OUTPUT,TAPE10)
00110 DIMENSION X(201),E(201),ALP2(201),ALP1(201),SUMN(201),ESC(201,10),VSC(10)
00120 DIMENSION EI(100),SUM0(100),A2(201),B2(201),A1(201),B1(201),ET(201,10)
00130 DIMENSION ESC(201,10),AMTAU(10),D0(10),D1(10),DT(10),DELTE(10),T(10)
00140 DIMENSION E0(201),ESC0(201),ESCT(201,100),TA(12)
00150 REAL ND(201),J1(201),J2(201),J0V(10),J0VA(12),J1V(10),J2V(10)
00160 REAL JEV(10),J0VXT(201,10),J1VXT(201,10),J2VXT(201,10)
00170 REAL J0VD
00180 REAL XR(101),XL(101),QR(101),QL(101),EQ(201),EQR(201),EQL(201)
00190 REAL XL(101),XR(101),VR(101),VL(101),W(101),C(101),V(101)
00200 REAL NR(101),NL(101)
00210 REAL E(101),ET(101),N(101)
00220 REAL NAL,NAR,NSL,NSR,NDL,NDR,NTL,NTR,NBL,NBR
00230 REWIND 10
00240 WRITE(6,1000)
00250 1000 FORMAT(//1X,*ARE YOU FAMILIAR WITH DIODE MODEL? YES(1),NO(0)*)
00260 READ(5,*) IFLAG
00270 IF(IFLAG.EQ.1) GO TO 334
00280 WRITE(6,10)
00290 10 FORMAT(6X,//* THIS PROGRAM CALCULATES AVALANCHE VOLTAGE, TOTAL */
00300+ * VOLTAGE, CONDUCTANCE, SUSCEPTANCE, OUTPUT POWER, AND */
00310+ * EFFICIENCY FOR A READ-READ DOUBLE DRIFT DEVICE.  THE */
00320+ * STRUCTURE AND NOMENCLATURE FOR EACH HALF IS SHOWN IN */
00330+ * THE FOLLOWING SKETCH.*///
00340+,T9,*NB:*,T35,*----------------------*)
00350 DO 20 I=1,5
00360 WRITE(6,30)
00370 30 FORMAT(1X,T11,*:*,T35,*I*)
00380 20 CONTINUE
00390  WRITE(6,40)
00400 40 FORMAT(1X,T9,*NS*,T11,*:*,T15,*---*,T35,*I*)
00410 DO 50 I=1,2
00420 WRITE(6,60)
00430 60 FORMAT(1X,T11,*:*,T15,*I.I*,T35,*I*)
00440 50 CONTINUE
00450 WRITE(6,70)
00460 70 FORMAT(1X,T11,*: ->I.I<- WS*,T35,*I*)
00470 DO 80 I=1,3
00480 WRITE(6,60)
00490 80 CONTINUE
00500 WRITE(6,90)
00510 90 FORMAT(1X,T9,*NT*,T11,*:*,T12,*   I.I     *,*       -----I*)
00520 DO 100 I=1,5
00530 WRITE(6,105)
00540 105 FORMAT(1X,T11,*:*,T15,*I.I*,T30,*I     .*)
00550 100 CONTINUE
00560 WRITE(6,110)
00570 110 FORMAT(1X,T9,*NA*,T11,*:*,T12,*----.I*,T30,*I     .*)
00580 DO 120 I=1,5
00590 WRITE(6,130)
00600 130 FORMAT(1X,T11,*:*,T16,*.I*,T30,*I*,T35,*.*)
```

```
00610 120 CONTINUE
00620 WRITE(6,140)
00630 140 FORMAT(1X,T9,*ND*,T11,*:*,T14,*  .--------------     .*)
00640 DO 150 I=1,5
00650 WRITE(6,160)
00660 160 FORMAT(1X,T11,*:*,T16,*.*,T30,*.*,T35,*.*)
00670 150 CONTINUE
00680 WRITE(6,170)
00690 170 FORMAT(1X,T11,*.....................................................*)
00700 WRITE(6,180)
00710 180 FORMAT(1X,T11,*0*,T16,*XS*,T29,*XD*,T34,*XT*///)
00720 WRITE(6,190)
00730 190 FORMAT(1X,*     IN THIS FIGURE:*/
00740+*          NB IS THE BUFFER OR SUBSTRATE DOPING*/
00750+*          NS IS THE SPIKE DOPING*/
00760+*          NT IS THE TERMINATION LAYER DOPING*/
00770+*          NA IS THE AVALANCHE REGION DOPING*/
00780+*          ND IS THE DRIFT REGION DOPING*/
00790+*          WS IS THE SPIKE WIDTH*/
00800+*          XS IS THE SPIKE POSITION*/
00810+*          XD IS THE DEPLETION/TERMINATION INTERFACE POSITION*/
00820+*          XT IS THE TERMINATION/ BUFFER INTERFACE POSITION*/
00830+*  */
00840+*  */
00850+*    LEFT AND RIGHT HALF QUANTITIES ARE DENOTED WITH L AND R*/
00860+* SUBSCRIPTS, I.E., NAL AND NAR ARE LEFT AND RIGHT AVALANCHE*/
00870+* REGION DOPINGS.*/
00880+*  */
00890+*  */
00900+*     HYBRID-READ AND UNIFORMLY DOPED DOUBLE DRIFT DEVICES*/
00910+* CAN BE SIMULATED BY LETTING NA=NS=ND FOR THE APPROPIATE REGIONS.*//)
00920 334 PI=4.*ATAN(1.)
00930 Q=1.6E-19
00940 EP=12.5E-11/(36.*PI)
00950 AREA=4.5E-5
00960 WRITE(6,200)
00970 200 FORMAT(/1X,*INPUT DATA-- DOPINGS(E16),DISTANCES(E-4)*//)
00980 WRITE(6,1010)
00990 1010 FORMAT(1X,*IS INPUT ON TAPE(10) OR TERMINAL(5)?*)
01000 READ(5,*) INPT
01010 WRITE(6,210)
01020 210 FORMAT(//1X,*WHAT ARE THE VALUES FOR NAL AND NAR?*)
01030 READ(INPT,*) NAL,NAR
01040 IF(INPT.EQ.10) WRITE(6,*) NAL,NAR
01050 1020 FORMAT(1X,2F15.3)
01060 NAL=NAL*1.E16
01070 NAR=NAR*1.E16
01080 WRITE(6,220)
01090 220 FORMAT(1X,*NSL,NSR?*)
01100 READ(INPT,*) NSL,NSR
01110 IF(INPT.EQ.10) WRITE(6,*) NSL,NSR
01120 NSL=NSL*1.E16
01130 NSR=NSR*1.E16
01140 WRITE(6,230)
01150 230 FORMAT(1X,*NDL,NDR?*)
01160 READ(INPT,*) NDL,NDR
01170 IF(INPT.EQ.10) WRITE(6,*) NDL,NDR
01180 NDL=NDL*1.E16
01190 NDR=NDR*1.E16
01200 WRITE(6,240)
01210 240 FORMAT(1X,*NTL,NTR?*)
01220 READ(INPT,*) NTL,NTR
01230 IF(INPT.EQ.10) WRITE(6,*) NTL,NTR
01240 NTL=NTL*1.E16
01250 NTR=NTR*1.E16
01260 WRITE(6,250)
```

```
01270 250 FORMAT(1X,*NBL,NBR?*)
01280 READ(INPT,*) NBL,NBR
01290 IF(INPT.EQ.10) WRITE(6,*) NBL,NBR
01300 NBL=NBL*1.E16
01310 NBR=NBR*1.E16
01320 WRITE(6,260)
01330 260 FORMAT(1X,*WHAT ARE THE POSITIONS OF THE SPIKES?*)
01340 READ(INPT,*) XSL,XSR
01350 IF(INPT.EQ.10) WRITE(6,*) XSL,XSR
01360 XSL=XSL*1.E-4
01370 XSR=XSR*1.E-4
01380 WRITE(6,265)
01390 265 FORMAT(1X,*WHAT ARE THE WIDTHS OF THE SPIKES?*)
01400 READ(INPT,*) WSL,WSR
01410 IF(INPT.EQ.10) WRITE(6,*) WSL,WSR
01420 WSL=WSL*1.E-4
01430 WSR=WSR*1.E-4
01440 WRITE(6,270)
01450 270 FORMAT(1X,*XDL,XDR?*)
01460 READ(INPT,*) XDL,XDR
01470 IF(INPT.EQ.10) WRITE(6,*) XDL,XDR
01480 XDL=XDL*1.E-4
01490 XDR=XDR*1.E-4
01500 WRITE(6,280)
01510 280 FORMAT(1X,*XTL,XTR?*)
01520 READ(INPT,*) XTL,XTR
01530 IF(INPT.EQ.10) WRITE(6,*) XTL,XTR
01540 XTL=XTL*1.E-4
01550 XTR=XTR*1.E-4
01560 XR(1)=0.
01570 XL(1)=0.
01580 DELTX=.01E-4
01590 NR(1)=NAR
01600 NL(1)=NAL
01610 VR(1)=0.
01620 VL(1)=0.
01630 QR(1)=0.
01640 QL(1)=0.
01650 DO 290 I=2,101
01660 XR(I)=DELTX*FLOAT(I-1)
01670 XL(I)=DELTX*FLOAT(I-1)
01680 NR(I)=NAR
01690 IF(XR(I).GT.(XSR-WSR/2.)) NR(I)=NSR
01700 IF(XR(I).GT.(XSR+WSR/2.)) NR(I)=NDR
01710 IF(XR(I).GT.XDR) NR(I)=NTR
01720 IF(XR(I).GT.XTR) NR(I)=NBR
01730 NL(I)=NAL
01740 IF(XL(I).GT.(XSL-WSL/2.)) NL(I)=NSL
01750 IF(XL(I).GT.(XSL+WSL/2.)) NL(I)=NDL
01760 IF(XL(I).GT.XDL) NL(I)=NTL
01770 IF(XL(I).GT.XTL) NL(I)=NBL
01780 QR(I)=QR(I-1)+(NR(I)+NR(I-1))*DELTX/2.
01790 QL(I)=QL(I-1)+(NL(I)+NL(I-1))*DELTX/2.
01800 VR(I)=VR(I-1)+(XR(I)*NR(I)+XR(I-1)*NR(I-1))*DELTX/2.
01810 VL(I)=VL(I-1)+(XL(I)*NL(I)+XL(I-1)*NL(I-1))*DELTX/2.
01820 EQL(I)=Q*QL(I)/EP
01830 EQR(I)=Q*QR(I)/EP
01840 290 CONTINUE
01850 K=0
01860 DO 300 I=2,101
01870 K=K+1
01880 IF(QR(I).LT.QL(I)) GO TO 330
01890 DO 310 L=I,101
01900 IF(QR(L).LT.QL(I)) GO TO 310
01910 DXL=(XR(L)-XR(L-1))*(QR(L)-QL(I))/(QR(L)-QR(L-1))
01920 W(K)=XL(I)+XR(L)-DXL
```

```
01930 V(K)=VL(1)+VR(L)-(XR(L)*NR(L)+XR(L-1)*NR(L-1))*DXL/2.
01940 IF(QR(L).GT.QL(I)) GO TO 320
01950 310 CONTINUE
01960 GO TO 320
01970 330 CONTINUE
01980 DO 340 L=2,I
01990 IF(QL(L).LT.QR(I)) GO TO 340
02000 DYL=(XL(L)-XL(L-1))*(QL(L)-QR(I))/(QL(L)-QL(L-1))
02010 W(K)=XR(I)+XL(L)-DYL
02020 V(K)=VR(I)+VL(L)-(XL(L)*NL(L)+XL(L-1)*NL(L-1))*DYL/2.
02030 IF(QL(L).GT.QR(I)) GO TO 320
02040 340 CONTINUE
02050 320 CONTINUE
02060 300 CONTINUE
02070 E(1)=0.
02080 V(1)=0.
02090 DO 370 I=1,200
02100 X(I)=DELTX*FLOAT(I)
02110 IF(I.LT.100) EQ(I)=EQL(101-I)
02120 IF(I.GE.100) EQ(I)=EQR(I-99)
02130 370 CONTINUE
02140 TEMP=22.
02150 AVG=2.*2222.2222
02160 EPINV=1./EP
02170 V1=6.E+6
02180 V2=6.E+6
02190 NPX=200
02200 DO 73 I=1,NPX
02210 A1(I)=1.85E+5*(1.+.07*(TEMP-22.)/100.)
02220 A2(I)=4.10E+5*(1.+.07*(TEMP-22.)/100.)
02230 B1(I)=5.79E+5*(1.+.11*(TEMP-22.)/100.)
02240 B2(I)=6.34E+5*(1.+.11*(TEMP-22.)/100.)
02250 73 CONTINUE
02260 M1=2
02270 M2=2
02280 IFLAG=0
02290 JJ=2
02300 EI(1)=4.0E+5
02310 EI(2)=1.1*EI(1)
02320 LL=2
02330 DELTE(1)=0.
02340 DELTE(2)=1.
02350 380 CONTINUE
02360 IFLAG=IFLAG+1
02370 DO 390 J=1,100,1
02380 EI(1)=EI(JJ-1)
02390 EI(2)=EI(JJ)
02400 IF(J.GT.2) EI(J)=EI(J-1)-ALOG(SUMO(J-1))*(EI(J-1)-EI(J-2))/
02410+(ALOG(SUMO(J-1))-ALOG(SUMO(J-2)))
02420 SUM1=0.
02430 SUM2=0.
02440 SUM3=0.
02450 SUM4=0.
02460 J1(1)=0.0
02470 J2(1)=ABS(1.-J1(1))
02480 SUMN(1)=0.0
02490 VOLT=0.0
02500 VOLTA=0.0
02510 E(1)=EI(J)-EQ(1)
02520 EO(1)=E(1)+ESC(1,1)
02530 IF(EO(1).LT.1.E-5) EO(1)=1.E-6
02540 B1OE=B1(1)/EO(1)
02550 B2OE=B2(1)/EO(1)
02560 IF(B2OE.GT.25.) B2OE=25.
02570 IF(B1OE.GT.25.) B1OE=25.
02580 ALP1(1)=A1(1)*EXP(-B1OE**M1)
```

```
02590 ALP2(I)=A2(I)*EXP(-B2OE**M2)
02600 DO 400 I=2,NPX,1
02610 E(I)=EI(J)-EQ(I)
02620 EO(I)=E(I)+ESC(I,1)
02630 IF(EO(I).GT.1.E-5.AND.EO(I-1).LT.1.E-5) IL=I-1
02640 IIL=IL+1
02650 XL=X(IL)
02660 IF(EO(I).LT.1.E-5.AND.EO(I-1).GT.1.E-5) IR=I
02670 XR=X(IR)
02680 IF(EO(I).LT.1.E-5) EO(I)=1.E-6
02690 B1OE=B1(I)/EO(I)
02700 B2OE=B2(I)/EO(I)
02710 IF(B2OE.GT.25.) B2OE=25.
02720 IF(B1OE.GT.25.) B1OE=25.
02730 ALP1(I)=A1(I)*EXP(-B1OE**M1)
02740 ALP2(I)=A2(I)*EXP(-B2OE**M2)
02750 A2M1=(ALP2(I)-ALP1(I)+ALP2(I-1)-ALP1(I-1))/2.
02760 TERM1=A2M1*DELTX
02770 SUM11=SUM1
02780 SUM1=SUM1+TERM1
02790 TERM2=(ALP1(I)*EXP(SUM1)+ALP1(I-1)*EXP(SUM11))*DELTX/2.
02800 TERM3=(ALP2(I)*EXP(SUM1)+ALP2(I-1)*EXP(SUM11))*DELTX/2.
02810 SUM2=SUM2+TERM2
02820 SUM3=SUM3+TERM3
02830 SUMN(I)=SUM2
02840 J1(I)=SUM3*EXP(-SUM1)
02850 J2(I)=ABS(1.-J1(I))
02860 IF(J1(I).GT..854.AND.J1(I-1).LT..854) XM1=X(I-1)+
02870+(.854-J1(I-1))*(X(I)-X(I-1))/(J1(I)-J1(I-1))
02880 IF(J2(I).LT..854.AND.J2(I-1).GT..854) XM2=X(I-1)+
02890+(.854-J2(I-1))*(X(I)-X(I-1))/(J2(I)-J2(I-1))
02900 TERMV=(EO(I)+EO(I-1))*DELTX/2.
02910 VOLT=VOLT+TERMV
02920 IF(J1(I).GT..05.AND.J2(I).GT..05) VOLTA=VOLTA+TERMV
02930 400 CONTINUE
02940 SUMO(J)=SUM2
02950CWRITE(6,3333) SUM2,EI(J)
02960 3333 FORMAT(1H ,2F15.4,2I5)
02970 IF(J.GT.3) JJ=J
02980 IF(ABS(SUM2-1.).LT.1.E-2.AND.J.GT.3) GO TO 410
02990 390 CONTINUE
03000 410 CONTINUE
03010 SUM4=0.
03020 ESC(1,1)=SUM4
03030 ESCO(1)=ESC(1,1)
03040 TMAXO=ABS(ESCO(1)-ESC(1,1))
03050 DO 420 I=2,NPX
03060 ESCO(I)=ESC(I,1)
03070 TERM=EPINV*AVG*((J1(I-1)+J1(I))/V1-
03080+(J2(I-1)+J2(I))/V2)*DELTX/2.
03090 IF(EO(I).LT.1.E-5) TERM=0.
03100 SUM4=SUM4+TERM
03110 ESC(I,1)=SUM4
03120 ESCT(I,IFLAG)=ESC(I,1)
03130 IF(MOD(IFLAG,3).EQ.1.AND.IFLAG.GT.1) ESC(I,1)=ESCT(I,IFLAG)-
03140+(ESCT(I,IFLAG)-ESCT(I,IFLAG-1))**2/(ESCT(I,IFLAG)-2.*
03150+ESCT(I,IFLAG-1)+ESCT(I,IFLAG-2)+1.E-5)
03160 TMAX=ABS(ESCO(I)-ESC(I,1))
03170 IF(TMAX.LT.TMAXO) TMAX=TMAXO
03180 420 CONTINUE
03190 IF(TMAX.LT.1.E-2.AND.IFLAG.GT.2) GO TO 430
03200 GO TO 380
03210 430 DO 440 I=1,NPX,1
03220 XD=1.E4*X(I)
03230 EF=1.E-5*EO(I)
03240 EFSC=1.E-5*ESC(I,1)
```

```
03250CIF(MOD(I,5).EQ.0) WRITE(6,2222) XO,J1(I),J2(I),EF,EFSC
03260 2222 FORMAT(1X,6F10.4)
03270 440 CONTINUE
03280 WRITE(6,5555)
03290 5555 FORMAT(//)
03300 CUR=AVG*AREA*1.E3
03310 WRITE(6,3737) VOLTA
03320 3737 FORMAT(1X,*AVALANCHE VOLTAGE =*,F7.2,* VOLTS*)
03330 WRITE(6,450) VOLT
03340 450 FORMAT(1X,*TOTAL VOLTAGE      =*,F7.2,* VOLTS*)
03350 WRITE(6,460) CUR
03360 460 FORMAT(1X,*CURRENT            =*,F7.2,* MA*)
03370 FREQ=40.
03380 WRITE(6,2000) FREQ
03390 2000 FORMAT(1X,*FREQUENCY          =*,F7.2,* GHZ*//)
03400CGO TO 5000
03410 NPT=10
03420 NPTA=NPT+2
03430 DELTT=1./FLOAT(NPT-1)
03440 DO 470 J=1,NPT
03450 T(J)=DELTT*FLOAT(J-1)
03460 470 CONTINUE
03470 WRITE(6,92)
03480 92 FORMAT(1X,*  VRF/VDC       G          B          PO       PIN*,
03490+*       EFF.*)
03500 WRITE(6,91)
03510 91 FORMAT(1X,*     (%)      (MMHOS)   (MMHOS)   (WATTS)   (WATTS)*,
03520+*    (%)*/)
03530 DO 3000 III=1,6
03540 VFACT=.1*FLOAT(III)
03550 VO=VFACT*VOLT
03560 AJO=AVG
03570 DO 480 J=1,NPT
03580 D1(J)=0.
03590 480 CONTINUE
03600 IFLAGA=0
03610 IFLAG2=0
03620 IFLAG3=0
03630 IFREQ=40
03640 FREQ=FLOAT(IFREQ)
03650 TAU=1.E-9/FREQ
03660 DO 490 M=1,50
03670 IFLAG3=IFLAG3+1
03680 DO 500 J=1,NPT
03690 DO(J)=D1(J)
03700 JOV(J)=AJO*EXP(-DO(J))
03710 500 CONTINUE
03720 DO 510 J=1,NPT
03730 DO 520 I=IL,IR
03740 IF(X(I).LT.XM2) GO TO 530
03750 IF(X(I).GT.XM1) GO TO 540
03760 J1VXT(I,J)=J1(I)*JOV(J)
03770 J2VXT(I,J)=J2(I)*JOV(J)
03780 GO TO 550
03790 540 T1D=T(J)-(X(I)-XM1)/(TAU*V1)
03800 IF(T1D.LT.0.) T1D=1.+T1D
03810 K=IFIX(FLOAT(NPT-1)*T1D+1.5)
03820 CALL INTERP(T1D,JOV,JOVA,JOVD,K,T,TA,NPT,NPTA)
03830 J1VXT(I,J)=J1(I)*ABS(JOVD)
03840 J2VXT(I,J)=J2(I)*JOV(J)
03850 GO TO 550
03860 530 T2D=T(J)+(X(I)-XM2)/(TAU*V2)
03870 IF(T2D.LT.0.) T2D=1.+T2D
03880 K=IFIX(FLOAT(NPT-1)*T2D+1.5)
03890 CALL INTERP(T2D,JOV,JOVA,JOVD,K,T,TA,NPT,NPTA)
03900 J2VXT(I,J)=J2(I)*ABS(JOVD)
```

```
03910 J1VXT(I,J)=J1(I)*JOV(J)
03920 550 CONTINUE
03930 520 CONTINUE
03940 510 CONTINUE
03950 DO 560 I=1,NPX
03960 DO 570 J=1,NPT
03970 JOVXT(I,J)=J1VXT(I,J)+J2VXT(I,J)
03980 570 CONTINUE
03990 6666 FORMAT(1X,10E11.3)
04000 560 CONTINUE
04010 DO 580 J=1,NPT
04020 SUM=0.
04030 DO 590 I=IIL,IR
04040 TERM=(JOVXT(I-1,J)+JOVXT(I,J))*DELTX/2.
04050 SUM=SUM+TERM
04060 590 CONTINUE
04070 JEV(J)=SUM/(XR-XL)
04080 580 CONTINUE
04090 SUMA=0.
04100 DO 600 J=2,NPT
04110 TERM=(JEV(J-1)+JEV(J))*DELTT/2.
04120 SUMA=SUMA+TERM
04130 600 CONTINUE
04140 AJO=AJO*AVG/SUMA
04150 DO 700 J=1,NPT
04160 J1VXT(IL,J)=J1VXT(IL,J)*AVG/SUMA
04170 J2VXT(IL,J)=J2VXT(IL,J)*AVG/SUMA
04180 SUM4=0.
04190 ESC(IL,J)=SUM4
04200 DO 710 I=IIL,IR
04210 J1VXT(I,J)=J1VXT(I,J)*AVG/SUMA
04220 J2VXT(I,J)=J2VXT(I,J)*AVG/SUMA
04230 TERM=EPINV*((J1VXT(I-1,J)+J1VXT(I,J))/V1
04240+          -(J2VXT(I-1,J)+J2VXT(I,J))/V2)*DELTX/2.
04250 IF(EO(I).LT.1.E-9) TERM=0.
04260 SUM4=SUM4+TERM
04270 ESC(I,J)=SUM4
04280 710 CONTINUE
04290 700 CONTINUE
04300 DO 720 J=1,NPT
04310 SUM=0.
04320 DO 730 I=2,NPX
04330 TERM=(ESC(I-1,J)+ESC(I,J))*DELTX/2.
04340 IF(EO(I).LT.1.E-9) TERM=0.
04350 SUM=SUM+TERM
04360 730 CONTINUE
04370 VSC(J)=SUM
04380 720 CONTINUE
04390 DO 740 L=1,10
04400 IF(L.EQ.1) DELTE(1)=DELTE(LL-1)
04410 IF(L.EQ.2) DELTE(2)=DELTE(LL)
04420 IF(L.GT.2) DELTE(L)=DELTE(L-1)-DT(L-1)*(DELTE(L-1)
04430+        -DELTE(L-2))/(DT(L-1)-DT(L-2))
04440 DO 750 I=IL,IR
04450 DO 760 J=1,NPT
04460 ET(I,J)=EO(I)+DELTE(L)+VO*SIN(2.*3.14159*FLOAT(J-1)/FLOAT(NPT-1))
04470+/(XR-XL)+ESC(I,J)-VSC(J)/(XR-XL)
04480 760 CONTINUE
04490 750 CONTINUE
04500 DO 770 J=1,NPT
04510 SUM1=0.
04520 SUMN=0.
04530 SUMD=0.
04540 IF(ET(IL,J).LT.1.E-9) ET(IL,J)=1.E-10
04550 B1OE=B1(IL)/ET(IL,J)
04560 B2OE=B2(IL)/ET(IL,J)
```

```
04570 IF(B2OE.GT.25.) B2OE=25.
04580 IF(B1OE.GT.25.) B1OE=25.
04590 ALP1(IL)=A1(IL)*EXP(-B1OE**M1)
04600 ALP2(IL)=A2(IL)*EXP(-B2OE**M2)
04610 DO 780 I=IIL,IR
04620 IF(ET(I,J).LT.1.E-9) ET(I,J)=1.E-10
04630 B1OE=B1(I)/ET(I,J)
04640 B2OE=B2(I)/ET(I,J)
04650 IF(B1OE.GT.25.) B1OE=25.
04660 IF(B2OE.GT.25.) B2OE=25.
04670 ALP1(I)=A1(I)*EXP(-B1OE**M1)
04680 ALP2(I)=A2(I)*EXP(-B2OE**M2)
04690 A2M1=(ALP2(I)-ALP1(I)+ALP2(I-1)-ALP1(I-1))/2.
04700 TERM1=A2M1*DELTX
04710 SUM11=SUM1
04720 SUM1=SUM1+TERM1
04730 TERMN=(ALP1(I)*EXP(SUM1)+ALP1(I-1)*EXP(SUM11))*DELTX/2.
04740 TERMD=(J1(I)*J2(I)*EXP(SUM1)+J1(I-1)*J2(I-1)*EXP(SUM11))*DELTX/2.
04750 SUMN=SUMN+TERMN
04760 SUMD=SUMD+TERMD
04770 780 CONTINUE
04780 AMTAU(J)=TAU*(1.-SUMN)/((1./V1+1./V2)*SUMD)
04790 770 CONTINUE
04800 D1(1)=0.
04810 DO 275 J=2,NPT
04820 D1(J)=D1(J-1)+(AMTAU(J-1)+AMTAU(J))*DELTT/2.
04830 275 CONTINUE
04840 DT(L)=D1(NPT)
04850 333 FORMAT(1X,4F15.10)
04860 IF(L.GT.3) LL=L
04870 IF(ABS(DT(L)).LT.1.E-9) GO TO 4000
04880 740 CONTINUE
04890 4000 CONTINUE
04900 SUM=0.
04910 DO 790 J=1,NPT
04920 TERM=(EXP(-D1(J-1))+EXP(-D1(J)))*DELTT/2.
04930 SUM=SUM+TERM
04940 555 FORMAT(1X,2F15.10)
04950 790 CONTINUE
04960 TAJO=AVG/SUM
04970 IF(IFLAG3.EQ.1) AJO=TAJO
04980 DO 800 J=1,NPT
04990 J1V(J)=AJO*EXP(-D1(J))
05000 800 CONTINUE
05010 TMAX=1.E-9
05020 IF(IFLAG2.EQ.0) DMAX=1.E-9
05030 DO 810 J=2,NPT
05040 IF(IFLAG2.EQ.0) DMAX=AMAX1(DMAX,ABS(D1(J)))
05050 TMAX=AMAX1(TMAX,ABS(D1(J)-DO(J))/DMAX)
05060 810 CONTINUE
05070 IFLAG2=1
05080 TAVG=ABS(AVG-SUMA)/AVG
05090 IF(TMAX.LT.1.E-3.AND.TAVG.LT.1.E-3) GO TO 495
05100 490 CONTINUE
05110 495 CONTINUE
05120 BCAP=2.*3.14159/(EPINV*(XR-XL)*TAU)
05130 SUMR=0.
05140 SUMI=0.
05150 DO 820 J=2,NPT
05160 TERMR=(JEV(J-1)*SIN(2.*3.14159*FLOAT(J-2)/FLOAT(NPT-1))+
05170+JEV(J)*SIN(2.*3.14159*FLOAT(J-1)/FLOAT(NPT-1)))*DELTT/2.
05180 TERMI=(JEV(J-1)*COS(2.*3.14159*FLOAT(J-2)/FLOAT(NPT-1))+
05190+JEV(J)*COS(2.*3.14159*FLOAT(J-1)/FLOAT(NPT-1)))*DELTT/2.
05200 SUMR=SUMR+TERMR
05210 SUMI=SUMI+TERMI
05220 820 CONTINUE
```

```
05230 SUMR=AREA*SUMR*2.
05240 G=SUMR/VO
05250 SUMI=AREA*SUMI*2.
05260 B=SUMI/VO+AREA*BCAP
05270 SUMI=B*VO
05280 RS=.0
05290 PS=(SUMR**2+SUMI**2)*RS/2.
05300 PO=-SUMR**2/(2.*G)
05310 PO=PO-PS
05320 G=G*1.E3
05330 B=B*1.E3
05340 PIN=VOLT*CUR*1.E-3
05350 EFF=100.*PO/PIN
05360 VFACT=100.*VFACT
05370 WRITE(6,83) VFACT,G,B,PO,PIN,EFF
05380 83 FORMAT(1X,6F9.2)
05390 DO 74 J=1,NPT
05400 74 CONTINUE
05410 3000 CONTINUE
05420 5000 CONTINUE
05430 4444 CONTINUE
05440 END
05450 SUBROUTINE INTERP(TND,JOV,JOVA,JOVD,K,T,TA,NPT,NPTA)
05460 DIMENSION T(NPT),TA(NPTA)
05470 REAL JOVD,JOV(NPT),JOVA(NPTA)
05480 KK=K+1
05490 JOVA(KK-1)=JOV(K-1)
05500 JOVA(KK)=JOV(K)
05510 JOVA(KK+1)=JOV(K+1)
05520 JOVA(1)=JOV(NPT-1)
05530 JOVA(NPTA)=JOV(2)
05540 TA(KK-1)=T(K-1)
05550 TA(KK)=T(K)
05560 TA(KK+1)=T(K+1)
05570 TA(1)=-1./FLOAT(NPT-1)
05580 TA(NPTA)=1.+1./FLOAT(NPT-1)
05590 DEN=TA(KK)*TA(KK+1)**2-TA(KK+1)*TA(KK)**2
05600+    -TA(KK-1)*TA(KK+1)**2+TA(KK+1)*TA(KK-1)**2
05610+    +TA(KK-1)*TA(KK)**2-TA(KK)*TA(KK-1)**2
05620 ANUM0=JOVA(KK-1)*(TA(KK)*TA(KK+1)**2-TA(KK+1)*TA(KK)**2)
05630+     -JOVA(KK)*(TA(KK-1)*TA(KK+1)**2-TA(KK+1)*TA(KK-1)**2)
05640+     +JOVA(KK+1)*(TA(KK-1)*TA(KK)**2-TA(KK)*TA(KK-1)**2)
05650 ANUM1=JOVA(KK)*TA(KK+1)**2-JOVA(KK+1)*TA(KK)**2
05660+     -JOVA(KK-1)*TA(KK+1)**2+JOVA(KK+1)*TA(KK-1)**2
05670+     +JOVA(KK-1)*TA(KK)**2-JOVA(KK)*TA(KK-1)**2
05680 ANUM2=TA(KK)*JOVA(KK+1)-JOVA(KK)*TA(KK+1)
05690+     -JOVA(KK+1)*TA(KK-1)+JOVA(KK-1)*TA(KK+1)
05700+     +JOVA(KK)*TA(KK-1)-JOVA(KK-1)*TA(KK)
05710 A0=ANUM0/DEN
05720 A1=ANUM1/DEN
05730 A2=ANUM2/DEN
05740 JOVD=A0+A1*TND+A2*TND**2
05750 RETURN
05760 END
READY.
```

```
GET,TAPE10
READY.

LIST,F=TAPE10
10,5
40,100
3,.7
70,100
200,200
.1,.07
.04,.02
.36,.36
.70,.70
READY.

RUN

 ARE YOU FAMILIAR WITH DIODE MODEL? YES(1),NO(0)
? 0

 THIS PROGRAM CALCULATES AVALANCHE VOLTAGE, TOTAL
 VOLTAGE, CONDUCTANCE, SUSCEPTANCE, OUTPUT POWER, AND
 EFFICIENCY FOR A READ-READ DOUBLE DRIFT DEVICE.  THE
 STRUCTURE AND NOMENCLATURE FOR EACH HALF IS SHOWN IN
 THE FOLLOWING SKETCH.
```

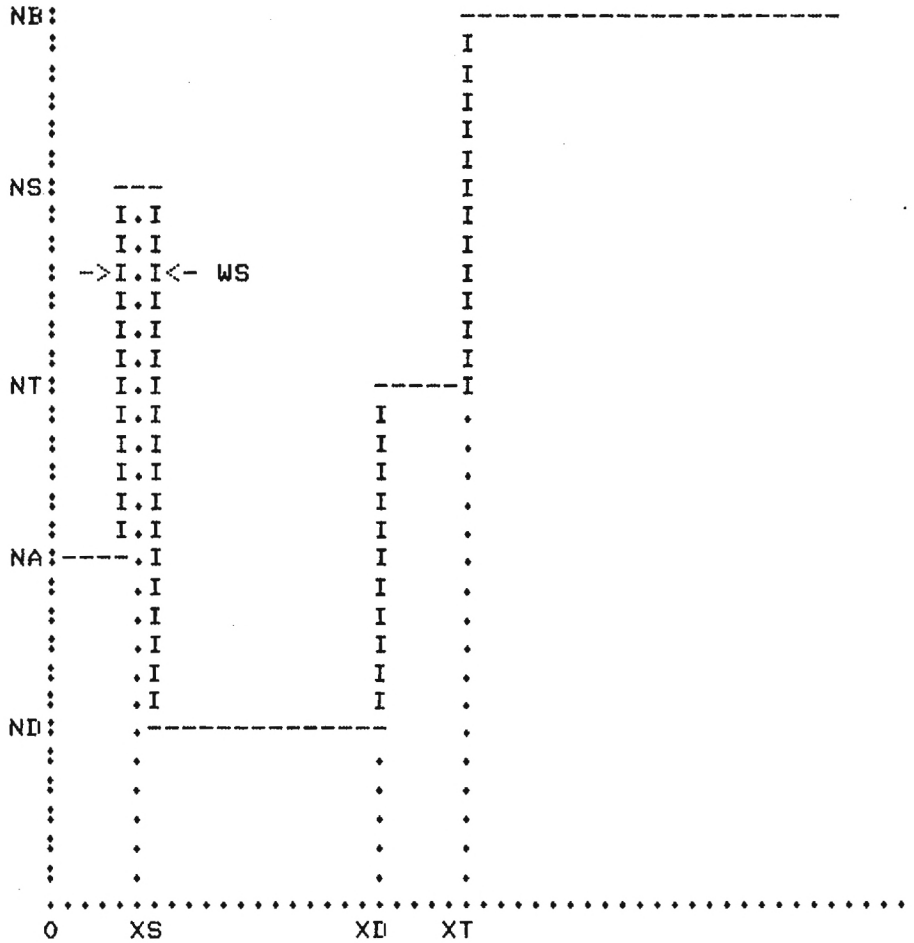

```
      IN THIS FIGURE:
          NB IS THE BUFFER OR SUBSTRATE DOPING
          NS IS THE SPIKE DOPING
          NT IS THE TERMINATION LAYER DOPING
          NA IS THE AVALANCHE REGION DOPING
          ND IS THE DRIFT REGION DOPING
          WS IS THE SPIKE WIDTH
          XS IS THE SPIKE POSITION
          XD IS THE DEPLETION/TERMINATION INTERFACE POSITION
          XT IS THE TERMINATION/ BUFFER INTERFACE POSITION


   LEFT AND RIGHT HALF QUANTITIES ARE DENOTED WITH L AND R
SUBSCRIPTS, I.E., NAL AND NAR ARE LEFT AND RIGHT AVALANCHE
REGION DOPINGS.


    HYBRID-READ AND UNIFORMLY DOPED DOUBLE DRIFT DEVICES
CAN BE SIMULATED BY LETTING NA=NS=ND FOR THE APPROPIATE REGIONS.


INPUT DATA-- DOPINGS(E16),DISTANCES(E-4)


IS INPUT ON TAPE(10) OR TERMINAL(5)?
? 10


WHAT ARE THE VALUES FOR NAL AND NAR?
10. 5.
NSL,NSR?
40. 100.
NDL,NDR?
3. .7
NTL,NTR?
70. 100.
NBL,NBR?
200. 200.
WHAT ARE THE POSITIONS OF THE SPIKES?
.1 .07
WHAT ARE THE WIDTHS OF THE SPIKES?
.04 .02
XDL,XDR?
.36 .36
XTL,XTR?
.7 .7



AVALANCHE VOLTAGE =   7.00 VOLTS
TOTAL VOLTAGE     =  19.25 VOLTS
CURRENT           = 200.00 MA
FREQUENCY         =  40.00 GHZ


  VRF/VDC      G          B          PO         PIN        EFF.
    (%)     (MMHOS)    (MMHOS)   (WATTS)    (WATTS)      (%)

    10.00   -27.12      94.36       .05       3.85       1.30
    20.00   -23.21     107.30       .17       3.85       4.47
    30.00   -18.94     119.09       .32       3.85       8.20
    40.00   -15.11     127.81       .45       3.85      11.63
    50.00   -12.21     133.97       .57       3.85      14.68
    60.00   -10.02     138.37       .67       3.85      17.35

SRU    173.479 UNTS.

RUN COMPLETE.
```

APPENDIX B

Computer Program CVTEST

```
00100 PROGRAM CVTEST(INPUT,OUTPUT,TAPE5=INPUT,TAPE6=OUTPUT,TAPE10)
00110 REAL XR(101),XL(101),QR(101),QL(101),EQ(201),EQR(201),EQL(201)
00120 REAL VR(101),VL(101),W(101),C(101),V(101)
00130 REAL NR(101),NL(101)
00140 REAL NAL,NAR,NSL,NSR,NDL,NDR,NTL,NTR,NBL,NBR
00150 REAL E(101),ET(101),N(101)
00160 REWIND 10
00170 PRINT*," "
00180 WRITE(6,312)
00190 312 FORMAT(1X,*DO YOU WANT A DRAWING OF THE STRUCTURE? YES(1),NO(0)*)
00200 READ(6,*) IDRAW
00210 PRINT*," "
00220 IF(IDRAW.EQ.0) GO TO 334
00230 WRITE(6,10)
00240 10 FORMAT(6X,*THIS PROGRAM CALCULATES CV DATA,ELECTRIC FIELD, AND */
00250+*BREAKDOWN VOLTAGE FOR A READ-READ DOUBLE DRIFT DEVICES.  THE */
00260+*STRUCTURE AND NOMENCLATURE FOR EACH HALF IS SHOWN IN THE FOLLOWING*/
00270+*SKETCH.*///
00280+,T9,*NB:*,T35,*----------------------*)
00290 DO 20 I =1,5
00300 WRITE(6,30)
00310 30 FORMAT (1X,T11,*"*T35,*I*)
00320 20 CONTINUE
00330 WRITE (6,40)
00340 40 FORMAT (1X,T9,*NS*,T11,*:*,T15,*---*,T35,*I*)
00350 DO 50 I=1,2
00360 WRITE(6,60)
00370 60 FORMAT (1X,T11,*:*,T15,*I,I*,T35,*I*)
00380 50 CONTINUE
00390 WRITE(6,70)
00400 70 FORMAT (1X,T11,*: ->I.I<- WS*,T35,*I*)
00410 DO 80 I=1,3
00420 WRITE(6,60)
00430 80 CONTINUE
00440 WRITE(6,90)
00450 90 FORMAT(1X,T9,*NT*,T11,*:*,T12,*   I.I     *,*        -----I*)
00460 DO 100 I=1,5
00470 WRITE(6,105)
00480 105 FORMAT (1X,T11,*:*,T15,*I.I*,T30,*I     .*)
00490 100 CONTINUE
00500 WRITE(6,110)
00510 110 FORMAT(1X,T9,*NA*,T11,*:*,T12,*----.I*,T30,*I     .*)
00520 DO 120 I=1,5
00530 WRITE(6,130)
00540 130 FORMAT(1X,T11,*:*,T16,*.I*,T30,*I*,T35,*.*)
00550 120 CONTINUE
00560 WRITE(6,140)
00570 140 FORMAT(1X,T9,*ND*,T11,*:*,T14,*  .-------------      .*)
00580 DO 150 I=1,5
00590 WRITE(6,160)
00600 160 FORMAT(1X,T11,*:*,T16,*.*,T30,*.*,T35,*.*)
00610 150 CONTINUE
00620 WRITE(6,170)
00630 170 FORMAT(1X,T11,*.....................................................*)
00640 WRITE(6,180)
00650 180 FORMAT(1X,T11,*0*,T16,*XS*,T29,*XD*,T34,*XT*///)
```

```
00660 WRITE(6,190)
00670 190 FORMAT(1X,*     IN THIS FIGURE*/
00680+*          NB IS THE BUFFER OR SUBSTRATE DOPING*/
00690+*          NS IS THE SPIKE DOPING*/
00700+*          NT IS THE TERMINATION LAYER DOPING*/
00710+*          NA IS THE AVALANCHE REGION DOPING*/
00720+*          WS IS THE SPIKE WIDTH*/
00730+*          XS IS THE SPIKE POSITION*/
00740+*          XD IS THE DEPLETION/TERMINATION INTERFACE POSITION*/
00750+*          XT IS THE TERMINATION/BUFFER INTERFACE POSITION*/
00760+*  */
00770+*  */
00780+*    LEFT AND RIGHT HALF QUANTITIES ARE DENOTED WITH L AND R*/
00790+* SUBSCRIPTS, I.E., NAL AND NAR ARE LEFT AND RIGHT AVALANCHE*/
00800+* REGION DOPINGS.*/
00810+*  */
00820+*  */
00830+*     HYBRID-READ AND UNIFORMLY DOPED DOUBLE DRIFT DEVICES*/
00840+* CAN BE SIMULATED BY LETTING NA=NS=ND FOR THE APPROPIATE REGIONS.*//)
00850 334 PI=4.*ATAN(1.)
00860 Q=1.6E-19
00870 EP=12.5E-11/(36.*PI)
00880 AREA=4.5E-5
00890 WRITE(6,200)
00900 200 FORMAT(1X,*INPUT DATA-- DOPINGS(E16),DISTANCES(E-4)*//)
00910 WRITE(6,212)
00920 212 FORMAT(1X,*INPUT ON TAPE(10) OR FROM TERMINAL(5)?*)
00930 READ(5,*) INCODE
00940 WRITE(6,216)
00950 216 FORMAT(//)
00960 WRITE(6,210)
00970 210 FORMAT(1X,*WHAT ARE THE VALUES FOR NAL AND NAR?*)
00980 READ(INCODE,*) NAL,NAR
00990 IF(INCODE.EQ.10) WRITE(6,*) NAL,NAR
01000 NAL=NAL*1.E16
01010 NAR=NAR*1.E16
01020 WRITE(6,220)
01030 220 FORMAT(1X,*NSL,NSR?*)
01040 READ(INCODE,*) NSL,NSR
01050 IF(INCODE.EQ.10) WRITE(6,*) NSL,NSR
01060 NSL=NSL*1.E16
01070 NSR=NSR*1.E16
01080 WRITE(6,230)
01090 230 FORMAT(1X,*NDL,NDR?*)
01100 READ(INCODE,*) NDL,NDR
01110 IF(INCODE.EQ.10) WRITE(6,*) NDL,NDR
01120 NDL=NDL*1.E16
01130 NDR=NDR*1.E16
01140 WRITE(6,240)
01150 240 FORMAT(1X,*NTL,NTR?*)
01160 READ(INCODE,*) NTL,NTR
01170 IF(INCODE.EQ.10) WRITE(6,*) NTL,NTR
01180 NTL=NTL*1.E16
01190 NTR=NTR*1.E16
01200 WRITE(6,250)
01210 250 FORMAT(1X,*NBL,NBR?*)
01220 READ(INCODE,*) NBL,NBR
01230 IF(INCODE.EQ.10) WRITE(6,*) NBL,NBR
01240 NBL=NBL*1.E16
01250 NBR=NBR*1.E16
01260 WRITE(6,260)
01270 260 FORMAT(1X,*WHAT ARE THE POSITIONS OF THE SPIKES?*)
01280 READ(INCODE,*) XSL,XSR
01290 IF(INCODE.EQ.10) WRITE(6,*) XSL,XSR
01300 XSL=XSL*1.E-4
01310 XSR=XSR*1.E-4
```

```
01320 WRITE(6,265)
01330 265 FORMAT(1X,*WHAT ARE THE WIDTHS OF THE SPIKES?*)
01340 READ(INCODE,*) WSL,WSR
01350 IF(INCODE.EQ.10) WRITE(6,*) WSL,WSR
01360 WSL=WSL*1.E-4
01370 WSR=WSR*1.E-4
01380 WRITE(6,270)
01390 270 FORMAT(1X,*XDL,XDR?*)
01400 READ(INCODE,*) XDL,XDR
01410 IF(INCODE.EQ.10) WRITE(6,*) XDL,XDR
01420 XDL=XDL*1.E-4
01430 XDR=XDR*1.E-4
01440 WRITE(6,280)
01450 280 FORMAT (1X,*XTL,XTR?*)
01460 READ(INCODE,*) XTL,XTR
01470 IF(INCODE.EQ.10) WRITE(6,*) XTL,XTR
01480 XTL=XTL*1.E-4
01490 XTR=XTR*1.E-4
01500 XR(1)=0.
01510 XL(1)=0.
01520 DELTX=.05E-5
01530 NR(1)=NAR
01540 NR(1)=7.E16
01550 NL(1)=NAL
01560 NL(1)=7.E16
01570 VR(1)=0.
01580 VL(1)=0.
01590 QR(1)=0.
01600 QL(1)=0.
01610 DO 290 I=2,101
01620 XR(I)=DELTX*FLOAT(I-1)
01630 XL(I)=DELTX*FLOAT(I-1)
01640 NR(I)=NAR
01650 IF(XR(I).GT.(XSR-WSR/2.)) NR(I)=NSR
01660 IF(XR(I).GT.(XSR+WSR/2.)) NR(I)=NDR
01670 IF(XR(I).GT.XDR) NR(I)=NTR
01680 IF(XR(I).GT.XTR) NR(I)=NBR
01690 NL(I)=NAL
01700 IF(XL(I).GT.(XSL-WSL/2.)) NL(I)=NSL
01710 IF(XL(I).GT.(XSL+WSL/2.)) NL(I)=NDL
01720 IF(XL(I).GT.XDL) NL(I)=NTL
01730 IF(XL(I).GT.XTL) NL(I)=NBL
01740 QR(I)=QR(I-1)+(NR(I)+NR(I-1))*DELTX/2.
01750 QL(I)=QL(I-1)+(NL(I)+NL(I-1))*DELTX/2.
01760 VR(I)=VR(I-1)+(XR(I)*NR(I)+XR(I-1)*NR(I-1))*DELTX/2.
01770 VL(I)=VL(I-1)+(XL(I)*NL(I)+XL(I-1)*NL(I-1))*DELTX/2.
01780 EQL(I)=Q*QL(I)/EP
01790 EQR(I)=Q*QR(I)/EP
01800 290 CONTINUE
01810 V(1)=0.
01820 W(1)=0.
01830 DO 300 I=2,101
01840 IF(QR(I).LT.QL(I)) GO TO 330
01850 DO 310 L=1,101
01860 IF(QR(L).LT.QL(I)) GO TO 310
01870 DXL=(XR(L)-XR(L-1))*(QR(L)-QL(I))/(QR(L)-QR(L-1))
01880 W(I)=XL(I)+XR(L)-DXL
01890 V(I)=VL(I)+VR(L)-(XR(L)*NR(L)+XR(L-1)*NR(L-1))*DXL/2.
01900 IF(QR(L).GT.QL(I)) GO TO 320
01910 310 CONTINUE
01920 GO TO  320
01930 330 CONTINUE
01940 DO 340 L=1,101
01950 IF(QL(L).LT.QR(I)) GO TO 340
01960 DYL=(XL(L)-XL(L-1))*(QL(L)-QR(I))/(QL(L)-QL(L-1))
01970 W(I)=XR(I)+XL(L)-DYL
```

```
01980 V(I)=VR(I)+VL(L)-(XL(L)*NL(L)+XL(L-1)*NL(L-1))*DYL/2.
01990 IF(QL(L).GT.QR(I)) GO TO 320
02000 340 CONTINUE
02010 320 CONTINUE
02020 300 CONTINUE
02030 E(1)=0.
02040 V(1)=0.
02050 PRINT*,' '
02060 PRINT*,' '
02070 PRINT*,'          TOTAL        JUNCTION        DEPLETION ',
02080+'         DOPING'
02090 PRINT*,'         VOLTAGE    CAPACITANCE         WIDTH   ',
02100+'         DENSITY'
02110 PRINT*,' '
02120 DO 350 K=2,100
02130 V(K)=Q*V(K)/EP
02140 C(K)=EP*AREA/W(K)
02150 IF(K.GT.2) E(K)=E(K-1)+(C(K)+C(K-1))*(V(K)-V(K-1))/(2.*EP*AREA)
02160 IF(K.GT.2) N(K)=-(C(K)+C(K-1))**3*(V(K)-V(K-1))/(8.*EP*Q*AREA**2*
02170+ (C(K)-C(K-1)))
02180 ET(K)=6.E5-E(K)
02190 IF(ET(K).GT.0.) WRITE(6,360) V(K),C(K),W(K),N(K)
02200 360 FORMAT(1X,4E15.3)
02210 350 CONTINUE
02220 END
READY.
```

```
RUN

 DO YOU WANT A DRAWING OF THE STRUCTURE? YES(1),NO(0)
? 0

 INPUT DATA-- DOPINGS(E16),DISTANCES(E-4)


 INPUT ON TAPE(10) OR FROM TERMINAL(5)?
? 10



 WHAT ARE THE VALUES FOR NAL AND NAR?
 10. 5.
 NSL,NSR?
 40. 100.
 NDL,NDR?
 3. .7
 NTL,NTR?
 70. 100.
 NBL,NBR?
 200. 200.
 WHAT ARE THE POSITIONS OF THE SPIKES?
 .1 .07
 WHAT ARE THE WIDTHS OF THE SPIKES?
 .04 .02
 XDL,XDR?
 .36 .36
 XTL,XTR?
 .7 .7
```

TOTAL VOLTAGE	JUNCTION CAPACITANCE	DEPLETION WIDTH	DOPING DENSITY
.218E-02	.583E-10	.853E-06	0.
.679E-02	.306E-10	.163E-05	.408E+17
.140E-01	.209E-10	.238E-05	.358E+17
.240E-01	.159E-10	.313E-05	.346E+17
.366E-01	.128E-10	.388E-05	.341E+17
.520E-01	.108E-10	.463E-05	.339E+17
.701E-01	.925E-11	.538E-05	.337E+17
.909E-01	.812E-11	.613E-05	.336E+17
.114E+00	.723E-11	.687E-05	.336E+17
.141E+00	.652E-11	.763E-05	.335E+17
.170E+00	.594E-11	.837E-05	.335E+17
.556E+00	.432E-11	.115E-04	.902E+17
.733E+00	.395E-11	.126E-04	.928E+17
.827E+00	.378E-11	.132E-04	.919E+17
.925E+00	.363E-11	.137E-04	.915E+17
.103E+01	.349E-11	.143E-04	.911E+17
.129E+01	.334E-11	.149E-04	.201E+18
.173E+01	.319E-11	.156E-04	.285E+18
.219E+01	.306E-11	.163E-04	.287E+18
.267E+01	.293E-11	.170E-04	.284E+18

.318E+01	.281E-11	.177E-04	.288E+18
.370E+01	.271E-11	.184E-04	.286E+18
.424E+01	.260E-11	.191E-04	.256E+18
.480E+01	.213E-11	.233E-04	.449E+17
.483E+01	.203E-11	.245E-04	.679E+16
.484E+01	.199E-11	.251E-04	.678E+16
.485E+01	.195E-11	.256E-04	.677E+16
.487E+01	.191E-11	.261E-04	.677E+16
.488E+01	.187E-11	.266E-04	.677E+16
.489E+01	.183E-11	.271E-04	.676E+16
.491E+01	.180E-11	.276E-04	.676E+16
.492E+01	.177E-11	.282E-04	.675E+16
.494E+01	.173E-11	.287E-04	.675E+16
.495E+01	.170E-11	.292E-04	.675E+16
.497E+01	.167E-11	.297E-04	.674E+16
.498E+01	.165E-11	.302E-04	.674E+16
.500E+01	.162E-11	.307E-04	.674E+16
.501E+01	.159E-11	.312E-04	.673E+16
.503E+01	.157E-11	.318E-04	.673E+16
.504E+01	.154E-11	.323E-04	.673E+16
.506E+01	.152E-11	.328E-04	.673E+16
.508E+01	.149E-11	.333E-04	.672E+16
.509E+01	.147E-11	.338E-04	.672E+16
.511E+01	.145E-11	.343E-04	.672E+16
.513E+01	.143E-11	.349E-04	.672E+16
.515E+01	.141E-11	.354E-04	.671E+16
.516E+01	.139E-11	.359E-04	.671E+16
.518E+01	.137E-11	.364E-04	.671E+16
.520E+01	.135E-11	.369E-04	.671E+16
.522E+01	.133E-11	.374E-04	.671E+16
.524E+01	.131E-11	.380E-04	.670E+16
.526E+01	.129E-11	.385E-04	.670E+16
.528E+01	.128E-11	.390E-04	.670E+16
.530E+01	.126E-11	.396E-04	.602E+16
.532E+01	.124E-11	.402E-04	.569E+16
.534E+01	.122E-11	.408E-04	.568E+16
.536E+01	.120E-11	.414E-04	.566E+16
.538E+01	.118E-11	.420E-04	.567E+16
.540E+01	.117E-11	.427E-04	.570E+16
.542E+01	.115E-11	.433E-04	.568E+16
.544E+01	.113E-11	.439E-04	.567E+16
.547E+01	.112E-11	.445E-04	.566E+16
.549E+01	.110E-11	.451E-04	.570E+16
.551E+01	.109E-11	.457E-04	.568E+16
.554E+01	.107E-11	.464E-04	.567E+16
.556E+01	.106E-11	.470E-04	.566E+16
.558E+01	.105E-11	.476E-04	.569E+16
.561E+01	.103E-11	.482E-04	.569E+16
.563E+01	.102E-11	.488E-04	.567E+16
.566E+01	.101E-11	.494E-04	.566E+16
.568E+01	.994E-12	.501E-04	.568E+16
.571E+01	.981E-12	.507E-04	.569E+16
.773E+01	.835E-12	.596E-04	.288E+17
.126E+02	.678E-12	.733E-04	.380E+17
.180E+02	.667E-12	.746E-04	.383E+18

SRU 3.342 UNTS.

RUN COMPLETE.